REFLECTIVE CRACKING OF SHEAR KEYS

IN MULTI-BEAM BRIDGES

A Thesis

by

GRAEME PETER SHARPE

Submitted to the Office of Graduate Studies of
Texas A&M University
in partial fulfillment of the requirements for the degree of

MASTER OF SCIENCE

August 2007

Major Subject: Civil Engineering

REFLECTIVE CRACKING OF SHEAR KEYS

IN MULTI-BEAM BRIDGES

A Thesis

by

GRAEME PETER SHARPE

Submitted to the Office of Graduate Studies of
Texas A&M University
in partial fulfillment of the requirements for the degree of

MASTER OF SCIENCE

Approved by:

Chair of Committee,	Harry Jones
Committee Members,	Ray James
	Harry Hogan
Head of Department,	David Rosowsky

August 2007

Major Subject: Civil Engineering

ABSTRACT

Reflective Cracking of Shear Keys

in Multi-beam Bridges. (August 2007)

Graeme Peter Sharpe, B.S., Carnegie Mellon University

Chair of Advisory Committee: Dr. Harry Jones

Multi-beam bridges made from precast concrete box girders are one of the most common bridge types used in the United States. One problem that affects these bridges is the development of longitudinal or reflective cracks on the road surface because of failure of the shear keys. Some states have attempted to correct this problem by redesigning the shear key or adding post-tensioning, but the problem persists in many new bridges.

The purpose of this study is to investigate why these shear key failures are occurring. This project studies two types of box girder designs, the common Precast/Prestressed Concrete Institute (PCI) box girder bridges and the Texas Department of Tranportation (TxDOT) box girder bridge. In the past, reflective cracking has occurred in bridges of both types.

The analysis procedure involves finite element analyses of bridge models with realistic support and loading conditions, and comparing the PCI and TxDOT bridges. The results indicate that both PCI and TxDOT box girder have sufficient strength to resist cracking from vehicular loads, but uneven temperature changes and shrinkage

strains cause high tensile stresses in the shear key regions and lead to reflective cracking. The analyses showed the highest stresses were often times near the supports, rather than at midspan.

Past studies have proposed using larger composite deck slabs, transverse post-tensioning, or full-depth shear keys to prevent shear key failure. Composite slabs were the most effective way to reduce high stresses in shear keys, and were effective for all loading cases considered. Post-tensioning and full-depth keys also showed a reduction in shear key stresses, but were less effective.

DEDICATION

This work is dedicated to my wonderful wife, Heather Joan Sharpe. She supported me in many ways during my time at Texas A&M, in both the jubilant times of gathering results to the despairs of lost data. She has my utmost respect as a fellow engineer, and has always inspired me to do my very best.

ACKNOWLEDGEMENTS

I would like to take this opportunity to acknowledge those individuals who have contributed to the completion of this thesis. My advisor, Dr. Harry Jones was a great leader and helped me explore the many details of this complicated engineering problem. His advice was always meaningful and I am appreciative for the time he spent on this project.

Dr. Ray James also taught me a great deal about this subject as a graduate assistant at the Texas Transportation Institute. I would like to thank him, TTI, and Dr. Jones once again for their assistance on that project and the funding it provided which allowed me to finish this thesis.

My fellow students at Texas A&M University deserve a lot of credit for helping me understand the many difficult aspects of computer modeling, and I would like to thank them. Special thanks go to Jong-Wha Bai, Yateesh Contractor, Tamas Liszkai, Fayez Moutassem, and Shashikant Sarada, who were always there for help and advice. Also special thanks to Natalie Brush, who was a great research partner and dedicated a lot of her time towards our project.

I would like to acknowledge the help from the Texas A&M Supercomputing Center and the High-Bay Structural and Materials Testing Laboratory. Their help and commitment to research activities were always appreciated.

TABLE OF CONTENTS

Page

ABSTRACT iii

DEDICATION v

ACKNOWLEDGEMENTS vi

TABLE OF CONTENTS vii

LIST OF FIGURES ix

LIST OF TABLES xiv

INTRODUCTION 1

RESEARCH OBJECTIVES 7

LITERATURE REVIEW 8

- Materials Selection 8
- Transverse Post-Tensioning 10
- Small Scale Tests 11
- Large Scale Tests 17
- Other Box Girder Bridge Literature 20
- Elastomeric Bearing Pad Literature 21

BRIDGES STUDIED 22

- TxDOT Box Girders 22
- PCI Box Girders 25

SOLID MODEL DESCRIPTION 29

- Introduction 29
- Box Girder Description 30
- Shear Key and Slab Description 30
- Material Properties 31
- Internal Diaphragms 32

Page

IDEALIZATION OF BEAM SUPPORTS 33

Introduction 33
Elastomeric Bearing Pads 33
Linear Spring Models 34
Linear Spring Stiffness 36

LOADS APPLIED 40

HS-25 Truck Loading 40
Initial Shrinkage Loads 44
Thermal Gradient Load 47

ANALYSIS PROCEDURE 50

Description of Program Output 50
Failure Criteria 52

SOLID MODEL VERIFICATION 55

Beam Bending 55
Transverse Bending 57
Submodel Analysis 63

RESULTS 80

Introduction 80
Results for Shrinkage Loading 82
Results for Temperature Loading 90
Results for Vehicular Loading 98
Discussion of Bridge Features 102

SUMMARY AND CONCLUSIONS 115

Summary of Project 115
Summary of Results 117
Conclusions 118
Recommendations for Further Research 119

REFERENCES 121

VITA 123

LIST OF FIGURES

Page

Figure 1: Schematic of Two Box Girders and a Shear Key 2

Figure 2: PCI 33” Box Girder with Shear Keys 5

Figure 3: TxDOT 34” Box Girder with Shear Keys 5

Figure 4: Test Specimen Under Tension 12

Figure 5: Test Specimen in Bending 12

Figure 6: Test Specimen in Shear 13

Figure 7: Typical TxDOT Box Girder Geometry 23

Figure 8: PCI Box Girder Typical Geometry 26

Figure 9: 5B34 Box Girder with Mesh 30

Figure 10: Shear Key Detail with Element Mesh 31

Figure 11: Bearing Pad Deformation and Behavior 34

Figure 12: Bearing Pad Vertical Spring Supports 35

Figure 13: Bearing Pad Schematic 36

Figure 14: Truck at Midspan Location 41

Figure 15: Truck at End of Span Location 41

Figure 16: Truck Axle Location on 2-Lane Bridge 42

Figure 17: Truck Axle Location on 3-Lane Bridge, Lane 1 42

Figure 18: Truck Axle Location for 3-Lane Bridge, Lane 2 43

Figure 19: Schematic of Shrinkage Effects 45

Page

Figure 20: Positive Temperature Profile for Thermal Gradient Load 48

Figure 21: Negative Temperature Profile for Thermal Gradient Load 49

Figure 22: Girder and Shear Key Cross Section 51

Figure 23: Transverse Normal Stress Profile 51

Figure 24: Beam Bending Test Bridge 56

Figure 25: Transverse Bending Test Bridge 58

Figure 26: Transverse Bending Shell Model 59

Figure 27: Transverse Bending Solid Model 60

Figure 28: Results for Transverse Bending Bridge Models 61

Figure 29: Shell Model vs. Solid Model Results 63

Figure 30: Global Model and Highlighted Submodel Region 65

Figure 31: Global Model Mesh 66

Figure 32: Submodel Mesh 67

Figure 33: Closer View of Submodel Shear Key 67

Figure 34: Submodel with Applied Constraints 68

Figure 35: Maximum Transverse Stress in Submodel due to Slab Shrinkage 69

Figure 36: Stress Profile for Slab Shrinkage 70

Figure 37: Maximum Transverse Stress in Submodel due to Shear Key Shrinkage 71

Figure 38: Stress Profile for Shear Key Shrinkage 72

Figure 39: Maximum Transverse Stress in Submodel due to Positive Temperature Gradient 73

Page

Figure 40: Stress Profile for Positive Temperature Gradient 74

Figure 41: Maximum Transverse Stress in Submodel due to Negative Temperature Gradient 75

Figure 42: Stress Profile for Negative Temperature Gradient 76

Figure 43: Maximum Transverse Stress in Submodel due to Truck Loading..... 77

Figure 44: Stress Profile for Truck Loading 78

Figure 45: Joint Numbering Scheme..... 81

Figure 46: Maximum Transverse Stress due to Slab Shrinkage in 2-Lane Bridges 83

Figure 47: Maximum Transverse Stress due to Slab Shrinkage in 3-Lane Bridges 84

Figure 48: Stresses in Joints for TxDOT Bridge due to Slab Shrinkage (2-Lane TB28 - 59) 85

Figure 49: Stresses in Joints for PCI Bridge due to Slab Shrinkage (2-Lane PB27 - 59)..... 85

Figure 50: Maximum Transverse Stress due to Shear Key Shrinkage in 2-Lane Bridges 87

Figure 51: Maximum Transverse Stress due to Shear Key Shrinkage in 3-Lane Bridges 88

Figure 52: Stresses in Joint for TxDOT Bridge Under Shear Key Shrinkage (2-Lane TB28 - 59) 89

Figure 53: Stresses in Joint for PCI Bridge under Shear Key Shrinkage (2-Lane PB27 - 59)..... 89

Page

Figure 54: Maximum Transverse Stress due to Positive Thermal Gradient in 2-Lane Bridges 91

Figure 55: Maximum Transverse Stress due to Positive Thermal Gradient in 3-Lane Bridges 92

Figure 56: Stresses in Joint for TxDOT Bridge due to Positive Temperature Gradient 93

Figure 57: Stresses in Joint for PCI Bridge due to Positive Temperature Gradient 93

Figure 58: Maximum Transverse Stress due to Negative Thermal Gradient in 2-Lane Bridges 95

Figure 59: Maximum Transverse Stress due to Negative Thermal Gradient in 3-Lane Bridges 96

Figure 60: Stresses in Joint for TxDOT Bridge due to Negative Thermal Gradient 97

Figure 61: Stresses in Joint for PCI Bridge due to Negative Thermal Gradient 97

Figure 62: Maximum Transverse Stress due to HS-25 Loading in 2-Lane Bridges 99

Figure 63: Maximum Transverse Stress due to HS-25 Loading in 3-Lane Bridges 100

Figure 64: Stresses in Joint for TxDOT Bridge due to Truck Loading (2-Lane TB28 - 59) 101

Figure 65: Stresses in Joint for PCI Bridge due to Truck Loading (2-Lane PB27 - 59) 101

Figure 66: TxDOT Bridge with no shear key under HS-25 loads (2-Lane TB28 – S 59) 103

Page

Figure 67: TxDOT Bridge with no shear key and (+) Thermal Gradient Loads
(2-Lane TB28 - S 59) 104

Figure 68: Texas Box Girder (TB28) with Full Depth Shear Key 105

Figure 69: PCI Box Girder (PB27) with Full Depth Shear Key 105

Figure 70: TxDOT Bridge with Full-Depth Key under HS-25 Loads
(2-Lane TB28 - FD 59) 107

Figure 71: TxDOT Bridge with Full-Depth Key under (-) Thermal Gradient Loads 107

Figure 72: Average Stress in TxDOT bridge from Post-Tensioning Force
(2-Lane TB28 – PT 59) 109

Figure 73: Post-Tensioned TxDOT Bridge without Loads Applied
(2-Lane TB28 – PT 59) 110

Figure 74: Post-Tensioned TxDOT Bridge without Loads Applied
(2-Lane TB28 – PT 59) 111

Figure 75: Post-Tensioned PCI Bridge without Loads Applied
(2-Lane PB27 – PT 59) 112

Figure 76: Post-Tensioned PCI Bridge without Loads Applied
(2-Lane PB27 – PT 59) 113

LIST OF TABLES

Page

Table 1: Small-scale specimen tests 16

Table 2: TxDOT Box Beam Typical Spans 24

Table 3: Table of TxDOT Box Girder Bridges 25

Table 4: PCI Box Beams and Typical Spans 26

Table 5: Comparison of PCI and TxDOT Box Beams 27

Table 6: Table of PCI Box Girder Bridges 28

Table 7: Bearing Pad Stiffnesses 39

Table 8: Shrinkage loads applied to bridge 47

Table 9: Beam Verification Results 57

Table 10: Bridge Suffix Identification Code 80

INTRODUCTION

Transportation departments across the U.S. have been using concrete box girder bridges since the 1950's. This bridge style accounts for a significant percentage of new and existing bridges (FHWA 2005). The section depth is one of the most important considerations for a new bridge, as the overhead clearance of a bridge affects many costs associated with bridge construction. The concrete box girder bridge is well suited for highway structures that require a limited section depth, short to medium spans, and rapid construction. The initial cost of the bridge is high when compared to other bridge types, but the advantages of box girder bridges often justify the higher cost.

The construction process for a multi-beam bridge occurs in distinct phases. The first phase is the construction of the box girders off-site, at a precast concrete manufacturing facility. The benefit of the precast process is that the manufacturer can maintain a high level of quality control over the materials used in the construction of the box girder. The next phase is the on-site construction of all the bridge sub-components, such as bent caps and approach slabs. When the site is ready for the placement of the box girders, they are lifted into place with a crane. Typically, the box girders rest on bearing pads that will accommodate the thermal elongation experienced by the box girders. The final phase of the construction process is the creation of joints, called shear keys, that link the individual box girders together and transfer vehicle loads from one beam to the next so they share the loads produced by vehicular traffic. In addition, a composite deck slab may be applied either as an integral part of the shear key casting

This thesis follows the style of *ASCE Journal of Bridge Engineering.*

The shear key gets its name from the transfer of vertical shear forces between adjacent girders. It has a geometry that causes the two girders to deflect as a single unit. When present, a composite deck slab also contributes to the transfer of forces between adjacent boxes. The multi-beam bridge cross section shown in Figure 1 is a Texas Department of Transportaion (TxDOT) standard and utilizes a large shear key.

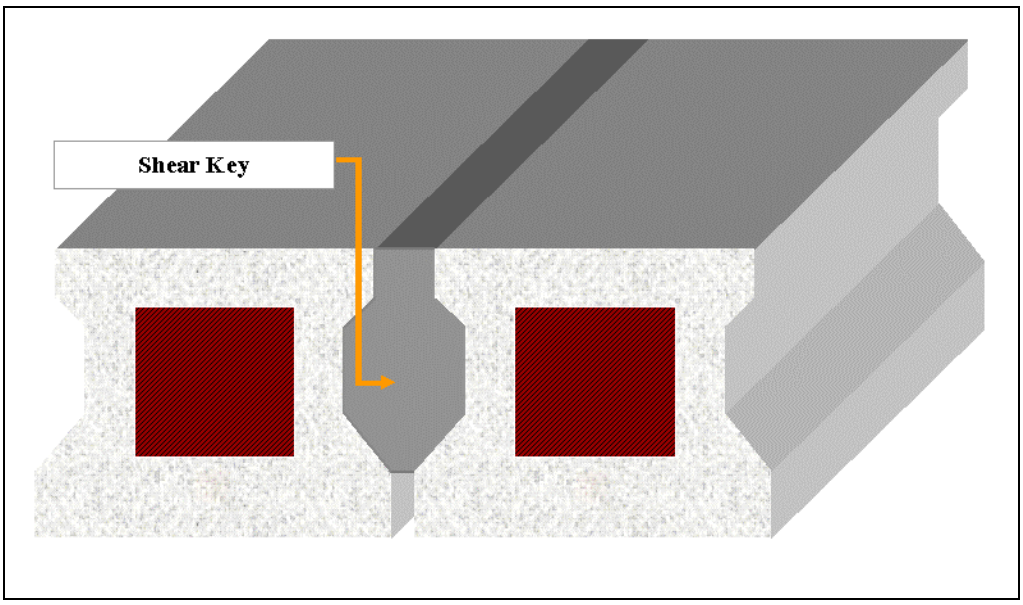

Figure 1: Schematic of Two Box Girders and a Shear Key

Reflective cracking in a multi-beam bridge refers to longitudinal cracks that can form on the roadway surface over the shear key area. TxDOT, as well as a number of other state DOT's, have reported reflective cracking problems severe enough to require corrective maintenance or replacement of the entire bridge. It is generally held that such cracking is associated with cracking which first occurs in the shear key below. The

reflection of keyway cracks in roadway surfaces can lead to spalling in a concrete deck and debonding of the asphalt layer when an overlaid riding surface is used. Field inspections of distressed multi-beam bridges by various transportation agencies suggests that shear key integrity deteriorates over time as a result of repetitive loads from passing traffic and causes more pronounced reflective cracking in the riding surface. Other field reports indicate that some bridges develop reflective cracks very soon after the bridge is completed, and sometimes before it is open for traffic.

Reflective cracks can be a major maintenance issue. Cracks in the roadway surface allow water and de-icing salts to corrode the reinforcing steel in the beams and the composite deck slab. Stains visible on the underside of the bridge and cracks on the road surface are considered unsightly. Also, transverse post-tensioning and tie bars, if present on the bridge, will be exposed to corrosive chemicals and begin to degrade. If the shear key damage is severe enough, it is possible for a girder to be overloaded because no load distribution to adjacent beams is occurring. This means that a girder may support loads greater than anticipated, and this can result in faster deterioration or structural failure. For example, a multi-beam box girder bridge experienced this type of failure in late 2005 (Grata and Saxton 2005), and the state of Pennsylvania had to close and inspect similar bridges.

The geometry of shear keys in use today seems to have evolved from early experiences and lacks any mechanics based procedure for rational design. In the last decade, however, growing awareness of common problems with shear keys led to new

efforts to design a better shear key. Reports since that time indicate that the problem continues, and further information is needed on this subject.

Some states have attempted to reduce reflective cracking through expensive alterations. TxDOT, for example, has issued new standard designs which mandate the use of a minimum 5 inch thick reinforced deck slab, adding cost and construction time to projects. Others have changed their designs to incorporate more extensive transverse post tensioning, which also increases cost significantly.

The two box girder designs considered in this study are the PCI/AASHTO (Precast/Prestressed Concrete Institute and American Association of State Highway and Transportation Officials) and the TxDOT version. The PCI – AASHTO design is used by more than half of the states in the U.S. The Texas DOT uses its own version with a more massive shear key. Figure 2 shows a PCI 33 inch deep box girder with associated shear keys as adopted by the Ohio DOT. Figure 3 shows a TxDOT 34 inch deep box girder and shear keys. The PCI girder has less concrete in the cross section and a much smaller shear key than the TxDOT girder. The bridges have similar structural properties, however, and are used for similar span lengths in multi-beam bridges. The primary reinforcement is prestressed steel strands at the bottom flange, and the amount of prestressing force along with section depth generally determines the span length and load capacity.

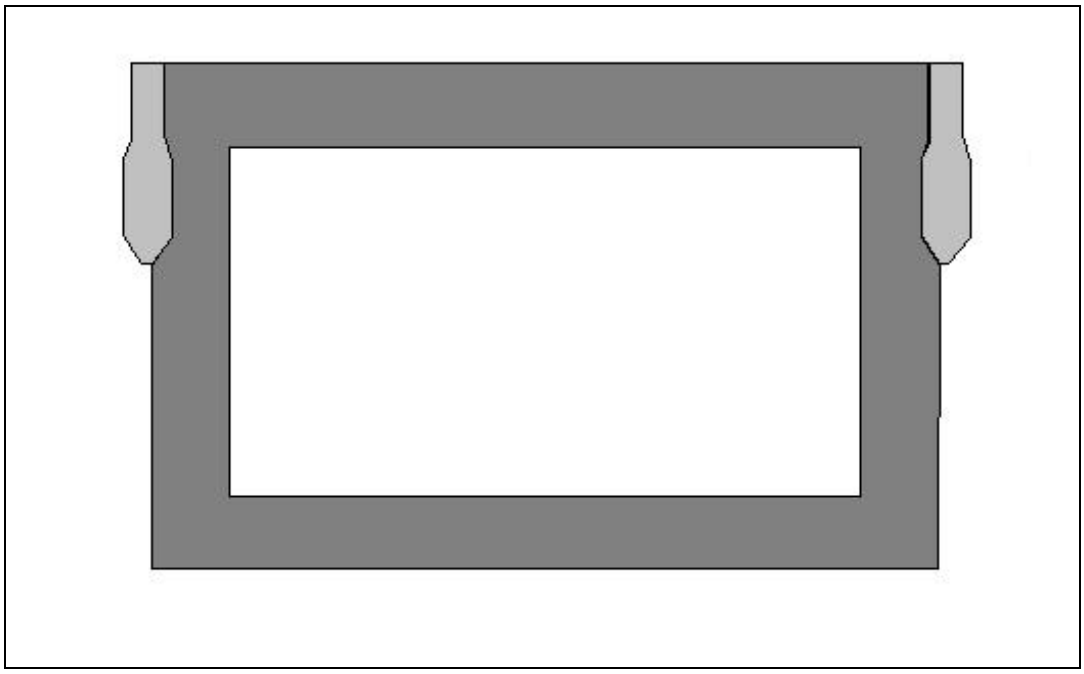

Figure 2: PCI 33" Box Girder with Shear Keys

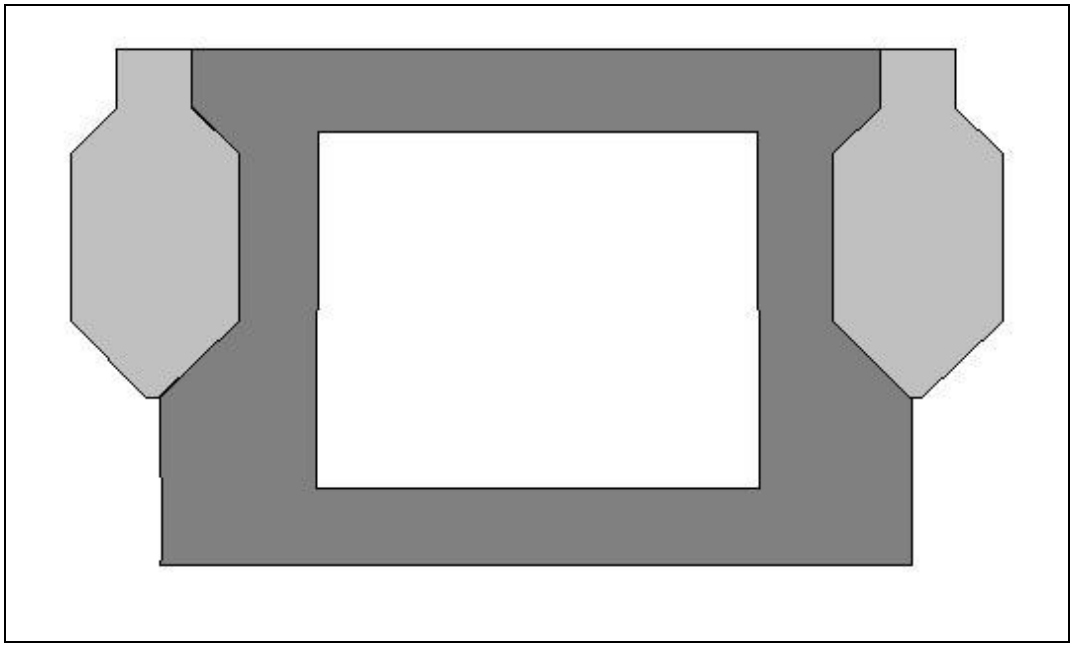

Figure 3: TxDOT 34" Box Girder with Shear Keys

The PCI and Texas shear keys share several other characteristics. They are both set high up in the section and make up part of the roadway surface. Also, the gap in the bottom is small so that a stop can be placed to contain the grout or concrete in the keyway. The keyway inset into the soffit of the box beam is usually very shallow or slanted in order to prevent air pockets from forming and weakening the joint.

The complex geometry of box girder bridges means that numerical methods or laboratory tests are necessary to determine stresses in the shear key. The AASHTO lateral load distribution factors can be used to determine the shear forces transferred between adjacent box girders due to traffic loads, but experience shows that the reflective cracking will occur if the shear keys are designed only to resist vertical shear. This happens because transverse normal stresses in the shear key from shrinkage, thermal effects, and wheel loads are also acting on the shear key. In this study, FEA was used to examine the stress state in the shear key. This approach also allows for incorporating the effects of composite deck slabs and transverse post-tensioning on the stress field in the shear key.

It is believed that both these elements work to reduce the tensile stresses in the shear key and prevent or reduce cracking. Field experience, however, demonstrates that the addition of these elements doesn't ensure the elimination of shear key cracking. This study was undertaken in an attempt to correlate the state of stress in the shear key with observed deterioration reported in both TxDOT and PCI concrete box girder bridges.

RESEARCH OBJECTIVES

The objectives of this study are:

1) Determine the state of stress in the shear key resulting from different loading situations
2) Determine what loads are likely to damage shear key connections in multi-beam box girder bridges
3) Determine the effectiveness of post-tensioning and composite slabs in reducing shear key failure
4) Compare the behavior of the PCI and TxDOT box girders which represent the two extremes of shear key design

LITERATURE REVIEW

In this section previous work relating to the failure of shear keys is reviewed in order to fully describe the problem at hand, and to understand what solutions have already been proposed. The research conducted on shear keys is divided into five categories; the first addresses materials selection, the second addresses the effect of transverse post-tensioning, the third reviews small-scale tests, and the fourth group investigates the performance of shear keys in full-scale constructed multi-beam bridges. The final section discusses the general design and construction, as well as the history of box girder bridges.

Materials Selection

The most common material choices for a shear key are unreinforced concrete or cementitious grout. However, other materials have been used, and research into the effectiveness of alternative materials has been conducted previously. Tensile and compressive strength are the most often cited properties of a shear key material. Just as important are several other factors such as amount of shrinkage, bond strength, chloride permeability, and ease of application. Higher performing materials will have higher cost, and a balance must be struck between the need for a reasonably priced material and the need for reliable performance.

The materials used in shear keys and their ASTM specifications are described in "Evaluation of Keyway Grout Test Methods for Precast Concrete Bridges" (Gulyas et al. 1995). This article details the work that Master Builders Technologies researchers have

conducted on the benefits of using cementitious materials other than grout in shear keys. The authors discuss important information related to the shrinkage and bond strength of both non-shrink grout and “Set-45” or magnesium ammonium phosphate (Mg-NH4-PO4) mortar. The Set-45 mortar tested much better in both the bond strength test and shrinkage test.

In a follow up commentary to the last article (Nottingham et al. 1995), an engineering firm discusses their experience with using Set-45 on a dock structure on the coast of Alaska. The shear keys there have performed well in a precast panel deck. However, the authors state that inappropriate joint details can lead to poor performance and early failure in typical installations.

Another alternative material discussed in the literature is epoxy based glue. The article “Epoxy Glue Joints in Precast Concrete Segmental Bridge Construction” (Moreton 1981) focused on how an epoxy glue joint would behave if two beams were joined and subjected to bending. The results published by the author indicate that the joints performed well if the mating surfaces were prepared carefully and the glue is allowed to cure under the appropriate conditions. In this study, epoxy was applied by hand and the specimens had to be pressed together for several days to achieve the right bond, indicating the need for some type of transverse post-tensioning system.

Further research into the use of alternative materials such discussed above is in the article "Performance of Transverse Joint Grout Materials in Full-Depth Precast Concrete Bridge Deck Systems" (Issa et al. 2003). The article details the authors’ efforts to compare different materials, including grout, Set-45 (Mg-NH4-PO4), Set-45 HW (for

hot weather), and polymer concrete. The authors concluded that conventional grout is the best material choice because it provides high strength and ease of use. Further, the authors state that they recommend polymer concrete over the Set-45 mortar where extreme conditions warrant a more expensive solution.

Transverse Post-Tensioning

An important factor cited in some earlier work is transverse post-tensioning. Some previous studies have suggested that reflective cracking can be remedied with large amounts of post-tensioning. Post tensioning has the ability to reduce debonding and tension failures by applying transverse compression across the shear keys. However, the amount of force and spacing of the post-tensioning strands needed to obtain satisfactory behavior in a general case is unclear. In addition, TxDOT as well as some other state DOT's, are cautious about using transverse post-tensioning because it can add significant cost and make the multi-beam bridges more troublesome than other types of bridge construction.

In Japan, where shear keys seldom fail, a large amount of transverse post-tensioning is used. In the article "Transverse Design of Adjacent Precast Prestressed Concrete Box Girder Bridges" (El Remaily et al. 1996), the authors detail Japan's efforts and adapt them to conventional bridges in the U.S. Some details of this design are full-depth shear keys with cast in place concrete filled diaphragms at the quarter-point locations of the bridge where post-tensioning strands can be used, and a relatively high post-tensioning force.

The article “Shear Strength of Post-Tensioned Grouted Keyed Connections” relates the strength of a shear key joint to the amount of transverse post-tensioning (Annamalai and Brown 1990). Their experiments show that increased post-tensioning improves both the strength and the monolithic behavior of a shear key. They state that the successful performance of grouted shear keys depend primarily on the amount of compressive stress present.

Two articles that present in-depth analyses of shear keys and their failure are "Fracture Mechanics Approach for Failure of Concrete Shear Key I: Theory" (Kaneko et al. 1993a) and "Fracture Mechanics Approach for Failure of Concrete Shear Key II: Verification" (Kaneko et al. 1993b). In these papers, the authors use the principles of fracture mechanics to derive the failure conditions for a concrete shear key. The results from the first paper were based on certain fracture mechanics assumptions, but may not be applicable for every shear key geometry or loading scenario. A closed form solution that gives the shear strength or peak load of a shear key is presented. However, this equation assumes that post-tensioning will be present and that vertical shear controls the failure, but if these assumptions are not met then the equation will not give meaningful results.

Small Scale Tests

Several of the articles in the literature include results from small-scale tests performed on shear key specimens. These tests are intended to characterize the strength per unit width of a shear key design for a given material and address the capacity of a

shear key in shear, moment, or tension. The testing configuration for tension is shown in Figure 4, moment testing is shown in Figure 5, and shear testing is shown in Figure 6.

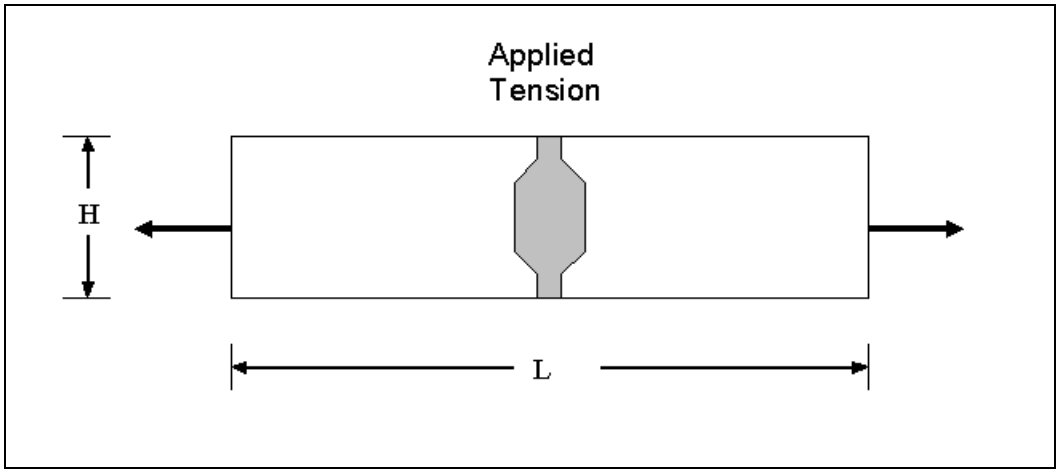

Figure 4: Test Specimen Under Tension

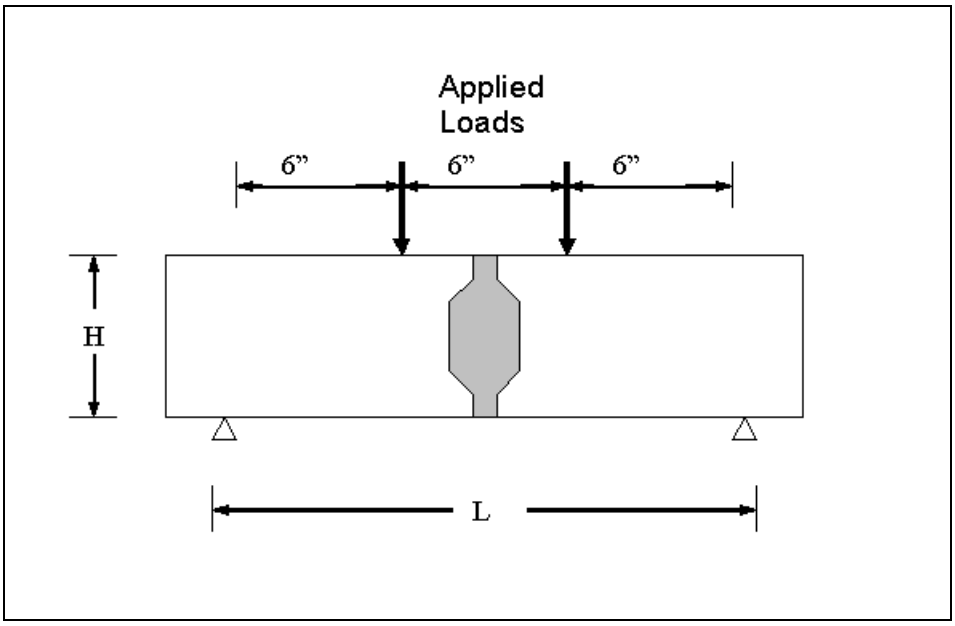

Figure 5: Test Specimen in Bending

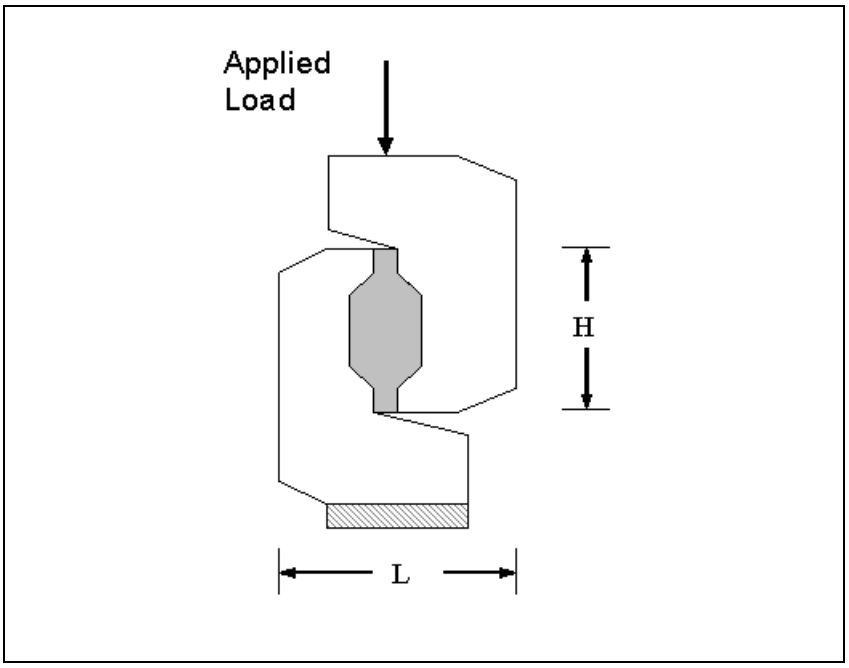

Figure 6: Test Specimen in Shear

The above referenced article about material selection (Issa et al. 2003) presents the results for the specimens that were tested in several failure modes. The specimens represented a typical transverse joint for a full-depth concrete bridge deck and the shear keys were 6 to 8 inches deep and 5 to 6 inches wide. The test results for conventional grout material yielded shear key strengths of 358 psi in direct shear, 223 psi in direct tension, and 620 psi in flexural tests.

Gulyas et al. include information about failures of small-scale specimens in the article mentioned earlier. In their tests, grouted shear key specimens 8 to 12 inches deep and 3.25 inches wide were subjected to various loading conditions. Their results

indicated that the specimens with grout failed at 75 psi in direct tension, 61 psi in longitudinal shear, and failed in vertical shear at about 223 psi.

The article concerning fracture mechanics as applied to shear keys (Kaneko et al. 1993b) references a test where a specimen composed of concrete that had a shear key 6 inches deep and 3 inches wide failed when the average stress in the shear key was 1520 psi. This test was done for vertical shear loading where a large amount of transverse prestressing was used; the value of prestress force given in the article is 6000 pounds of compression.

Detailed information about all of the small-scale tests can be found in Table 1. This data was recorded by researchers and published in their research reports. The type of loading, ultimate load, and failure mode as well as the stress is included in the table. The stress data was calculated for this study and uses simple formulas for average axial and shear stress (P/A, V/A), or maximum bending stress (M*y/I), depending upon the loading and the specimen geometry. This data represents the ultimate strength of shear keys. It can be seen from looking at failure modes that samples using grout or other cementitious materials are weakest in direct tension, and will fail at loads lower than their material strengths would indicate. This means the bond between the keyway face and the shear key itself is very important. If the key debonds from the box girder, there is no steel reinforcement to keep the joint intact.

The data from the table also notes the failure mode of the samples, indicating if a joint line failure (debonding), material failure (cracking), or a mixed failure (combination of debonding and cracking) was the result of the test. As can be seen in

the table, debonding or mixed failures are the result for every case except the prestressed sample that failed by crushing. This means that debonding is the most likely cause of failure regardless of loading, and therefore a cementitious material is unlikely to achieve full strength in a shear key design since the shear key will separate from the face of the box girder prematurely.

Table 1: Small-scale specimen tests

Material Information				Geometry				Failure Information		
Authors	Material	fc' (psi)	ft (psi)	Depth (in)	Length (in)	Width (in)	Type of Test	Failure (lbs)	Stress (psi)	Notes
Issa, et al.	Grout	7700	658	6	5	9	Vertical Shear	10749	358	Mixed failure
	"	"	"	8	5	20	Tension	8948	224	Mixed failure
	"	"	"	6	6	18	(2Pt) Flexural	22331	620	Mixed failure
	Set-45	5820	572	6	5	9	Vertical Shear	9756	325	Joint failure
	"	"	"	8	5	20	Tension	8036	201	Joint failure
	"	"	"	6	6	18	(2Pt) Flexural	9817	273	Joint failure
Kaneko, et al.	Concrete	7105	632	6	3	10	Vertical Shear	20880	1160	6000 lbs prestress
Gulyas, et al.	Grout	5870	390	12	3.25	6.5	Longitudinal Shear	2400	62	Bond line failure
	"	"	"	12	3.25	6.5	Vertical Shear	5850	150	Bond line failure
	"	"	"	8	3.25	6.5	Vertical Shear	7850	302	Bond line failure
	"	"	"	8	3.25	6.5	Tension	1940	75	Bond line failure
	Set-45	7260	557	12	3.25	6.5	Longitudinal Shear	14300	367	Mixed failue
	"	"	"	12	3.25	6.5	Vertical Shear	16500	423	Mixed failue
	"	"	"	8	3.25	6.5	Vertical Shear	20250	779	Mixed failue
	"	"	"	8	3.25	6.5	Tension	5730	220	Mixed failue

Large Scale Tests

Full-scale tests were discussed in some of the articles reviewed. The benefit of these studies is that the shear keys can be tested in a manner similar to how they will be used in the field. However, there are some problems with large-scale tests. First, determining the existence and extent of cracking or failure in the shear key is difficult. Second, construction of full-scale bridges is costly and so only a limited number of studies can be carried out.

Cusens and Pama (1965) investigated the design of shear keys and the transverse loads experienced in multi-beam bridges. The authors discuss the appropriate way to analyze a bridge, including those with shear keys and composite slabs. They recommend the use of modified orthotropic plate equations derived from mechanics of materials. The authors discuss how to account for the stiffness of the bridge in the transverse direction, even if the shear key is not full-depth or cracked.

More recently, the Ohio Department of Transportation sponsored several projects to improve the behavior and strength of concrete multi-beam box girder bridges with grouted shear keys. In the first article by Huckelbridge et al. (1995), the authors instrumented an existing box girder bridge and measured displacements between adjacent girders to determine how much shear transfer took place. They found that the shear keys in some regions of the bridge had failed almost entirely and the beam prestressing strands were corroded from leaking water. The authors concluded that design changes to the bridge were necessary, as the current design had insufficient strength.

In a later study sponsored by the Ohio DOT (Huckelbridge and El-Esnawi 1997), the authors attempted to correct the design flaws of the shear key. This project involved a thorough investigation of the design forces in the bridge using a 3D finite element analysis of a multi-beam box girder bridge subjected to a vehicular wheel load. The authors concluded that the stresses in the shear key were large enough to cause failure after repeated loadings, and so changes needed to be made to the shear key design. The transverse post-tensioning alternative was investigated and found to be uneconomical, as strands would need to be located every 2.5 feet in order to apply an effective compressive stress across the entire length of the bridge. An improved design with the shear key relocated at mid-depth of the girder was investigated and it failed at a load 2.3 times higher than the original design. Therefore, the authors recommended moving the shear key to mid-depth and using conventional grouting procedures.

The latest Ohio DOT study (Miller et al. 1998) details the results of a full-scale bridge with the improved shear key designs as compared to the original detailing. Three tests were performed, one with the conventional shear key design with grout, the same design with epoxy, and a new design with a grouted key at mid-depth. Surprisingly, the shear keys with grouted keys began to crack before any load was applied. The specimens were dismantled, cleaned and new shear keys were installed, but the same failures occurred. A combination of thermal cycling and off-axis beam orientation was cracking the shear keys within a few days. In fact, it was found that throughout testing, vehicle loading did not initiate any cracking but only propagated existing cracks. The mid-depth shear key design had a higher resistance to both crack formation and crack

propagation. The epoxy joints did not crack at any point during loading. The authors noted that the worst crack locations still transferred a significant amount of load to adjacent girders, but longer fatigue testing may continue to degrade a shear key.

The article "Full Depth Shear-Key Performance in Adjacent Prestressed-Beam Bridges" (Lall et al. 1997), sponsored by the New York DOT discusses the performance of box girder bridges in New York. The New York State DOT had recently switched to a full-depth design with a transverse tie system and was reporting on the effectiveness of the new bridge design. From the questionnaires sent to different state officials, it was clear that the design changes had reduced the cracking problems but had not eliminated them. Further design recommendations were introduced, including more transverse post-tensioning. Other recommendations included a tighter control of construction practices, full-width bearing pads to prevent off-axis tilting, and a higher amount of steel reinforcement in the concrete deck overlay.

One report was written specifically about Texas bridges and their reflective cracking problems (Jones 1999). This report includes a survey of existing bridges with problems as well as data from a bridge instrumented with strain gages in order to determine loading effects and strains in the bridge. The paper also addresses the failure of bridges that had a composite deck slab and were built without a shear key. A three-dimensional beam analysis program developed by the author identified high transverse moments in the deck slab as a potential problem in the bridges analyzed. The report shows design forces for a wide range of Texas bridges and gives live load distribution factors for a number of box girder geometries used in Texas bridges.

Other Box Girder Bridge Literature

The design and construction process for TxDOT box girder bridges is detailed in documents from their website (TxDOT 2001). The documents include information on the standardized bridge designs, dimensions of all box girders, construction drawings for slabs, and details about elastomeric bearing pads. This information was consulted for material specifications and bridge geometry of the models used in this study.

Similar to the Texas standards, the Ohio bridge design manual and box beam standards (ODOT 2005) were consulted to obtain the specifications for a PCI type box girder. These documents were posted on the Ohio DOT website. The Ohio standards were chosen because these are PCI sections that have been studied in the past and many results are available in the literature regarding the design and construction of these bridge types. Also, Ohio uses a minimal amount of transverse post-tensioning so the comparison with TxDOT examples is more meaningful than a bridge with extensive post-tensioning.

The AASHTO LRFD Bridge Design Specifications (AASHTO 2004) and Standard Specifications for Highway Bridges (AASHTO 1992) books were consulted to find the current practices of construction and design, as well as how to correctly model design loads for the bridges.

Elastomeric Bearing Pad Literature

One article about the support conditions of bridge girders on elastomeric bearing pads was consulted (Yazdani et al. 2000). This article details the role that the stiffness of the bearing pads play in the behavior of precast concrete bridges. The article concludes that the bearing pad stiffness must be taken into account if the actual bending behavior of a girder is to be accurately modeled. The recommended stiffnesses for bearing pads are found in the AASHTO documents, but the researchers found that bearing pads grew stiffer as they aged, and that this can significantly alter the bending behavior. Also, the stiffnesses of the bearing pads can affect the lateral distribution of loads between girders.

BRIDGES STUDIED

For this study, 39 different multi-beam box girder bridges were analyzed with ANSYS, a general finite element computer program. The focus of the study was the behavior of each bridge under realistic loading conditions. The lengths and widths of the bridges were based on current bridge design standards used by TxDOT. The selected bridges have no slope in the transverse direction, no curvature along their length, a constant cross section, and no skew.

Of the 39 different bridges, 28 use TxDOT boxes and 11 incorporate the PCI box girder. These bridge types were chosen because they represent the two extremes of shear key design. The overall width of each bridge depends upon the number and type of box girder used in construction. A typical way to represent this for a 26 ft wide TxDOT box girder bridge would be 5Bxx + 4[4Bxx] + 5Bxx, where the bridge is made up of a 5 ft wide box girder at one edge then (4) – 4 ft wide interior box girders, then another 5 ft wide box girder at the other edge. The Bxx indicates a Box Girder section with "xx" as the depth of the girder.

TxDOT Box Girders

When the Texas bridge design engineers originally considered the box girder issue, they felt that the PCI sections used shear keys that were too small to resist the vehicular loads, so a new design was created (TxDOT 2001). The Texas box girder uses the soffit form developed in the 1950's for prestressed concrete I-beams. The result, as seen in Figure 7, is an abnormally large shear key. The benefit of using this detail was

that the concrete beam fabricators had the ability to make either an I-beam or a box girder with the same form. One disadvantage is that the shear key and box girder uses more concrete or grout than the PCI design. Thus, there is an extra material cost as well as the additional dead load that must be supported by the bridge superstructure, possibly resulting in the use of deeper sections or more prestressing than other designs.

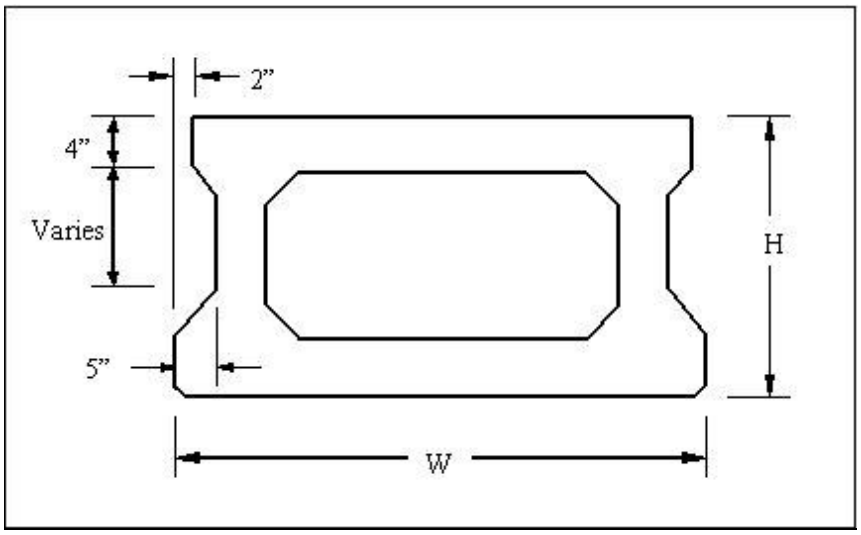

Figure 7: Typical TxDOT Box Girder Geometry

Texas bridge designers can specify four standard depths, and two standard width boxes, for a possible eight cross sections. Box girder dimensions in Figure 7 are available in the state Bridge Design Guide (TxDOT 2001). Typical span lengths for each cross section are listed in Table 2 (Jones 1999). The B40 section is rarely used and so was not included in this study.

Table 2: TxDOT Box Beam Typical Spans

		Span Length (ft)		
Section Name	Depth (in)	Shortest	Medium	Longest
B20	20	39	49	59
B28	28	39	59	79
B34	34	65	79	92
B40	40	79	92	105

The shear key is constructed after the bridge box girders have seated on the bent caps and a backer rod is used to seal the bottom of the keyway. Grout or concrete is then poured into the keyway, and as soon as it has reached design strength the bridge is complete. In its latest design standard, TxDOT encourages the use of a concrete composite topping slab in an attempt to reduce longitudinal cracking in the riding surface. A nominal depth of 5 inches is required, but the slab can be thicker. If an asphalt topping is chosen instead of the composite slab, the minimum thickness is 2 inches and the bridge must have transverse post-tensioning according to TxDOT specifications.

Texas has built multi-beam box girder bridges in many different configurations, reflecting the combinations available. Table 3 shows the TxDOT box girder bridges that were used in this study, including the most important characteristics of each one. The purpose of including the large number of bridges is to investigate what role each component plays on the stresses present in the shear key.

Table 3: Table of TxDOT Box Girder Bridges

Bridge Name	Span (ft)	Section Depth (in)	Overall Width (ft)	Shear Key	Composite Slab	Post-Tensioning	Full-Depth Key
2 Lane TB20 - 30	30	20	26	Yes	Yes	--	--
2 Lane TB20 - 39	39	20	26	Yes	Yes	--	--
2 Lane TB20 - 59	59	20	26	Yes	Yes	--	--
2 Lane TB20 - S 59	59	20	26	--	Yes	--	--
2 Lane TB20 - SK 59	59	20	26	Yes	--	--	--
3 Lane TB20 - 30	30	20	40	Yes	Yes	--	--
3 Lane TB20 - 39	39	20	40	Yes	Yes	--	--
3 Lane TB20 - 59	59	20	40	Yes	Yes	--	--
2 Lane TB28 - 39	39	28	26	Yes	Yes	--	--
2 Lane TB28 - 59	59	28	26	Yes	Yes	--	--
2 Lane TB28 - S 59	59	28	26	--	Yes	--	--
2 Lane TB28 - SK 59	59	28	26	Yes	--	--	--
2 Lane TB28 - FD 59	59	28	26	--	--	--	Yes
2 Lane TB28 - PT 59	59	28	26	Yes	--	Yes	--
2 Lane TB28 - 79	79	28	26	Yes	Yes	--	--
3 Lane TB28 - 39	39	28	40	Yes	Yes	--	--
3 Lane TB28 - 59	59	28	40	Yes	Yes	--	--
3 Lane TB28 - 79	79	28	40	Yes	Yes	--	--
2 Lane TB34 - 59	59	34	26	Yes	Yes	--	--
2 Lane TB34 - S 59	59	34	26	--	Yes	--	--
2 Lane TB34 - SK 59	59	34	26	Yes	--	--	--
2 Lane TB34 - 79	79	34	26	Yes	Yes	--	--
2 Lane TB34 - 92	92	34	26	Yes	Yes	--	--
2 Lane TB34 - 104	104	34	26	Yes	Yes	--	--
3 Lane TB34 - 59	59	34	40	Yes	Yes	--	--
3 Lane TB34 - 79	79	34	40	Yes	Yes	--	--
3 Lane TB34 - 92	92	34	40	Yes	Yes	--	--
3 Lane TB34 - 104	104	34	40	Yes	Yes	--	--

NOTES:
1) 26 ft roadway composed of (4) - 4ft-0in wide box girders with (2) - 5ft-0in wide girders, (1) on each end
2) 40 ft roadway composed of (8) - 5ft-0in wide box girders

PCI Box Girders

The more common PCI box girder has a smaller shear key, but is made of similar sizes as the Texas box girders and has similar section properties. The PCI box girder also comes in two standard widths, but these are 3 ft and 4 ft rather than the Texas 4 ft and 5 ft. See Figure 8 for a typical PCI box girder.

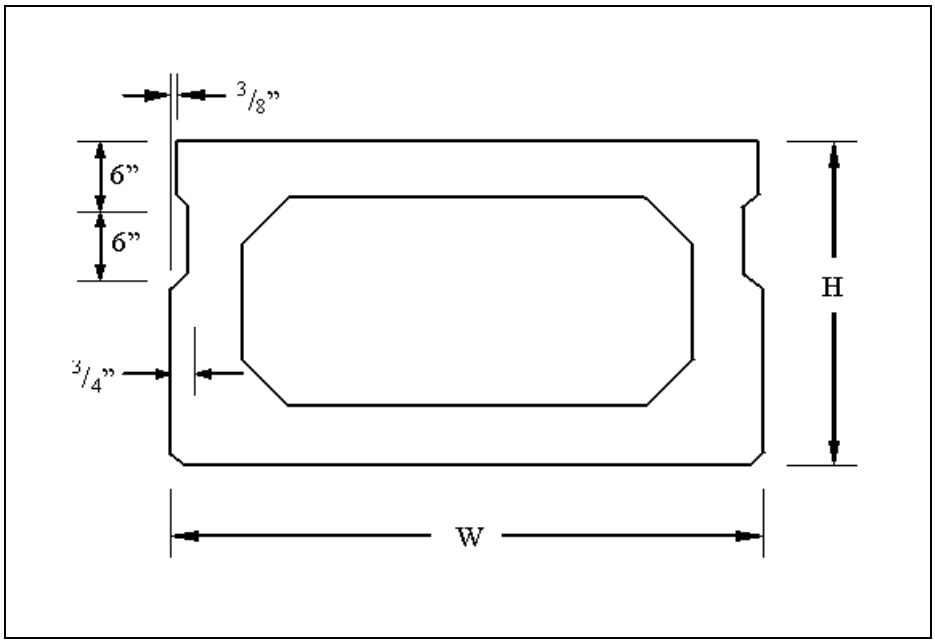

Figure 8: PCI Box Girder Typical Geometry

The applications for the PCI sections are similar to the Texas sections, but only the 27" and 33" sections are used. The 39" box girder section will not be included in this study due to infrequent use, but some of the relevant information is shown here for completeness. Table 4 shows the typical span lengths for a PCI box beam bridge (ODOT 2005).

Table 4: PCI Box Beams and Typical Spans

Section Name	Depth	Short	Medium	Long
BI	27	40	60	70
BII	33	50	65	85
BIII	39	60	65	100

Since both Texas and the PCI box girder are used for similar bridges, Table 5 was created to compare properties for three different examples. These box girders have similar cross sectional properties, and therefore if a shear key fails in one bridge type but not the other, then it indicates that the shear key itself is the difference.

Table 5: Comparison of PCI and TxDOT Box Beams

State of Use	Box Girder Type	Depth (in)	Area (in^2)	Moment of Inertia (in^4)
OH	BI-48	27	692.6	65,835
TX	4B28	28	678.8	68,745
OH	BII-48	33	752.6	110,333
TX	4B34	34	797.7	115,540
OH	BIII-48	39	812.6	168,377
TX	4B40	40	917.7	176,556

The PCI bridges in this study are similar to the TxDOT bridges in most respects, but are composed of 4 ft wide sections since no 5 ft wide section is available. For the smaller bridges used in this study, the difference between the PCI and TxDOT designs is small, about 2 feet, so the overall response to vehicular loads should be similar. However, for a wider 3 lane bridge the PCI design would use 10 girders rather than the TxDOT design of 8 girders, and the results would be difficult to compare. Therefore only the 2 lane bridge design is modeled using the PCI box girders.

Each state has a different specification for the composite deck slab. Also, there are differences in the type and extent of transverse post-tensioning. In order to keep the analyses consistent, the effects of transverse reinforcing are ignored unless otherwise

noted. Also, the bridges chosen assume a 5 inch composite top slab is used. Thus, the only difference between the PCI and TxDOT bridge models are the box sections themselves and the size of the shear key. Table 6 shows the PCI bridges analyzed for this study.

Table 6: Table of PCI Box Girder Bridges

Bridge Name	Span (ft)	Section Depth (in)	Overall Width (ft)	Shear Key	Composite Slab	Post-Tensioning	Full-Depth Key
2 Lane PB27 - 39	39	27	24	Yes	Yes	--	--
2 Lane PB27 - 59	59	27	24	Yes	Yes	--	--
2 Lane PB27 - S 59	59	27	24	--	Yes	--	--
2 Lane PB27 - SK 59	59	27	24	Yes	--	--	--
2 Lane PB27 - FD 59	59	27	24	--	--	--	Yes
2 Lane PB27 - PT 59	59	27	24	Yes	--	Yes	--
2 Lane PB27 - 79	79	27	24	Yes	Yes	--	--
2 Lane PB33 - 59	59	33	24	Yes	Yes	--	--
2 Lane PB33 - 79	79	33	24	Yes	Yes	--	--
2 Lane PB33 - 92	92	33	24	Yes	Yes	--	--
2 Lane PB33 - 104	104	33	24	Yes	Yes	--	--

NOTES:

1) 24 ft roadway composed of (6) - 4ft-0in wide box girders

SOLID MODEL DESCRIPTION

Introduction

The multibeam bridges in this study were analyzed using the commercial finite element program ANSYS (ANSYS 2005). The finite element method is used to get a detailed prediction of shear key stresses. These stresses are used as a predictor of shear key cracking. An earlier study (Huckelbridge 1997) also used finite element analyses to predict stresses in the shear key. The bridge models contained in the current work presented here are similar, but seek to build upon the earlier work.

The finite element method uses an idealized mathematical model that incorporates all of the important features of an actual structure. There are certain modeling concerns that must be addressed with the finite element method. First, the correct elements must be chosen. Second, the element sizes must be sufficiently small so that the high stresses are not averaged out. Third, material properties must reflect actual values. Fourth, the support conditions and loads must reflect reality. The focus of this section is on how the idealized bridge models meet these requirements.

Box Girder Description

The box section, shear key, and slab were modeled using three dimensional solid brick elements. There was a limit on the number of elements and nodes available for a single model for the software license, so this forced the use of a relatively coarse mesh in beams to allow enough detail to study the shear keys. A box girder cross section with its mesh is shown in Figure 9. The elements are about 6 inches in the longitudinal dimension, because if a smaller spacing is used then the bridge models exceeded the software license restrictions.

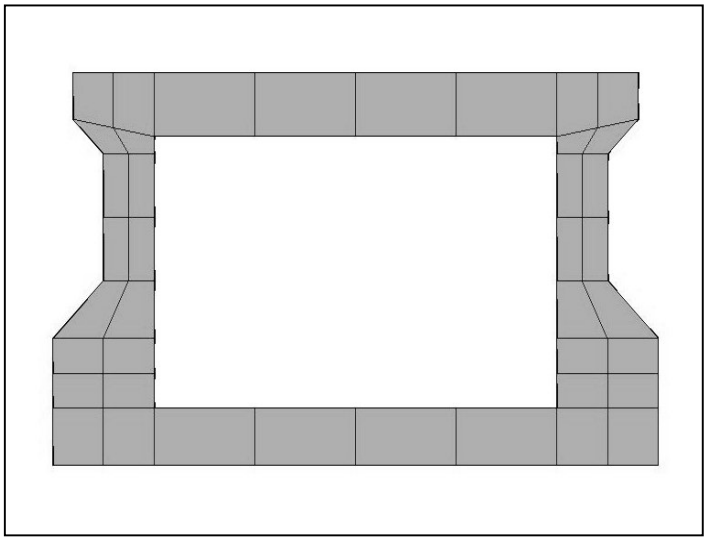

Figure 9: 5B34 Box Girder with Mesh

Shear Key and Slab Description

A composite deck slab used in some of the bridges studied. The slab was 5 inches thick and based on current TxDOT construction practice. The effect of adding an

asphalt riding surface was not considered. All parts of the bridge use solid 3D elements, and the nodes were rigidly connected to each other. The beams are all at the same elevation, and no cases with skewed supports are analyzed. A cross section of a PCI box girder shear key with mesh is shown in Figure 10. This figure also shows the nearby elements making up the rest of the box girder and the composite slab near the top.

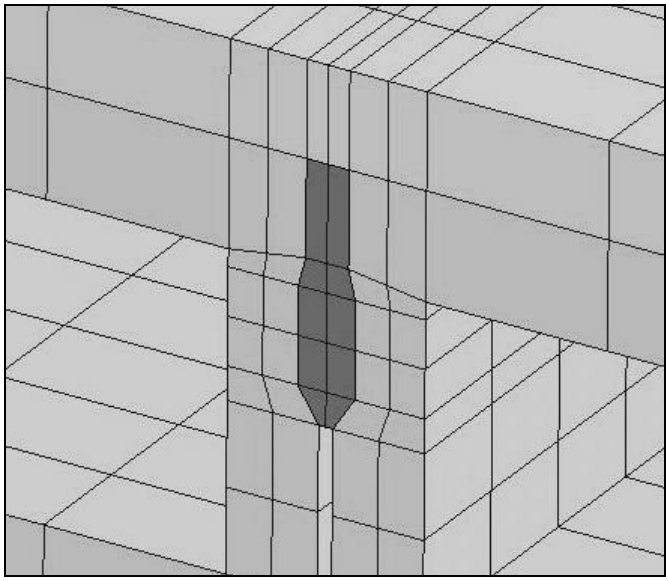

Figure 10: Shear Key Detail with Element Mesh

Material Properties

There were three material models used in the finite element analysis. All three were considered linear elastic isotropic materials. The modulus of elasticity for each material is based on the current ACI specifications (ACI 2002) for normal weight concrete, which is given by the relationship $E_c = 57{,}000\sqrt{f'c}$, and Poisson's ratio was

taken as 0.20. Thus, only the concrete compressive strength (psi) is needed to completely describe the material properties. The box girder concrete was assumed to have a compressive strength of 5500 psi. The composite deck slab, if present, was given a 4000 psi compressive strength, and the shear key was given a strength of 5000 psi.

Internal Diaphragms

As specified in the TxDOT standards, internal diaphragms are provided at the ends of each beam. These extend 1 ft into each end and serve to anchor reinforcing bars and limit deformations near the supports. These diaphragms are also included in the PCI/AASHTO box girders for consistency. If post-tensioning is used, then diaphragms are added at approximately 10 ft on center spacing in the exterior box girders, but none are added for interior box girders.

IDEALIZATION OF BEAM SUPPORTS

Introduction

The bridges examined in this study rest on elastomeric bearing pads. Earlier work (Jones 1999, and Yazdani 2000) suggests that appropriate representation of bearing pads is important and erroneous results can occur if box girder supports are treated as simple supports. This section explains how the beam supports were modeled and how the structural element properties were obtained.

Elastomeric Bearing Pads

Box Beam bridges usually rest on solid supports or bent caps with an elastomeric bearing pad to accommodate movement. The elastomeric bearing pad is typically very stiff in the vertical direction, but allows movement in the other two dimensions. This is done to accommodate the constant expansion and contraction of the box girders, while providing resistance against vertical deflection. A schematic of this behavior is shown in Figure 11.

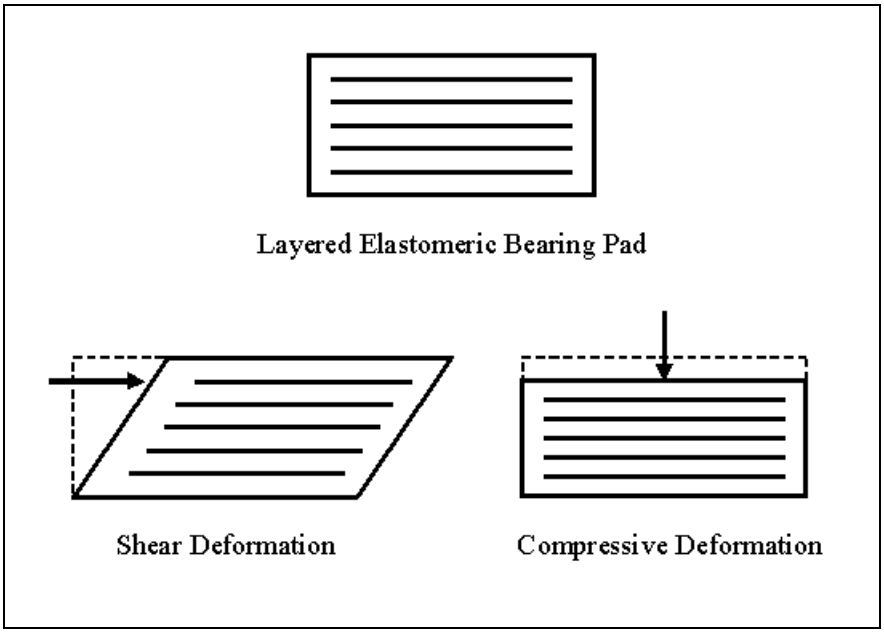

Figure 11: Bearing Pad Deformation and Behavior

In Texas, the box girder design specification states that a three point bearing setup must be used for new bridge construction. This is where a single large pad is placed under one end of the bridge and two smaller pads are located under the opposite edge. This is done to eliminate rocking if the pads have slightly different support elevations. In the models, all of the larger pads are on one side of the bridge and all the smaller double pads are on the other side of the bridge.

Linear Spring Models

In the model, these bearings are represented by linear spring elements connected to the bridge model at one node and are restrained at the other node. Because the bearing pads resist movement in three dimensions, each side of the bridge has two spring

sets with three spring elements each restrained in only one direction. A schematic showing the cross section view of the end of a beam with two pads is shown in Figure 12. In this view, the two horizontal springs are not shown for clarity.

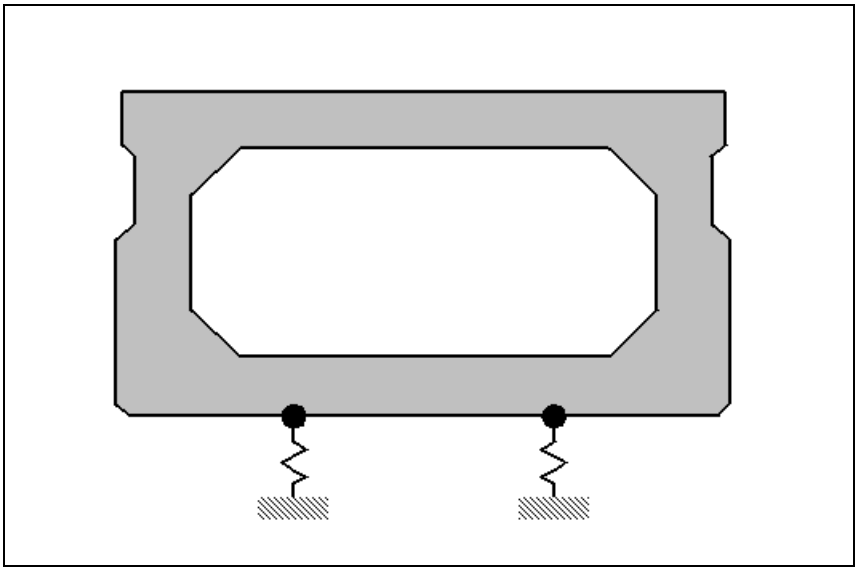

Figure 12: Bearing Pad Vertical Spring Supports

The springs are simple linear elements, known as LINK11 in the ANSYS element library (ANSYS 2005). This element will resist both compression and tension, but a real bearing pad can only resist compression. This means that a girder could potentially "lift-off" the bearing pad. In actuality, the pads are compressed under the dead load, so lift-off does not occur.

Linear Spring Stiffness

A value for stiffness, K (measured in lb/in), must be specified for each spring element. The stiffness values were based on Mechanics of Materials equations combined with recommendations from AASHTO (AASHTO 2004). The stiffness values were taken to be those of a new bearing pad, but it is known that the values may change as time and movement affect the pad, as previously discussed in the literature review (Yazdani et al. 2000).

The stiffness of an elastomeric bearing pad is based on the overall size and laminations used. A schematic of the bearing pad is shown in Figure 13, illustrating the parameters used for the stiffness equations.

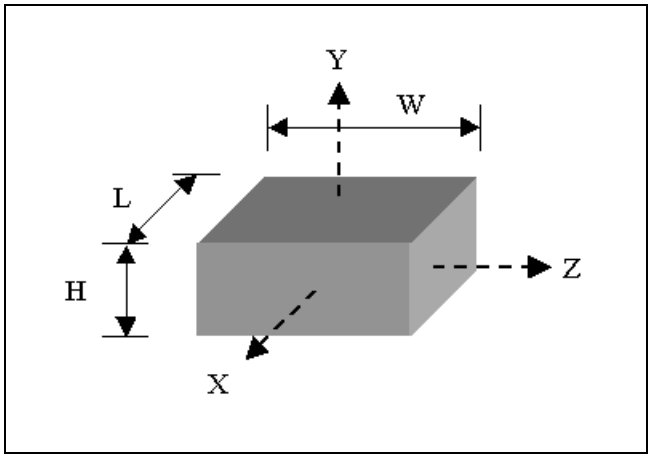

Figure 13: Bearing Pad Schematic

The first step in relating the spring stiffness to the bearing pad properties is to find a parameter 'S', which is the shape factor. This parameter takes into account the

steel laminations and elastomer to give an indication of how much each material contributes to the overall stiffness. The laminated steel sheets resist compression as well as bulging of the elastomer, while the elastomer permits movement in the two horizontal dimensions without much resistance. Once the shape factor is found, it is used in an equation along with the shear modulus, G, which gives an approximation of the compressive modulus of elasticity. The variable h_{ri} is the height of an individual lamination within the bearing pad.

The shape factor equation given in AASHTO is:

$$S = (L*W)/(2*h_{ri}*(L+W))$$

The compressive modulus of elasticity is:

$$E_c = 6*G*S^2$$

These equations are used to calculate the design compressive modulus for a given pad. After the bearing pad specifications have been found, the spring stiffness can be calculated using mechanics of materials. The following equations are used to find the spring constants:

Hookes law:

$$\sigma_x = E * \varepsilon_x$$

$$\tau_{xy} = G * \gamma_{xy}$$

average stress:

$$\sigma_x = P_x/A$$

$$\tau_{xy} = V_y/A$$

displacement:

$$\delta_x = \varepsilon_x * H$$

$$\delta_y = \tan(\gamma_{xy}) * H$$

spring constants:

$$k_x = P_x/\delta_x$$

$$k_y = P_y/\delta_y$$

An assumption is made that k_y and k_z are similar and that the orientation of the pad will not affect the horizontal stiffness greatly. To make the calculation of spring stiffnesses easier these equations can be condensed down to a single expression for each spring component (Yazdani, et al 2000), such that:

$$k_x = (E_c*A)/H$$

$$k_y = (G*A)/H$$

The shear modulus recommended by TxDOT is 100psi when taken at a standard 73 deg F. The size of the bearing pad used for a bridge is dependent upon the depth of the section used, but does not depend on the span length or other factors (assuming some standard conditions are met). In this study, similar pads are used for standard PCI sections for consistency. In reality, however, the use of four bearing pads rather than three is typical in many states. The state of New York even uses full-width bearing pads to prevent rotation at the ends of the beams (Lall 1997). A summary of the values used in this study is shown in Table 7 below.

Table 7: Bearing Pad Stiffnesses

Elastomeric Bearing Pad Information										
Beam Type	One-Pad Size (in)			Stiffness (lb/in)		Two-Pad Size (in)			Stiffness (lb/in)	
	W	L	T	Long.	Vert.	W	L	T	Long.	Vert.
B20	6	12	2 3/4	2618	1.01E+06	6	6	2 3/4	1309	2.83E+05
B28	6	14	2 3/4	3055	1.29E+06	6	7	2 3/4	1527	3.83E+05
B34	6	16	2 3/4	3491	1.60E+06	6	8	2 3/4	1745	4.92E+05

The table shows the sizes of the pads and the corresponding computed spring stiffnesses for the linear elements. The stiffness for the single-pad side of the beam is more than twice as stiff as the double-pad side stiffness, even though the gross area of the pads is the same for both sides. This is a consequence of the shape factor equation, which is non-linear. For the bearing pads used in this study, the stiffness of the vertical springs will be about twenty times greater than the stiffness of the two horizontal springs.

Elastomeric bearing supports have important consequences for box girder bridges. The horizontal springs alter the bending stiffness of the box girders, and can act as a partial restraint for end rotations. The vertical springs allow the box girders to deflect at the supports, spreading out the load to adjacent box girders. These effects are necessary to incorporate into the bridge models or else the stresses will not represent actual conditions.

LOADS APPLIED

In the actual bridges, dead load is carried by the box girders because the shear keys and composite slab are cast after erection. Live loads are resisted by the entire composite section including the shear keys and composite slabs. The live loads considered include HS-25 truck loading (AASHTO 2004), initial shrinkage loads, and thermal gradient loads. Previous work (Huckelbridge et al. 1995, and Miller et al. 1998) has indicated shrinkage and temperature effects can produce larger stresses than vehicular loads, and so they must be included in the analysis.

HS-25 Truck Loading

The vehicular loads applied to the bridge model are those recommended by the AASHTO HS-25 design loading. This loading pattern represents a heavy tractor-trailer and has three axles, each with two wheels acting on the top surface of the structure. The bridge is divided into a number of lanes depending on the width of the bridge, and there can only be a single truck in one lane at a time. In this study, multiple presence factors have not been considered, nor have live load factors.

The AASHTO specification states that the truck loads should be placed where they cause the largest stresses to the section of bridge under consideration. This location was found by varying the position of the truck along the span and across the width of each lane and checking the stress of the shear key and composite slab. The worst locations for most bridges were either at the very end of the bridge near the supports or at midspan. All locations had higher stresses when short wheelbases with 14’ spacing

were used for each axle. Schematics of sample truck locations on a two lane bridge are shown in Figure 14 and Figure 15.

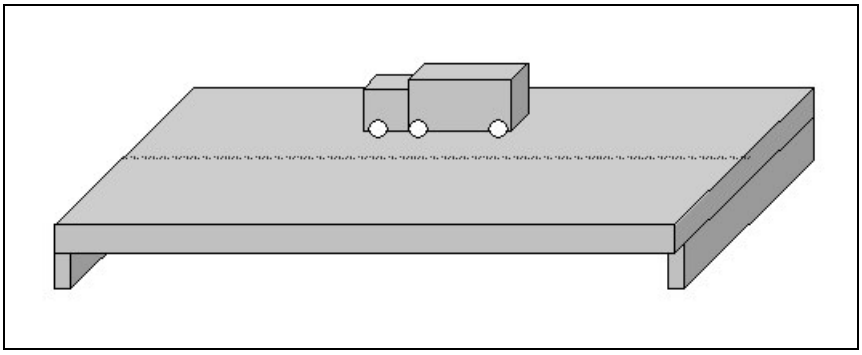

Figure 14: Truck at Midspan Location

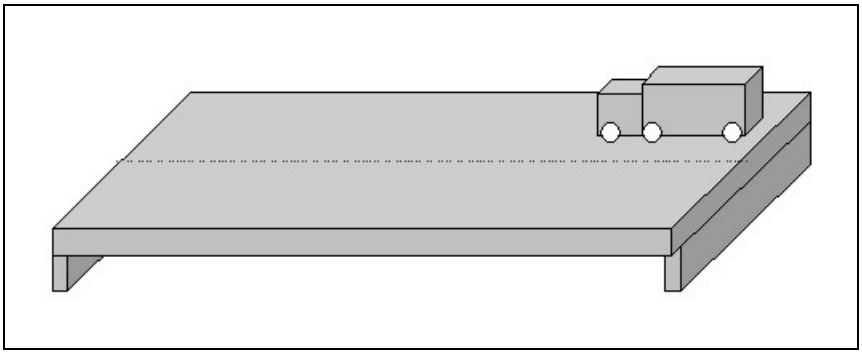

Figure 15: Truck at End of Span Location

The wheel locations for a two lane bridge are shown in Figure 16. The locations available for a three lane bridge are shown in Figure 17 and Figure 18. The wheel loads were applied as vertical concentrated forces at nodes. These loads are applied on the top

surface of the bridge and located at the nearest nodal location corresponding to a truck wheel.

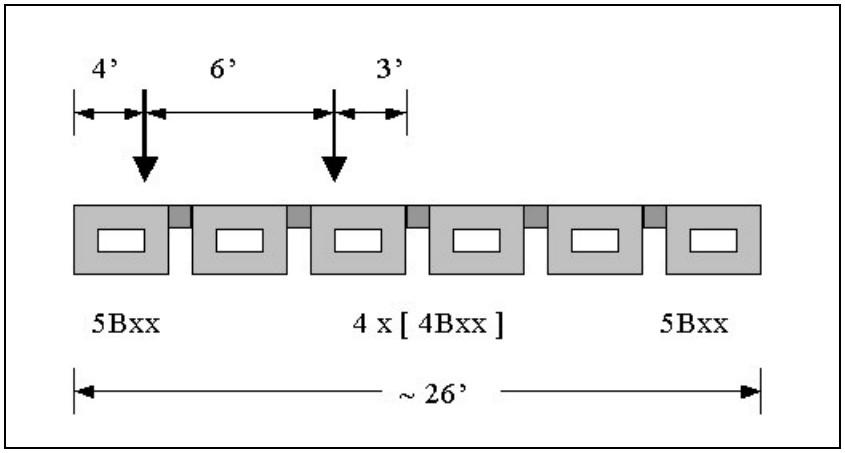

Figure 16: Truck Axle Location on 2-Lane Bridge

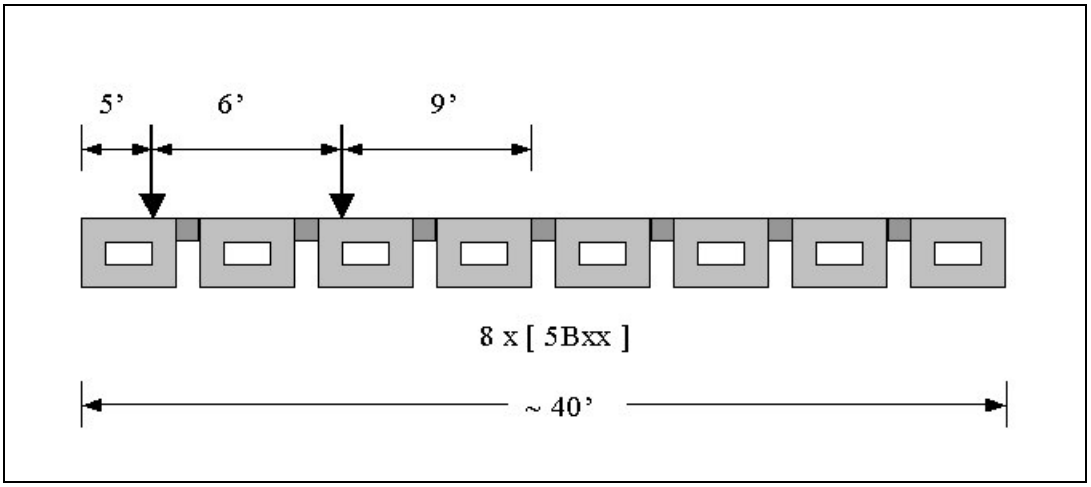

Figure 17: Truck Axle Location on 3-Lane Bridge, Lane 1

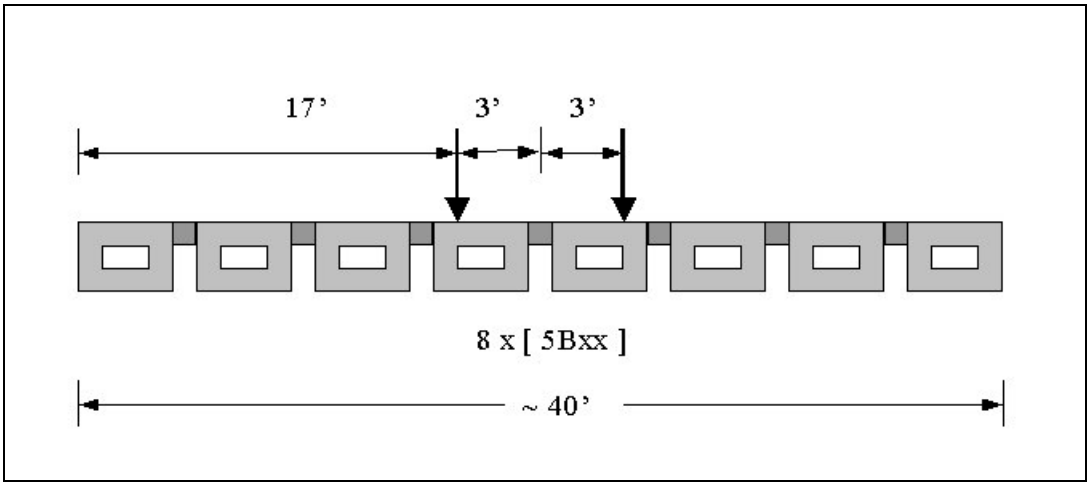

Figure 18: Truck Axle Location for 3-Lane Bridge, Lane 2

The location of the wheel loads was based upon the AASHTO guide concerning the application of truck loads inside a lane. The truck axles were moved from side to side and along the length of the bridge, in order to find the location where they caused the highest stresses. The highest tensile stresses were found when the axle was near a shear key, but not directly on top of it. Thus, the trucks axles were placed in their proper lane with at least one of the axles near the edge of a shear key.

As noted above, the wheel loads are applied as a single concentrated load rather than a pressure over a given area as AASHTO recommends. This is justified by using St. Venant's principle of statically equivalent systems. This principle states that the differences in stress between a load applied over a small area and a concentrated load will only be significant within a small distance from this area. This will be dealt with in more detail in the Solid Model Verification section.

Initial Shrinkage Loads

The second loading type was the stress induced by shrinkage. This load is applied to the elements that might be expected to experience any type of shrinkage after casting. Shrinkage is due to a number of factors including temperature changes during curing, loss of water, and general chemistry reactions within the slab. Grouted keyways are often created with non-shrink grout material. Non-shrink grout must conform to the specifications set by ASTM (ASTM 1993). This requires that the grout not lose any volume over a certain time period. This is usually achieved with the use of proprietary grout mixes with special additives.

Concrete members can be subjected to residual stresses if shrinkage effects are not addressed. This is particularly damaging in unreinforced concrete because there is no steel to prevent failure or redistribute stresses. Restrained shrinkage can impose large tensile stresses, and a schematic of this effect in a uniaxial specimen is shown in Figure 19. The effect in a shear key would be similar, but shrinkage would take place in all three dimensions.

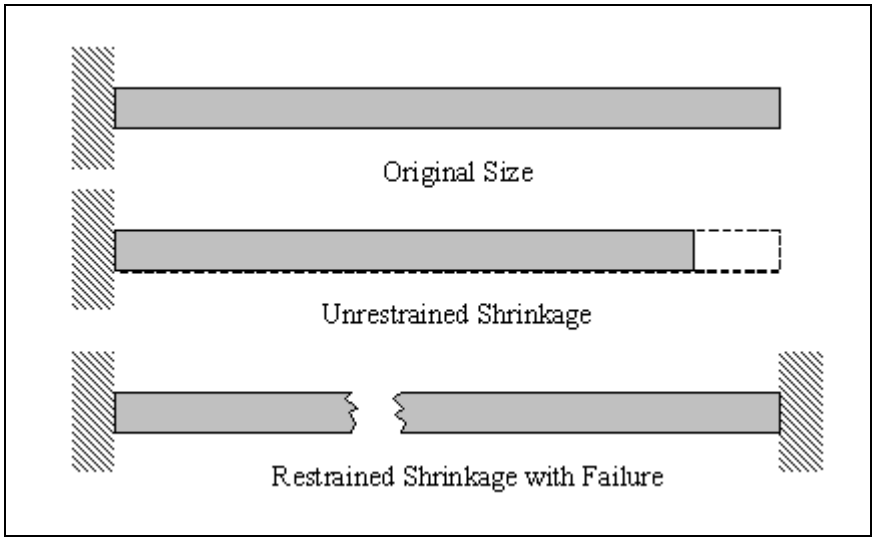

Figure 19: Schematic of Shrinkage Effects

In one of the studies referenced in the literature review (Issa et al. 2003), shrinkage measurements were taken for a variety of materials commonly used in keyways, including non-shrink grout. The total shrinkage measured at 28 days after casting was close to 900 microstrain, which is much higher than allowed by ASTM for this material. The authors pointed out that they used a greater amount of water than they expected in order to get the material to flow at the right consistency. The specimens followed the ASTM C 157 specifications, and were prisms of 1 in. x 1 in. x 11 ¼ in. The specimens were demolded six hours after casting and placed in lime-saturated water for 15 minutes.

The simple shrinkage specimens are placed in very specific laboratory conditions, and so the overall shrinkage measured will probably be different than the shrinkage experienced by a shear key in-situ. It is believed that shrinkage strains of 900 microstrain, as seen in the simple shrinkage specimens, are unrealistic in actual shear

keys because of the high volume to surface ratio present. In comparison to non-shrink grout, typical shrinkage strains of unreinforced concrete members is between 400-700 microstrain, and so the shrinkage reported in the study referenced above seems high. Therefore, 500 microstrain is the value of shrinkage strain used for the shear keys in this study, as this is between the reported shrinkage values of 900 microstrain and zero microstrain as reported in the literature review section.

A composite slab will also experience shrinkage, but the reinforcing steel will limit the ultimate shrinkage values. A typical slab is reinforced with steel in two directions, and the reinforcement is usually designed to limit the amount of shrinkage that can take place. For reinforced members, a shrinkage strain of 200 microstrain will be used for the composite slab based on previous research (Leet and Bernal 1995).

The box girders will not impose any shrinkage load on the shear keys because it is assumed that the girders will have reached ultimate shrinkage before the bridge is constructed. Therefore, the shrinkage load is only applied to the shear keys and top slab.

Although no method is provided in ANSYS to apply shrinkage directly on the model, the effect can be represented with a body force temperature applied that corresponds to the correct strain value. Using the value of the coefficient of thermal expansion, the shrinkage strain to temperature conversion is found using the equation:

$$\text{Temp} * C_{\text{thermal expansion}} = \varepsilon_{sh}$$

So, using a thermal expansion coefficient of 5.5E-6 $^{in}/_{in}$/deg F and 500 microstrain shrinkage value, a temperature of –91 deg F is applied to the shear key elements. When a composite slab is present on the top of the bridge deck, the shrinkage strain of 200

microstrain is applied as temperature loads to the slab elements. The temperature applied is –36 deg F. The values of shrinkage and their converted temperatures are reported in Table 8 below.

Table 8: Shrinkage loads applied to bridge

Category	Shrinkage (in/in)	α (in/in/deg F)	Temp (deg F)
Prestressed Box Beam	0	5.5E-06	0
Unreinforced Shear Key	-0.0005	5.5E-06	-91
Reinforced Concrete Slab	-0.0002	5.5E-06	-36

In reality, shrinkage will vary within the structural members. The top surface will dry faster than the interior surfaces and each part of the shear key will experience shrinkage at a different rate. However, it is assumed in this study that the shrinkage will be uniform through the depth of the concrete member and that the shrinkage values will reach the ultimate value at the same time.

Thermal Gradient Load

A thermal gradient load was applied based on that recommended by AASHTO specifications (AASHTO 2004). There are two cases, a positive thermal profile and a negative thermal profile. For the positive loading case, the nodes on the top surface have the highest temperature, and the temperature profile decreases through the depth of the bridge cross section. The temperatures are relative to ambient temperature, so a value of zero deg Fahrenheit indicates no difference from ambient temperature. A graph showing this temperature profile is shown in Figure 20.

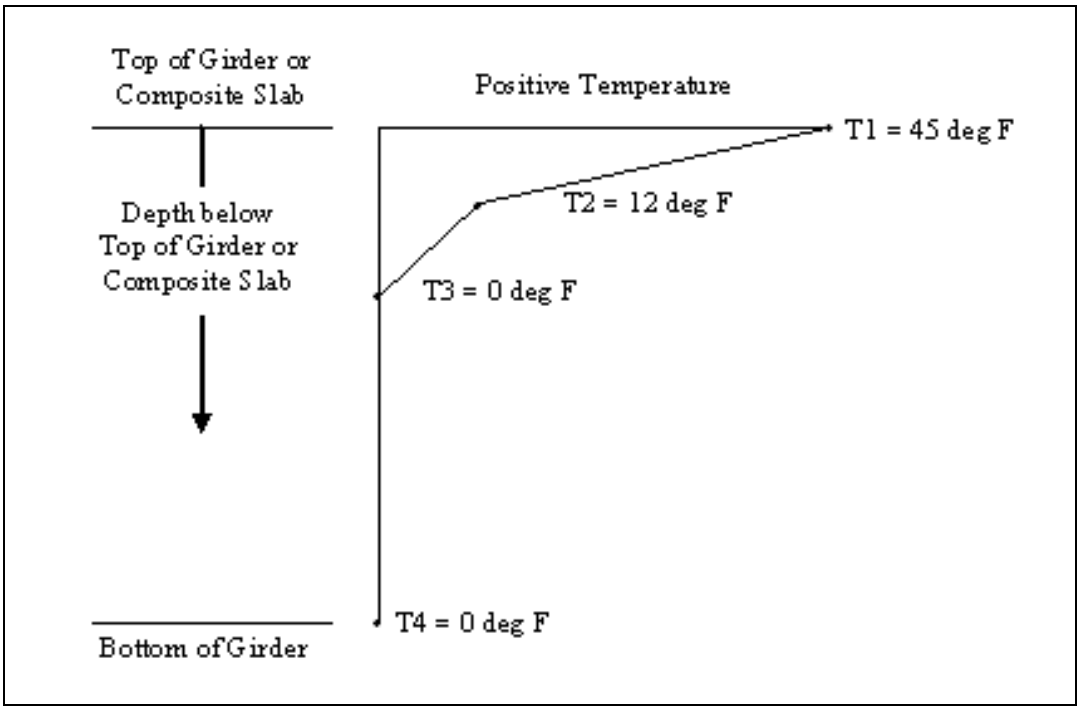

Figure 20: Positive Temperature Profile for Thermal Gradient Load

The temperature loads change according to the depth of the node below the top surface, representing the effect that solar radiation has on the bridge during a sunny day. The AASHTO provisions are based on a bridge where the bottom surface is cool, whereas the top surface is being heated by the sun. This creates a thermal expansion and can result in significant stresses built up in the bridge.

The reverse of this loading scenario is also considered where the interior and bottom of the bridge have warmed to the high daytime temperatures, but the top surface is now losing heat to the cooler atmosphere at night. This is specified by AASHTO to

have the similar profile as the positive case, but with negative temperatures applied to the bridge models, as shown in Figure 21.

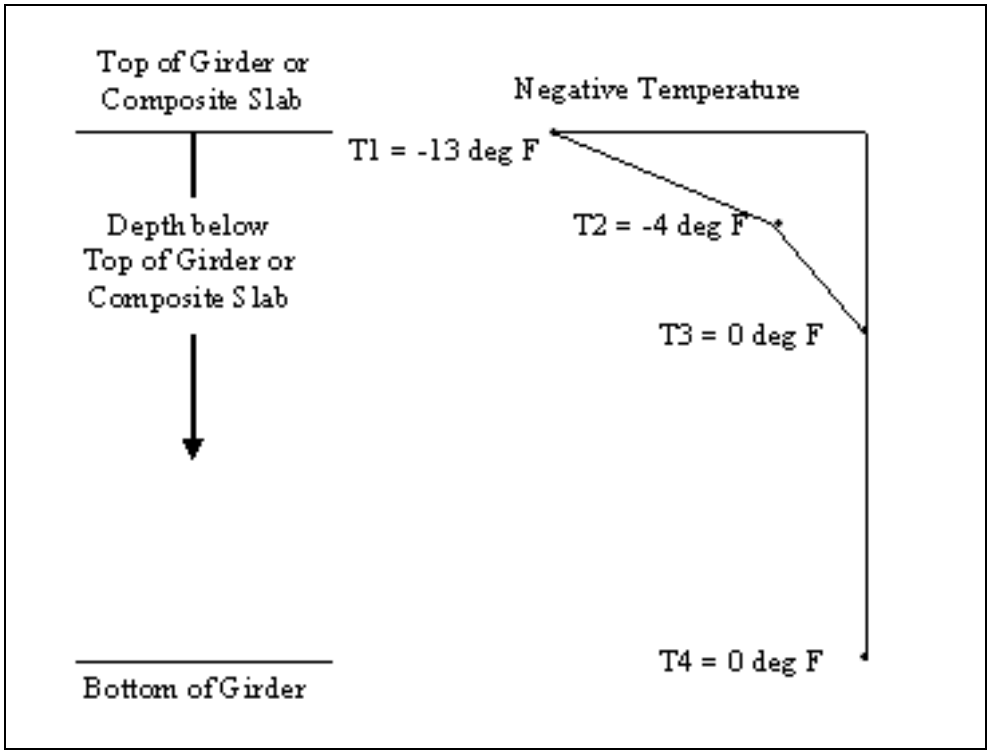

Figure 21: Negative Temperature Profile for Thermal Gradient Load

In the bridge models, the thermal loads are applied as nodal temperatures relative to ambient levels. The thermal gradients will produce bending in the box girders, but the transverse effects of thermal loads are not well known. As mentioned above and in the literature review, the reports from studies in Ohio (Hucklebridge et al. 1995, and Miller et al. 1998) suggested that thermal loads were the prime reason that shear keys were failing in the field.

ANALYSIS PROCEDURE

The program chosen for the structural analysis of the bridges was ANSYS Version 9.0 running on the UNIX based supercomputers hosted by Texas A&M. This program is a general finite element package, specializing in engineering simulations and stress analysis. The license held by the Texas A&M University computing center is one for research applications and is limited to 128,000 nodes, which imposed some constraints on modeling efforts.

Input files were written using the native ANSYS language, APDL, to facilitate generation of bridge models with similar geometry and loading conditions. Program output consisted of stresses, strains, and displacements at each nodal point. The ANSYS graphical user interface was used to produce many of the plots in this thesis.

Description of Program Output

The results of interest in this study are the normal and shear stresses in the shear key and composite slab. It is known that cracking of the shear key occurs along a vertical plane, so the stresses that are responsible for this are likely to act perpendicular to this plane. So to find this information, a computer routine was written to report the stresses though the depth of each shear key, from the top of the composite slab to the bottom of the keyway. A profile was then built along a vertical line at the center of the shear key as shown in Figure 22.

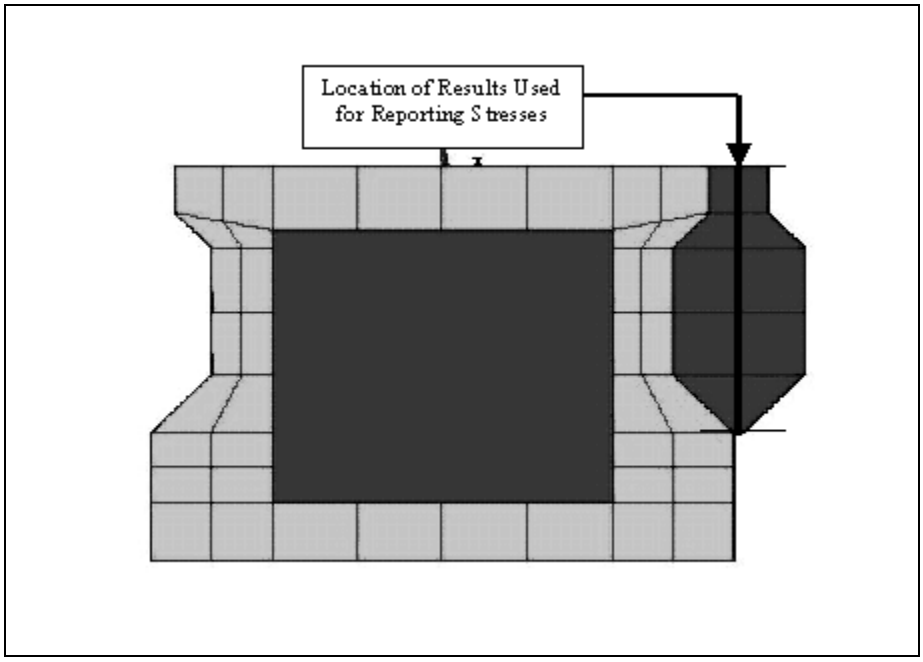

Figure 22: Girder and Shear Key Cross Section

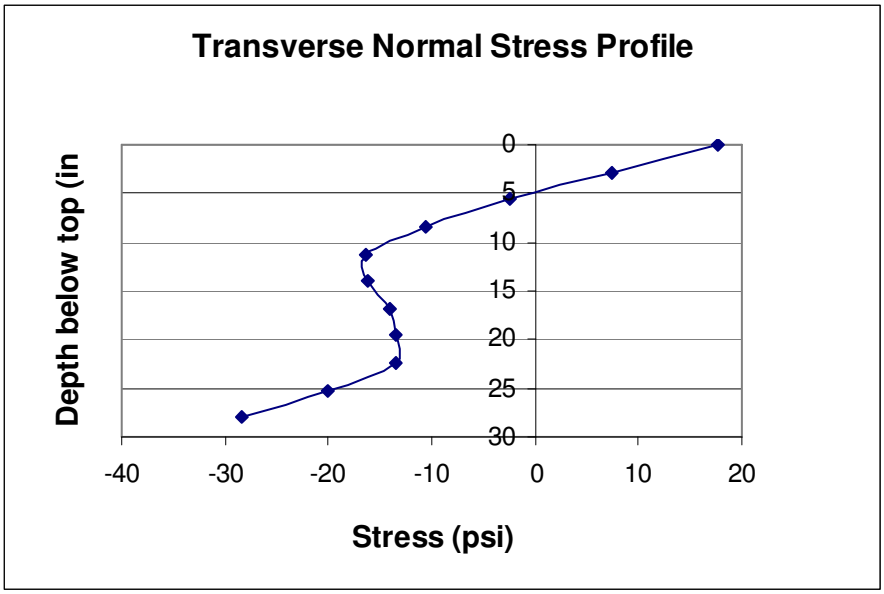

Figure 23: Transverse Normal Stress Profile

The resulting stress profile, showing transverse normal stress from the top surface to the bottom of the keyway is shown in Figure 23. This represents the stress at a single location on the bridge, and was taken from a bridge model with a concentrated load. The stresses represent the transverse normal stress at different depths along the vertical line of the cross section. The centerline of the shear key was chosen to represent data for the entire shear key. Transverse normal stresses in the middle of the shear key and those existing on the either side at the beam-shear key interfaces were essentially the same in every case.

The most important quantity in the stress profile is the maximum tensile stress as this will govern initiation of a crack. Consequently, this value was tabulated for each stress profile given by ANSYS and compared amongst all the bridges.

Failure Criteria

Shear keys typically fail in two different ways. The first is a fracture or cracking in the shear key. The second is debonding of the key material from the precast box girder. Both problems can be considered as cracks, and both allow water and chlorides to leak into the joint. This study considers both debonding and cracking as a shear key failure, as both are detrimental to the performance of the shear key and may result in reflective cracking.

Failure by Debonding

Debonding failure is a result of a poor bond between the shear key and precast box girder. The theoretical strength of the bond is that of the base material itself, but the bond strengths reported in the previous research usually did not achieve a bond that was this strong. In fact, the range of stresses in tensile failures for non-shrink grout reported in the literature varied between 75 – 224 psi. When other loading situations were considered (other than pure tension), the bond strengths reported were between 62 – 620 psi. The criterion for failure by debonding will be defined as a tensile stress exceeding 300 psi at the bond surface, as this is typical of the values reported in the literature.

Failure by Cracking

A cracking failure occurs when the concrete material separates due to tensile stresses. The ACI recommends that tension in unreinforced concrete is limited to a value of $6 \cdot \sqrt{f'c}$ for normal weight concrete. At the assumed compressive strength of $f'c = 5000$ psi used in this study, the failure stress is 424 psi.

Cracking failures have more serious consequences than debonding failures because the crack can happen on a vertical plane allow slip, reducing load transfer between girders. The loss of load transfer in the shear key depends on the location and extent of fracture, but previous studies (detailed in the literature review) show that the shear key can experience severe damage and cease performing its function in certain cases.

Shear keys usually will lose their bond with the adjacent girders before an internal fracture occurs, but some tests have indicated that fractures do occur if bond strength is sufficiently high. When the shear keys are cast from epoxy or polymer concrete debonding is unlikely and cracking would occur in the box girder if large transverse stresses are present.

SOLID MODEL VERIFICATION

Three different tests were performed in order to verify the finite element model. The goal of the verification tests was to confirm the element types and mesh used for the analysis were accurate. The first test measured beam bending behavior of bridge models and compared them to the results given by ordinary 2D beam theory. The second test compared transverse stresses for box girder bridge models built with different element types. The last test used a model with a very refined mesh to check convergence of the results.

Beam Bending

In this test, a single simply supported beam is subjected to a load at midspan. Two finite element models are created, one using BEAM189 elements and the other using SOLID45 elements. The results are also compared with a simple beam bending solution.

The purpose of modeling the beam in different ways is to find out if the finite element model agrees with expected results. Since the solution for a simply supported beam is well known, it is a good test of model behavior. Typically, 3-D solid elements are stiffer and require a fine mesh to correctly model bending behavior, so it is important to confirm that the model has an adequate mesh density.

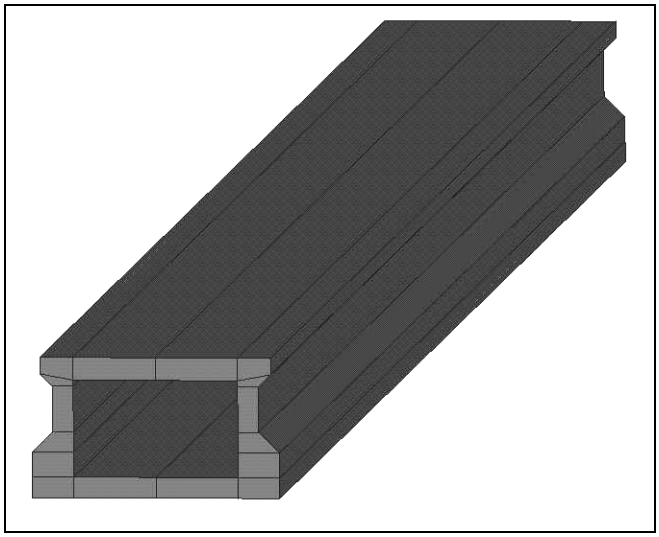

Figure 24: Beam Bending Test Bridge

The results discussed here are for a single 59 ft long Texas 4B34 box girder that has no composite slab, simple supports at both ends, and is made of material that has an elastic modulus of 4 million psi and a Poisson Ratio of 0.20. A view of the beam geometry used for this test is shown in Figure 24. Two load cases were considered, a distributed load and a concentrated load. The distributed load is from the concrete self-weight of 150 lb/ft^3 and the concentrated load is a 20,000 lbs load at midspan (distributed evenly across the width).

Table 9: Beam Verification Results

1 x 4B34 Beam Simply Supported				
Load Case	Results	Beam Eqns	Beam189	Solid45
Dead Load	Top Stress (psi)	-678	-673	-672
	Bottom Stress (psi)	603	603	603
	Deflection (in)	0.492	0.498	0.502
Point Load	Top Stress (psi)	-551	-543	-550
	Bottom Stress (psi)	490	487	490
	Deflection (in)	0.32	0.326	0.327

The results shown in Table 9 indicate that stresses and deflections were virtually the same for all cases. Overall, the results indicate that the beam is correctly modeled, because the stresses agree very closely with analytical solutions for both distributed loads and concentrated loads. The model built with solid 3D (SOLID45) elements used the same mesh density as the other bridges in this study. When the mesh was varied for the solid element models the results were similar to those shown in the table above.

Transverse Bending

A total of 6 finite element models were built to confirm transverse behavior. The purpose of using several different element types was to confirm that the elements chosen for the study gave reliable and accurate results. All the models were simply supported, with two Texas 4B34 box girders connected with a 5 inch composite slab, similar to that discussed for the beam bending section. The loading chosen for this bridge is a 20,000

lbs point load at the midspan location directly above the centroid of the left beam. A cross section of the test bridge is shown in Figure 25.

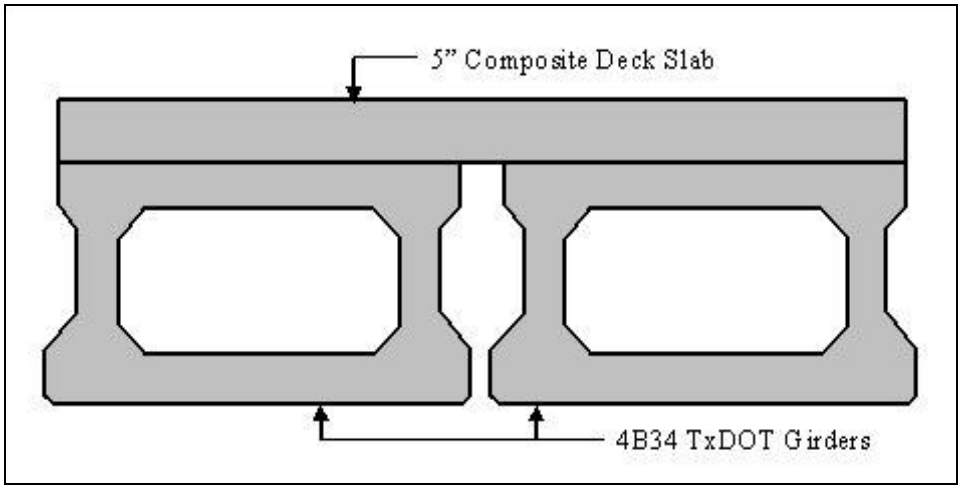

Figure 25: Transverse Bending Test Bridge

The first model used exclusively shell elements (ANSYS SHELL181) for the slab, girder webs, and girder top and bottom flanges. A screenshot of this bridge is shown in Figure 26 with offset nodal locations to best match the girder geometry. A review of the figure below shows the limitations of this element type for modeling complex geometries. The large gaps and overlapping elements resulted from trying to match the geometry of the box girders with the modeling requirements of the shell elements. The shell elements were not appropriate element types for use in this study, but they were included in this verification test for the sake of comparison.

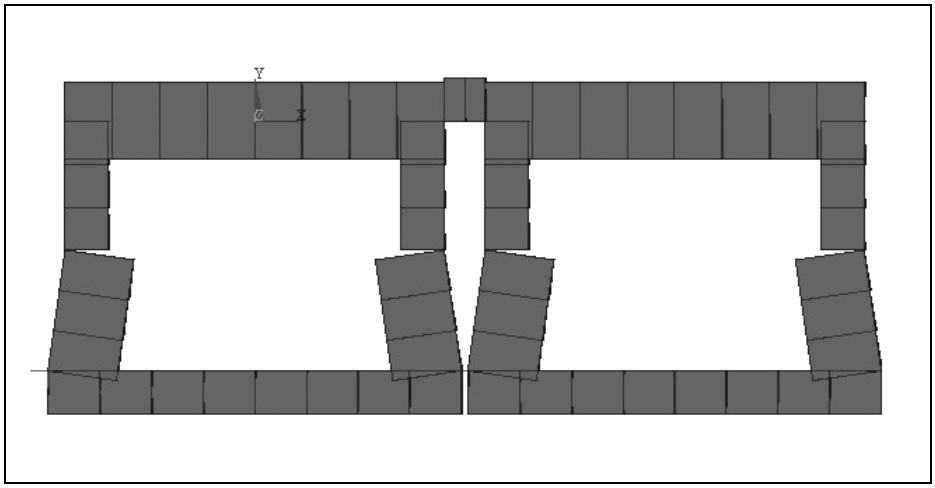

Figure 26: Transverse Bending Shell Model

Solid element types were used to create the remainder of the test models. Solid elements can be used to build finite element models of any geometry, but they use a larger amount of computing resources. The other problems with solid elements are that they are too stiff in bending situations and the shape of each element needs to be similar to a cube for best results (ANSYS 2005). The second bridge model used solid (ANSYS SOLID45) elements for the bridge throughout the model. The third model used Solid45 elements but with a mesh twice as dense in every dimension as the previous bridge model. Figure 27 shows a cross section of a bridge model with solid elements.

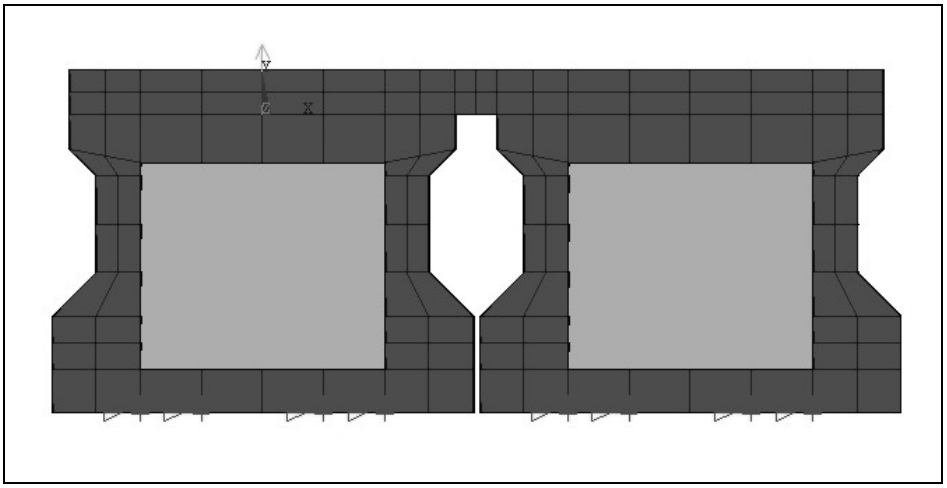

Figure 27: Transverse Bending Solid Model

The fourth model used an element supported by ANSYS called SOLSH190, which features shell behavior but uses 3-D solid topology (SOLid-SHell). The user must specify an out-of-plane orientation in addition to the nodal coordinates. This element was chosen because it is useful for structures that are governed by bending but need to interface with regular solid elements.

The last two bridge models used a combination of elements already described. The fifth model had SOLSH elements for the composite slab, but used Solid45 elements for the box girder. The sixth model used Solid45 element for the box girder but shell elements for the composite slab. Once again, the purpose of these tests was to find out whether Solid45 elements yield accurate results for transverse stresses.

Transverse moments were compared for the sake of convenience. For bridge models with solid elements in the slab, the transverse moment was calculated using the

stress values given at each nodal location and a moment of inertia based on slab thickness.

Figure 28 shows the transverse moments in the shear key from one end of the bridge model to the other. This is the transverse moment resulting from the application of the 20,000 lb point load applied above the centroid of one of the beams as discussed earlier. This data does not show the results for the bridge model built entirely from shell elements, which will be discussed later.

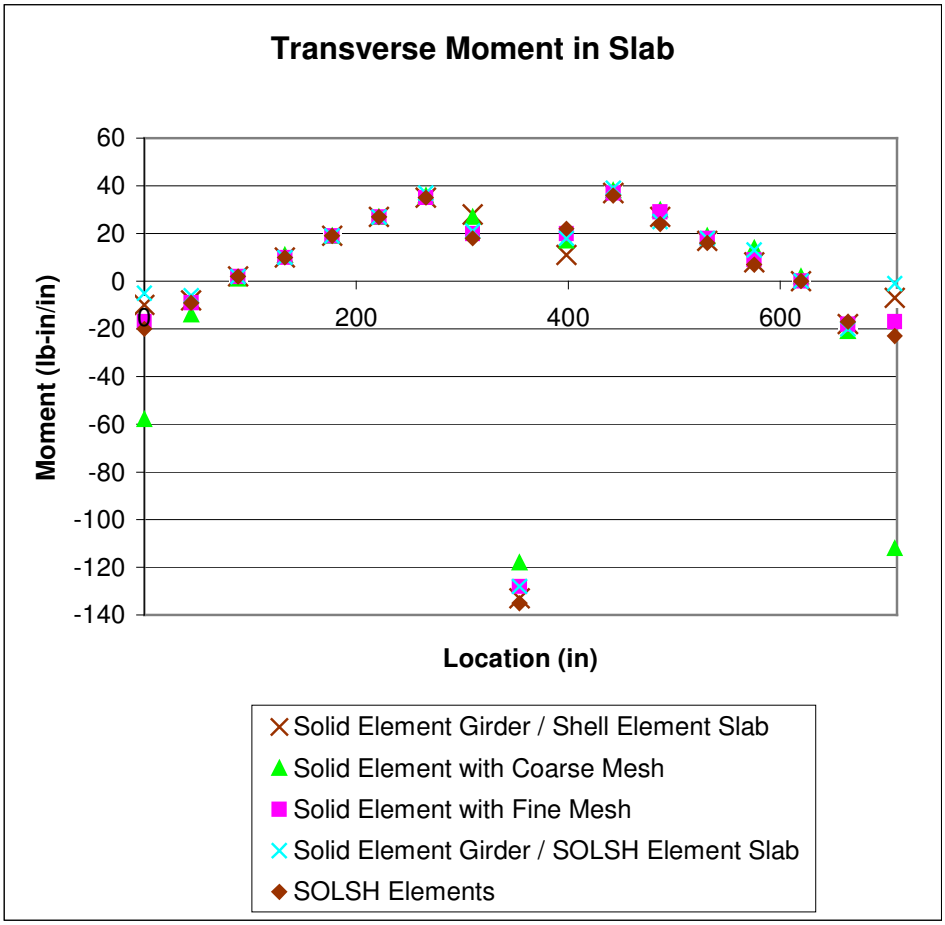

Figure 28: Results for Transverse Bending Bridge Models

The graph indicates that all bridge models behave similarly, regardless of element type or mesh fineness. This means that the bridge can be modeled using Solid45 elements with the proposed mesh without losing accuracy in the results.

One item to note is the moment near the ends for the Solid Model with Coarse Mesh versus all the other bridges. This was the only model without end diaphragms in the box girder. When end diaphragms were present, the transverse moment was lower because the girder did not experience as much deformation near the support locations and so less rotation was imposed on the slab. Thus, the presence of internal diaphragms was an important factor in the behavior of the bridges and was included in every model as discussed in the section regarding Solid Model Description.

Figure 29 shows the differences in transverse moment between the bridge model built only with shell elements and the model built only with solid elements. In this case, the shell model showed much higher moments than the solid model. As noted in the discussion on the shell element model, that element type was not appropriate for use in a box girder bridge with shear keys. The results shown in the graph indicate that the box girder bridge models with shell elements are more flexible than those with solid elements, even the SOLSH elements that use shell behavior. Therefore, a box girder bridge should be modeled with solid elements for accurate results.

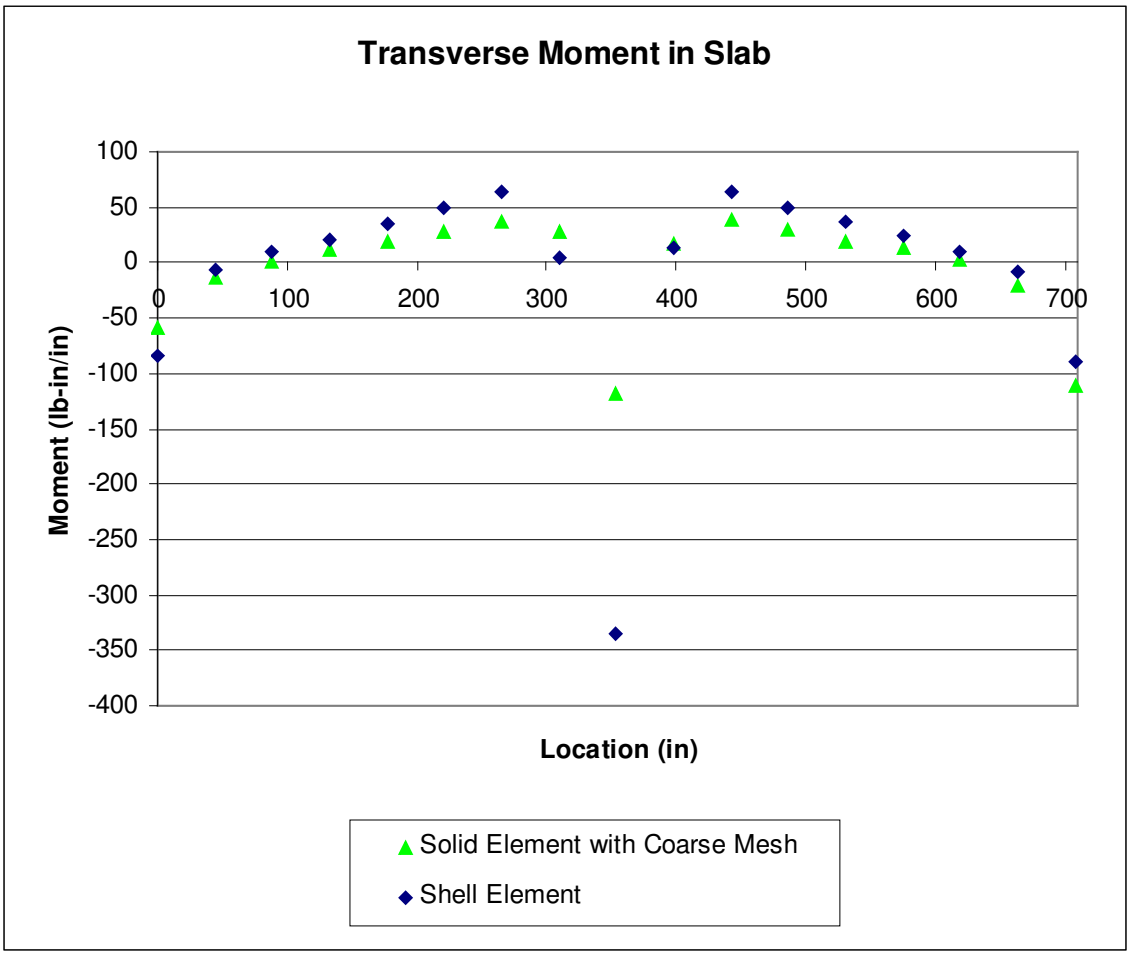

Figure 29: Shell Model vs. Solid Model Results

Submodel Analysis

The last verification test used a process called submodelling. In this technique, a small portion of the model is recreated with a higher mesh density in the areas of importance. A submodel can give more detailed results and is useful when a limit on the number of nodes prevents a small mesh size from being used. In this test, a submodel was built to verify that the mesh size chosen would give accurate answers.

The theory of submodeling is that a coarse mesh will give accurate results with regard to displacements, but the stresses (which are based on derivatives of displacement) may be inaccurate. If the stress varies greatly within a small region of the model, the solid elements will only be able to capture an approximation of that stress. Therefore, a fine mesh is desired in regions where stress varies greatly. However, a fine mesh was not an option due to limited computer resources. Submodeling allows a model to have a coarse mesh in a global model and a very fine mesh in regions where the stress results are important.

The process of submodeling superimposes the displacements from a large "global" model upon a smaller "submodel." In ANSYS, the user can specify the "cut boundaries," or the locations where the submodel will be sliced out of the larger model. The smaller submodel is then recreated in the same three dimensional space as the original model and the global model displacement field is applied to the submodel boundary. Because the submodel incorporates the effects of the global structure but has a significantly higher number of elements in the shear key, the profile of stresses through the depth of the joint should be more accurate.

A submodel with elastic springs used to simulate the effects of the global structure was used in the article "Evaluation of Improved Shear Key Designs for Multi-Beam Box Girder Bridges" (Hucklebridge and El-Esnawi 1997). The type of submodel used for the present study is somewhat different than that approach. The results for each individual loading situation are applied as constraints on a smaller model. The submodel

with imposed displacements on the boundaries is the most accurate type of submodel and is the best way to model the effects of temperature and shrinkage.

The bridge under consideration is a PCI box girder bridge with (6) – 4 ft wide, 27" deep girders, and a span of 59 feet. A standard PCI shear key and a 5" composite top slab is used, and no internal diaphragms or transverse post-tensioning is present. A 10 ft slice of the larger bridge near midspan is taken from one side of the bridge to investigate. A screenshot from the global model is shown in Figure 30. This model shows the general configuration of the bridge, and the region chosen for the submodel is highlighted.

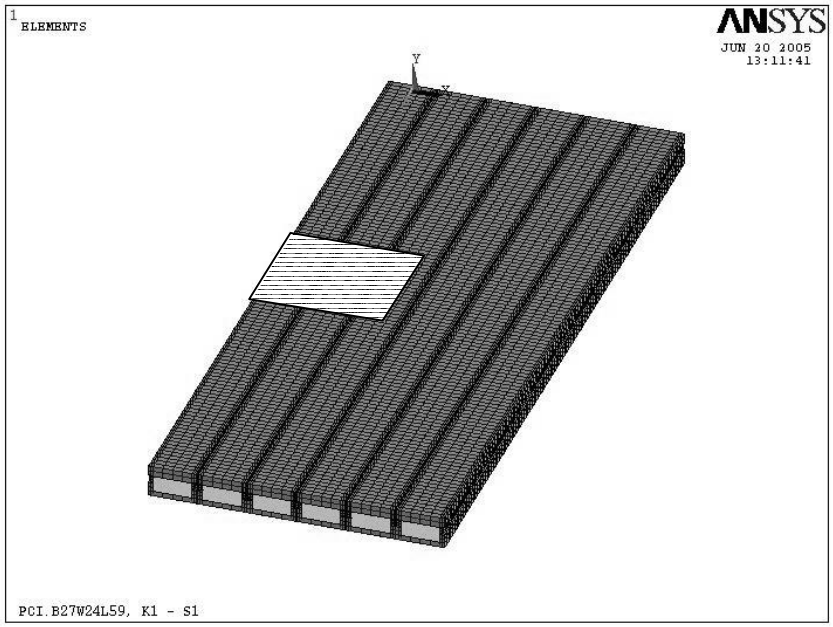

Figure 30: Global Model and Highlighted Submodel Region

The mesh size used for the global model is shown in a closer view of the model in Figure 31. The element size shown is similar to that used for all the other bridge models in this study. The mesh size is generally about 4" - 6" per side, but some elements have sides up to 10" when they are away from the shear key region.

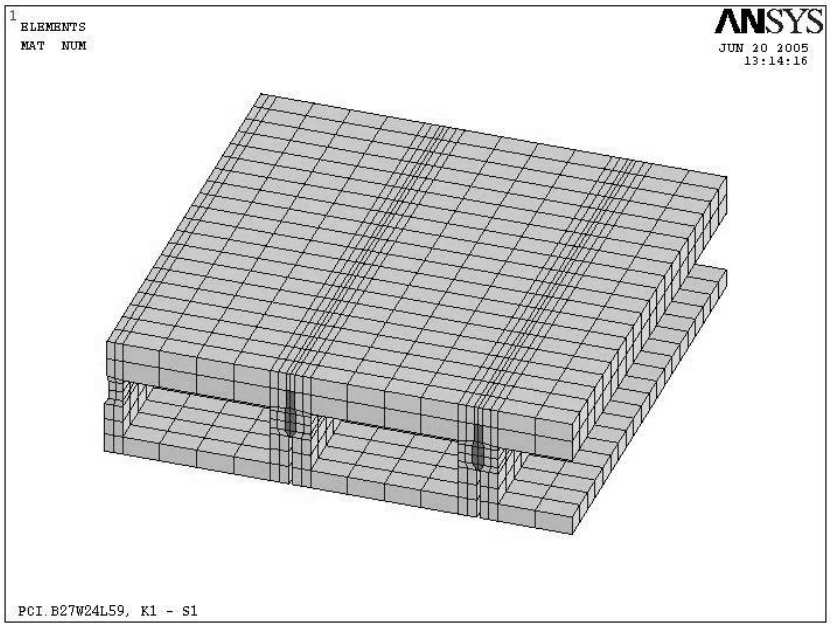

Figure 31: Global Model Mesh

The submodel is shown in Figure 32, where the elements are about 2 inches on each side. A close-up of the shear key region is shown in Figure 33. The results from the global model analysis are superimposed on the boundary of the submodel and the loads are applied to the submodel in the same manner as on the global model.

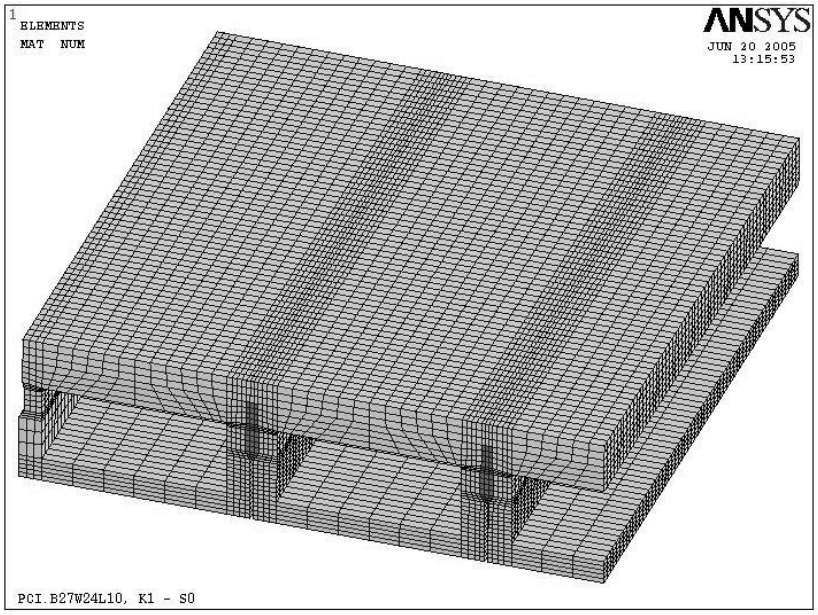

Figure 32: Submodel Mesh

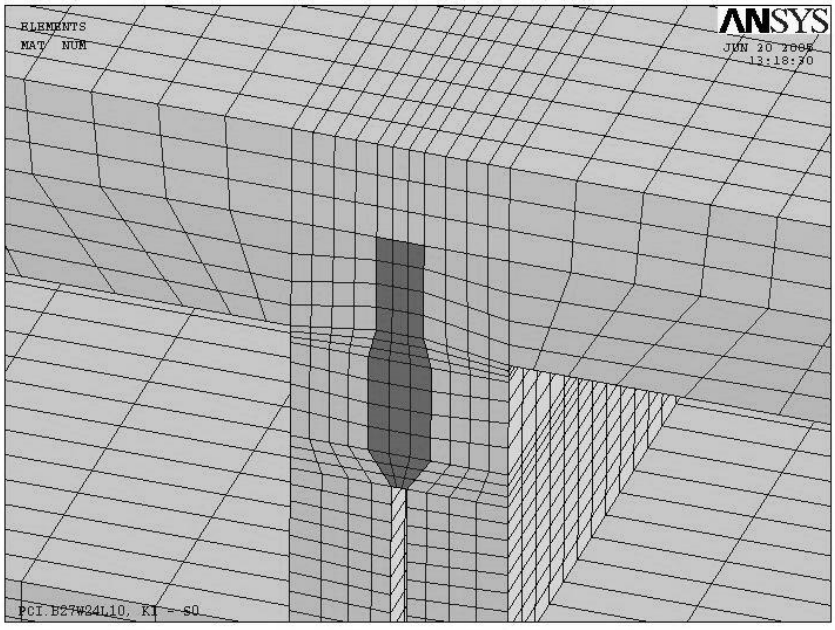

Figure 33: Closer View of Submodel Shear Key

The screenshot in Figure 34 shows the displacement field from the global model applied as constraints to the "cut boundary". The cut boundary is any part of the submodel that is not a free surface in the global model. Also visible in the screenshot are two wheel patch loads, each of which covers a 20" x 10" surface with 20,000 lb applied over the nodes.

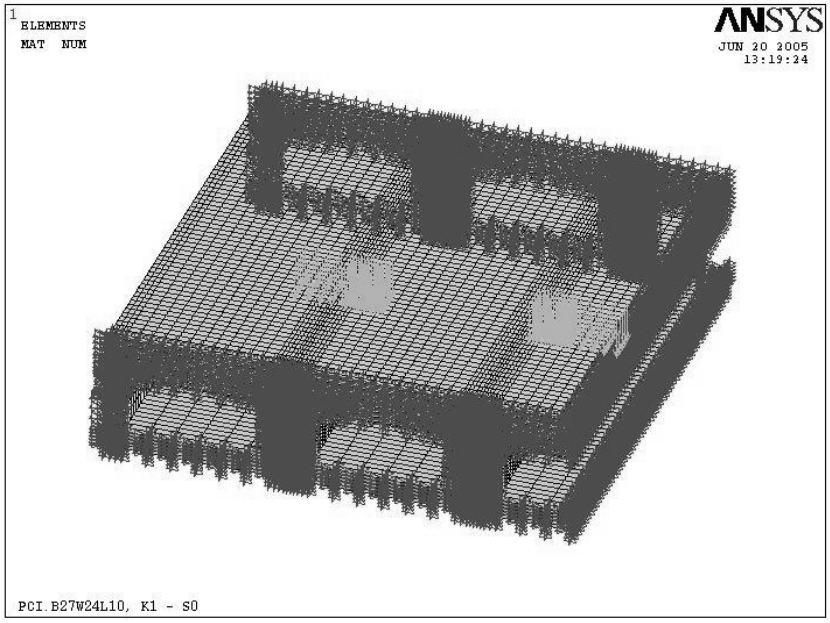

Figure 34: Submodel with Applied Constraints

The transverse stress results for the worst location in any shear key and the stress profile through the depth of the second shear key from the edge (listed as J2 in the graphs following) are compared between the full bridge model and the submodel. The results indicate that the full model generally gives equivalent results as the submodel,

but some loading situations show discrepancies. The results for each loading are discussed below in more detail.

Shrinkage in the Slab

The maximum transverse normal stress in the shear key or composite slab due to slab shrinkage is shown in Figure 35. In this case, the full model shows a fairly consistent value around 750 psi near midspan. The submodel shows a value near 900 psi. The results indicate that the full bridge model underestimates maximum transverse normal stresses by about 20%.

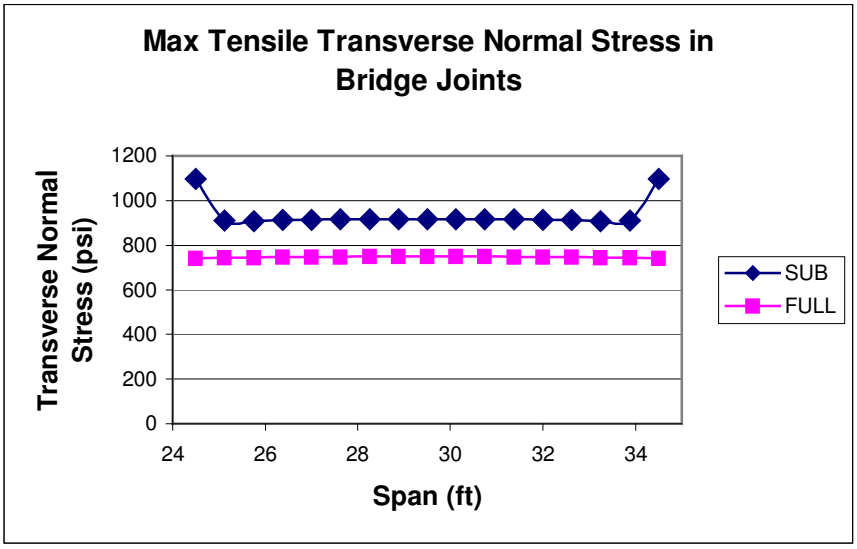

Figure 35: Maximum Transverse Stress in Submodel due to Slab Shrinkage

There are also peaks in stress near the edges of the submodel. These are a result of applied constraints which are interpolated from the global model and cause the stress

to spike in this area as a result. These spikes in stress near the submodel cut boundaries are typical of the data presented in this section. Since they are fictitious and only a result of the modeling technique, they will be disregarded.

The stresses through the depth of the shear key and composite slab are shown in Figure 36. The results here indicate that the stresses follow the same pattern, but that the submodel shows a wider variation in stresses in the upper portion of the shear key and lower portion of the composite slab. The full bridge model does not include this interaction between the slab and shear key because the elements are larger and the effects get averaged out.

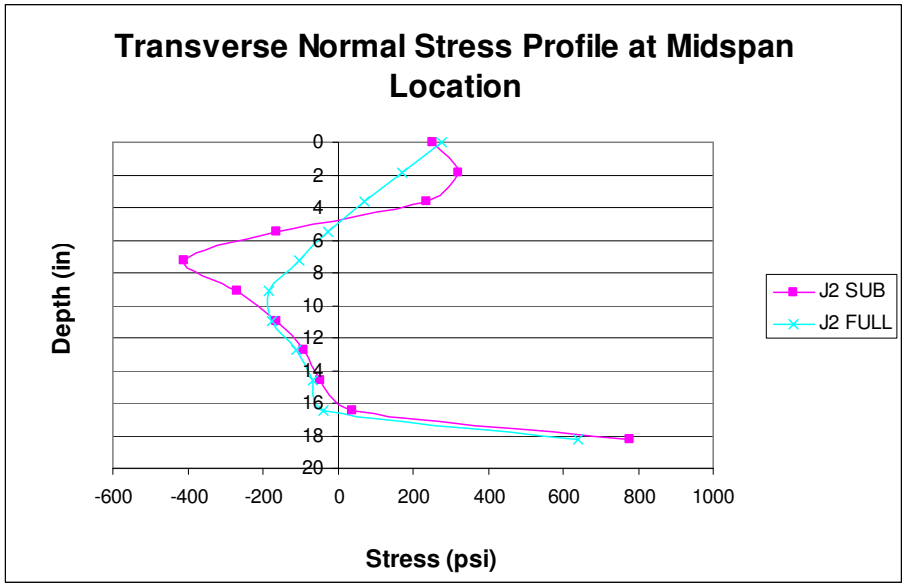

Figure 36: Stress Profile for Slab Shrinkage

Overall, the stress profile and maximum stresses compare favorably between each model when slab shrinkage is considered. The results provided by the full model should provide enough accuracy to use in the analysis of the shear key.

Shrinkage in the Shear Key

The maximum transverse normal stress in the shear key or composite slab due to shrinkage in the shear key is shown in Figure 37. The full bridge model shows a maximum normal stress near 700 psi whereas the submodel gives a result of about 450 psi. The full bridge model appears to overestimate maximum tensile stresses by about 50%.

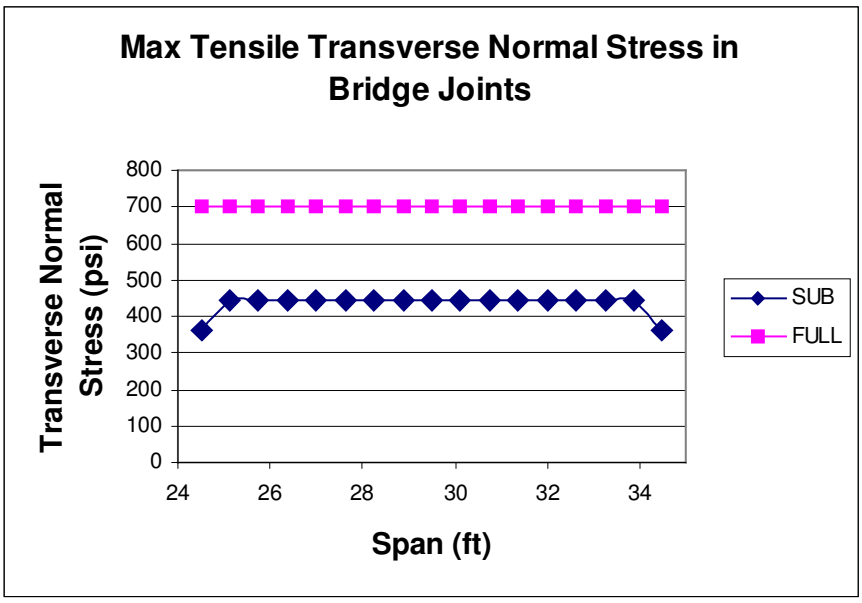

Figure 37: Maximum Transverse Stress in Submodel due to Shear Key Shrinkage

The stresses through the depth of the section are shown in Figure 38. In this case, the submodel shows that the stresses vary near the top of the section between compression and tension, and the area of the shear key near the top is under a significant amount of tensile stress. The full bridge model does not show tension in this region, so there is some concern that the full model does not include this effect. The stresses near the bottom of the shear key have the same pattern, but the submodel shows more compression and a less tension than the full bridge model.

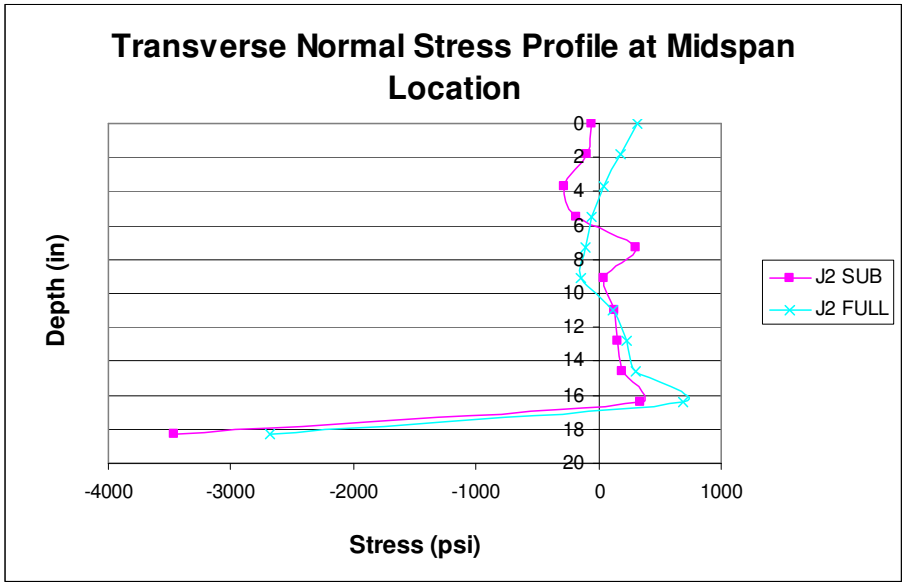

Figure 38: Stress Profile for Shear Key Shrinkage

The differences between the two models under shear key shrinkage loads are quite large. The full bridge model does a poor job of representing the worst tensile loads and shows the reverse stress conditions from the submodel at the top of the section. The

reason that this occurs is probably due to the size of the elements used in the shear key. The elements making up the shear key are the locations where loads are applied and they are also the locations where stresses are being measured, and this can introduce errors.

Positive Temperature Gradient

The maximum transverse normal stresses in the shear key due to a positive temperature gradient are shown in Figure 39. Both models show a stress near 170 psi, so there is little difference between the two models.

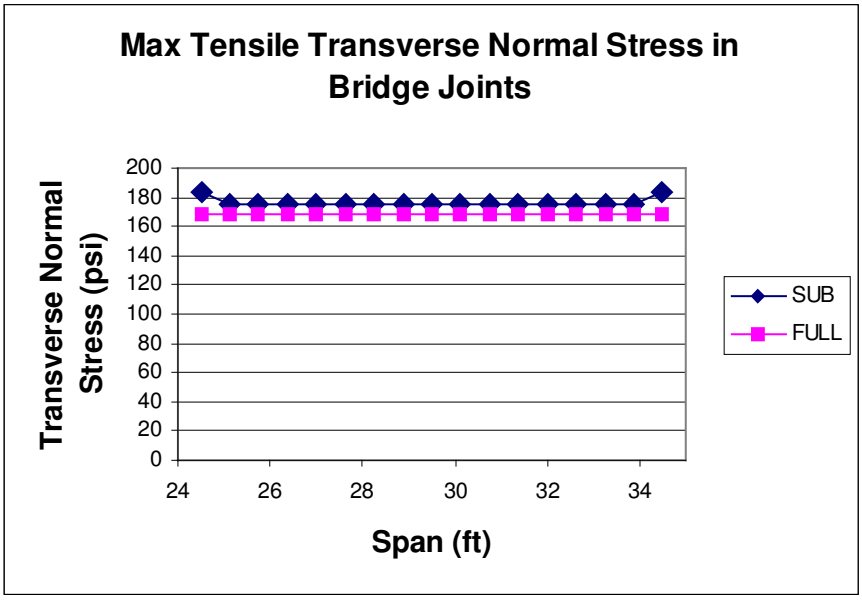

Figure 39: Maximum Transverse Stress in Submodel due to Positive Temperature Gradient

The stresses through the depth of the section are shown in Figure 40. Once again, the stresses are nearly identical for the entire cross section, showing only slight

variations. The top and bottom of the joint section are both in compression, while the stresses near the mid-depth region are all in tension.

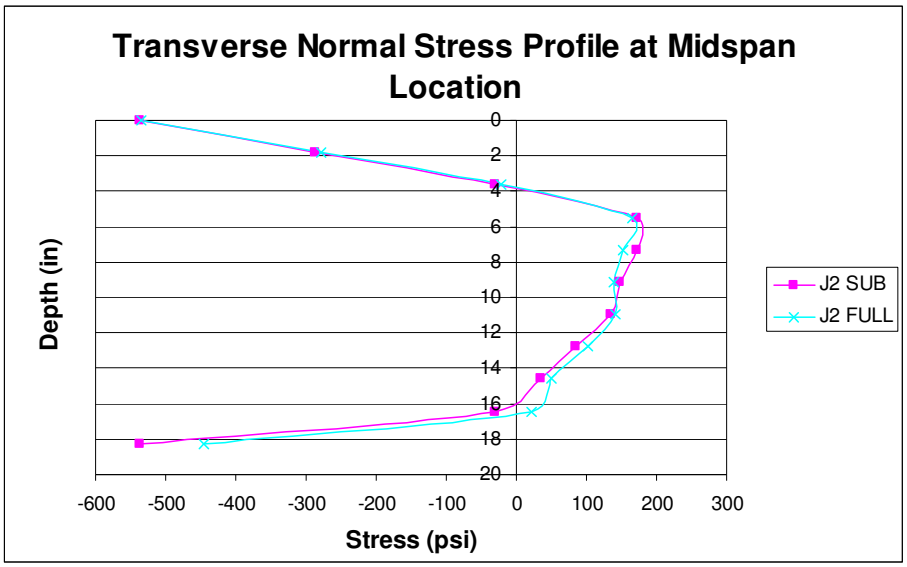

Figure 40: Stress Profile for Positive Temperature Gradient

From the data shown comparing the two models, it can be seen that the differences are small for this loading case. The results of the full bridge model agree closely with the submodel, so there is no adjustment needed.

Negative Solar Radiation Temperature Differential

The maximum transverse normal stresses in the shear key due to a positive temperature gradient are shown in Figure 41. This loading case is similar to the positive thermal gradient, but the temperature loads are reversed in sign and have a lower value.

The stresses for the submodel are near 200 psi, while the full bridge model stresses are near 160 psi, which means that the full model underestimates the stresses by about 20%.

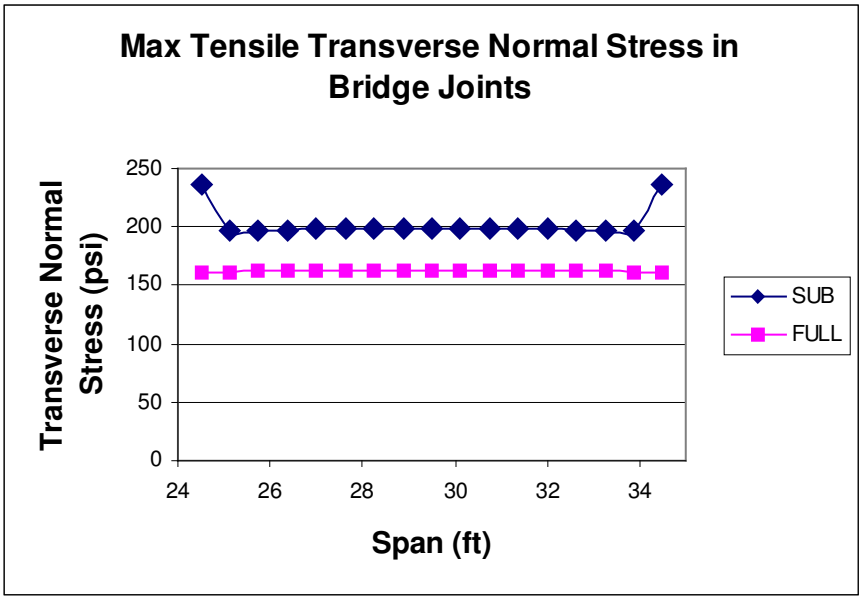

Figure 41: Maximum Transverse Stress in Submodel due to Negative Temperature Gradient

The stresses through the depth of the section are shown in Figure 42. The stresses shown for each model agree very closely except for the area near the bottom of the shear key. The stress profile here is opposite in sign from the one shown in the positive thermal gradient loading case, and so in this case the tension occurs at the very top and bottom of the section.

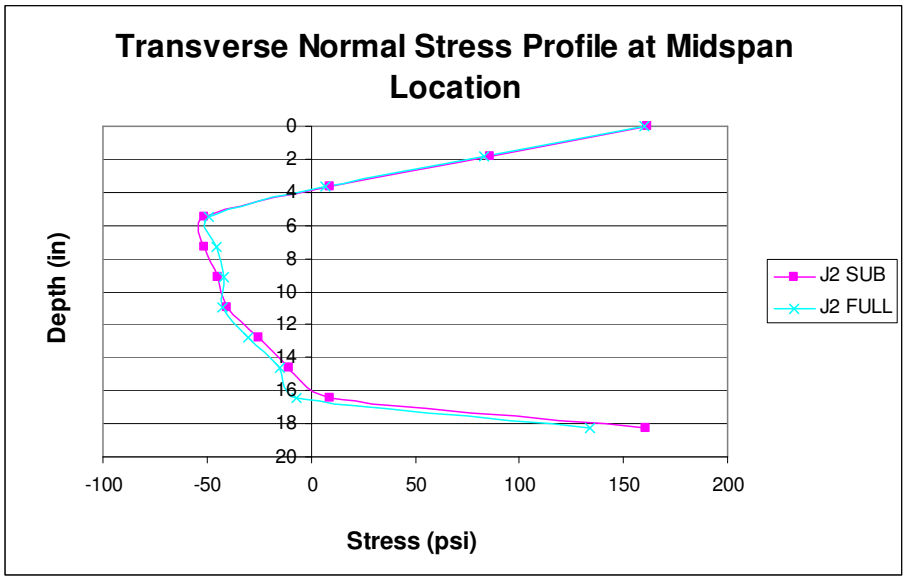

Figure 42: Stress Profile for Negative Temperature Gradient

In this loading case, the differences are noticeable, but not very large. The results from the full bridge model are accurate enough to use in the analysis with only a small amount of adjustment necessary.

HS-25 Truck Loading

The maximum transverse normal stresses due to HS-25 truck loading are shown in Figure 43. For this case, the results of full bridge model are compared with the results from two loading patterns of the submodel. The first loading case considered is similar to the full bridge model, where the HS-25 wheel loads are applied at a single node. The second loading case is where the HS-25 wheel loads are applied over an area that is the correct AASHTO specification. This "patch" loading means that the load pressure is

100 psi and distributed over an area according to the formula listed in the AASHTO documents (AASHTO 2004).

The maximum transverse stress results show that there is little difference between the submodel with a point load and the submodel with a patch load. However, the full bridge model underestimates the maximum stresses by about 20%.

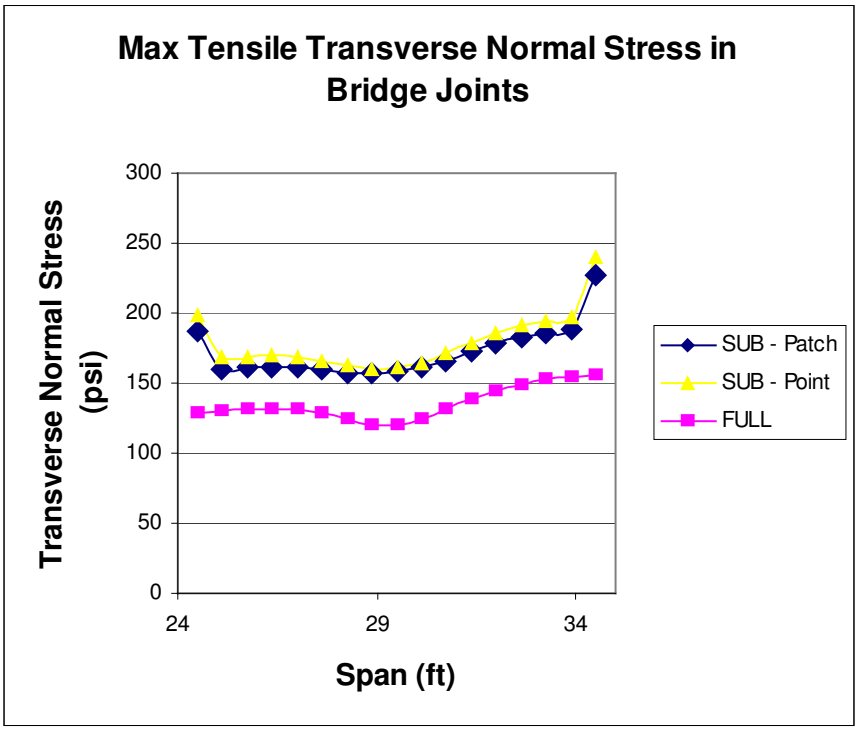

Figure 43: Maximum Transverse Stress in Submodel due to Truck Loading

The stresses through the depth of the section are shown in Figure 44. The graph shows the results for both submodel loading conditions and the full bridge model with point loads. At this location, both the submodel with patch loads and with point loads

agree closely with each other, but the full bridge model is a bit off from the submodel results. All models show a region of compression near the top of the section and a large tensile stress at the extreme bottom of the shear key. Using a point load instead of a patch load was found to have little consequence on the overall results, as both styles of loading showed similar patterns of stresses through the depth of the section.

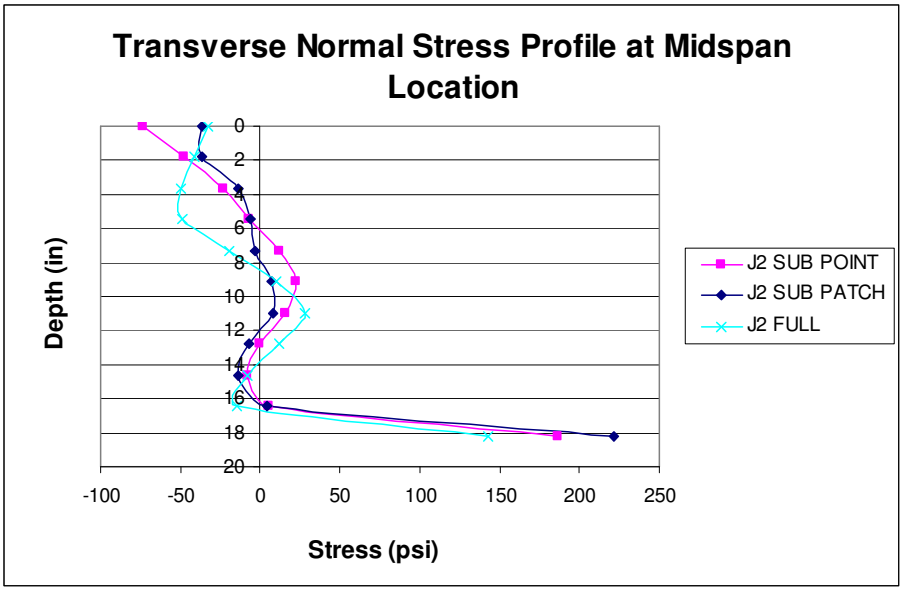

Figure 44: Stress Profile for Truck Loading

Summary of Submodel Verification Test

In general, the results from the submodel verification test show that the maximum transverse tensile and stress profile match well, but some adjustments need to be made in order to match the results from the submodel. First, the load case involving shear key shrinkage overestimates maximum transverse stresses by about 50%. Next,

the load cases involving slab shrinkage, negative temperature gradient, and truck loading all underestimate the maximum transverse stresses by about 20%. The results from the positive temperature gradient load case was found to agree closely with the maximum transverse stress found in the submodel, and so no adjustment is needed.

Also of important interest was the truck loading submodel results. AASHTO states that HS-25 truck loads should be applied as a pressure over a certain area (AASHTO 2004). The truck loads were applied as point loads in all tests, so it was important to find out if this would cause a difference when compared to an applied pressure.

RESULTS

Introduction

The results shown in this section compare the stresses from the bridge models to the failure criteria. The results are given independently for each load case. These results are shown in graphs that plot the highest tensile stress in a bridge joint as a function of span length. Additional graphs show the variation of stresses through the depth of each bridge joint at midspan for typical TxDOT and PCI bridges. The notation used to identify the various bridges analyzed in this study is shown in Table 10.

Table 10: Bridge Suffix Identification Code

Bridge Identification Code	
Prefix	Explanation
P	PCI style box girder and shear key
T	Texas style box girder and shear key
Section	
Bxx	Box girder section "xx", depth of girder section only
Suffix	
None	Assumes 5" slab and shear key present
- S	Assumes 5" slab, NO shear key present
- SK	NO slab present, shear key is present
- PT	NO slab present, post-tensioning and shear key used
- FD	NO slab present, full depth shear key used

As an example, a **TB20 – S (59)** indicates a Texas B20 section with no shear key and a 5 inch composite slab on a bridge span of 59 feet. A **PB33 (92)** indicates a PCI B33 (IIB) section with both a shear key and a 5 inch composite slab on a 92 ft. span. The span length is often used as one of the axes on each graph, so that information may

be unlisted if it would be redundant. Also, the results are separated by the number of design lanes, so each chart will be noted as 2-lane bridges or 3-lane bridges.

It should be noted the results show only the worst case transverse tensile stresses for a bridge joint. The transverse tensile stress is the most important stress component because it is the best predictor of failure in a shear key, and likely to be the cause of reflective cracking on the roadway surface.

In addition to the maximum transverse tensile stresses, graphs showing transverse stress through the depth of the joint section are given. The "joint section" is the part of the bridge that transfers forces from one box girder to the adjacent girders. For a bridge that has shear keys and a composite slab, the joint would be composed of both the shear key and the part of the slab directly above the shear key. The results for each joint are graphed versus section depth and begin at the top of the shear key or composite slab and extend to the bottom of the shear key, similar to that described in the previous section on the submodel. A sample joint numbering pattern is shown in Figure 45.

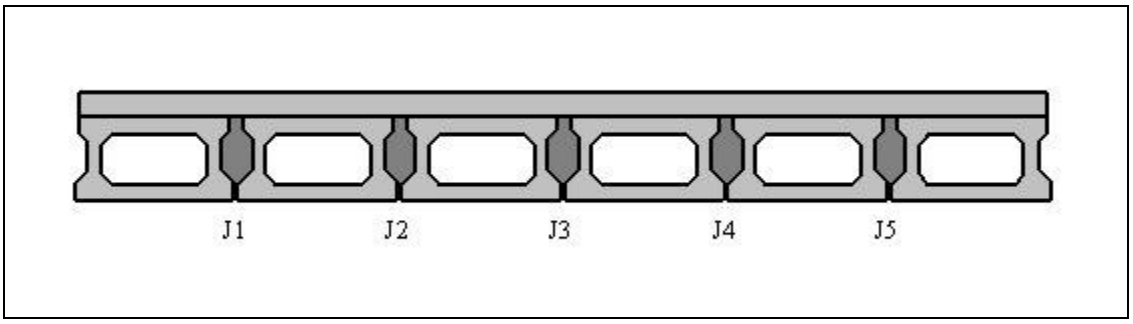

Figure 45: Joint Numbering Scheme

Only a selection of bridges for each load case will include stresses through the depth of the joint section because the other bridges will have a similar pattern for the same load case. Listing the full results for every bridge under every load case would be redundant and consume too much space for a worthwhile discussion.

Each load case also discusses the scaling factor required for the global model results to match the submodel results. This factor represents the difference between the coarse mesh "global model" and the fine mesh "submodel". In some cases, this difference accounted for a factor of 50% difference in the maximum tensile stress, but typically the difference was about 20%. This factor is mentioned in the description of each load case, but the factor has not been applied to any results. The values shown in the graphs are the actual stresses obtained from the analysis, and contain no scaling factors.

Results for Shrinkage Loading

Slab Shrinkage

As discussed in the section on loading values, the slab has a shrinkage strain equivalent to 200 microstrain. Because the analysis is linear, the stresses can be scaled up or down to obtain the results for an analysis performed with a shrinkage strain different from the 200 microstrain used.

The results shown in Figure 46 and Figure 47 show that the tensile stresses due to slab shrinkage in all bridges are higher than both the rupture strength and debonding

failure criteria. The highest tensile stresses occur in bridges without a shear key. Span length appears to be a factor for the PCI style bridges, but the Texas bridges do not show a dependence on span length.

The submodel analysis indicated that the global models would underestimate tensile stresses by 20%, so the stresses should be scaled up to reflect these conditions.

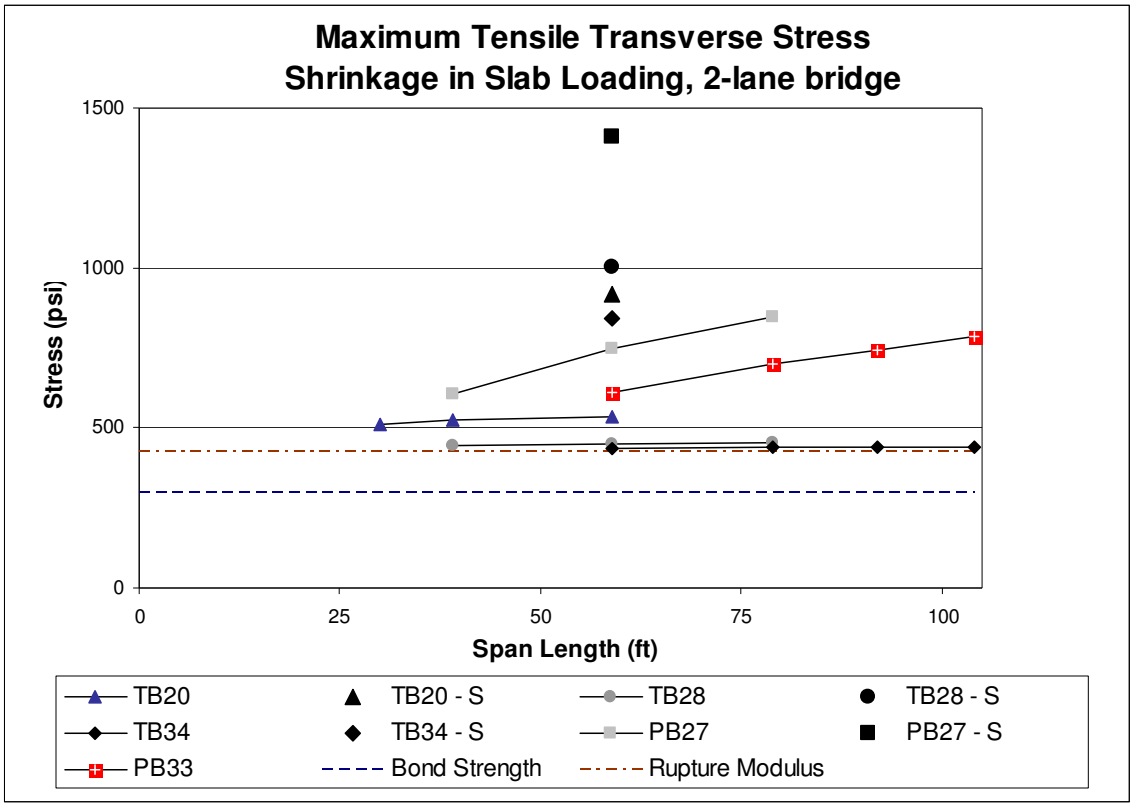

Figure 46: Maximum Transverse Stress due to Slab Shrinkage in 2-Lane Bridges

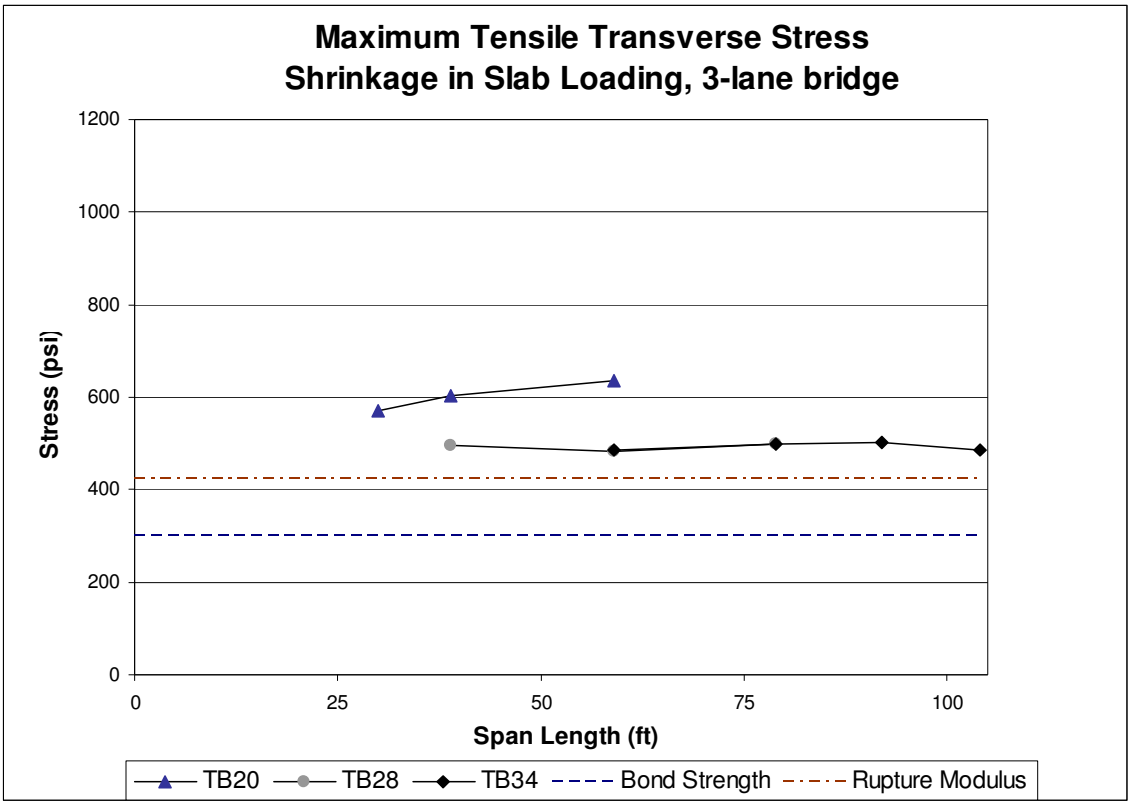

Figure 47: Maximum Transverse Stress due to Slab Shrinkage in 3-Lane Bridges

The transverse stresses at midspan in Figure 48 and Figure 49 indicate that the stresses caused by slab shrinkage are similar for all joint locations. The stress profiles through the depth of the section also show that tension stresses are highest at the top and bottom surfaces, and some compression exists in the middle region. Cracking at the top surface is possible due to this load case, and cracking could occur at every joint location.

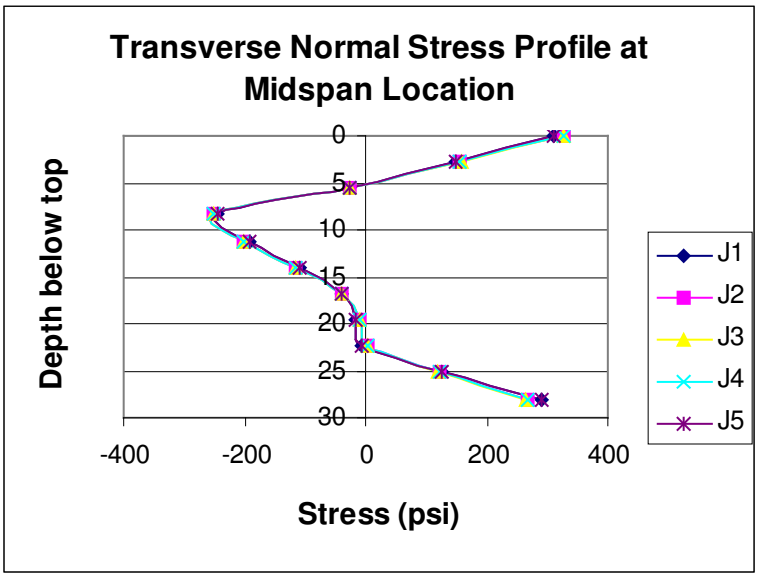

Figure 48: Stresses in Joints for TxDOT Bridge due to Slab Shrinkage (2-Lane TB28 - 59)

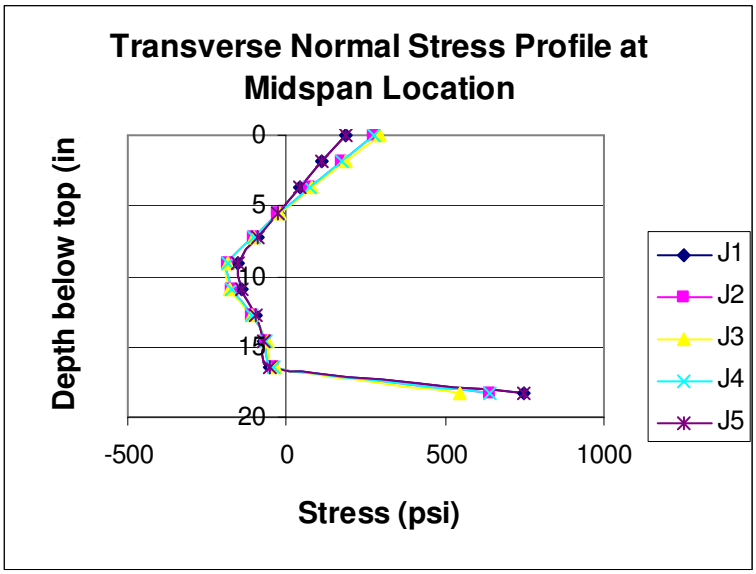

Figure 49: Stresses in Joints for PCI Bridge due to Slab Shrinkage (2-Lane PB27 - 59)

Shear Key Shrinkage

The shear key shrinkage load case is similar to that for shrinkage in the slab. The shrinkage loads are confined to the shear keys, and all other elements do not have any loads applied. The value used for shrinkage is 400 microstrain. The stress levels for shear key shrinkage should be reduced by approximately 50% to reflect the differences between the global model and the submodel. The bridge models that do not have a shear key have been removed from this data set as no loads can be applied to them.

The results for shrinkage in the shear key are shown in Figure 50 and Figure 51. For this load case, most TxDOT bridges and some of the PCI bridges without a composite slab are above the failure criteria, after considering the scaling factor needed to match the submodel results. In this load case, the span length is not a factor contributing to maximum tensile stress. However, the size of the shear key is a factor. The use of full depth shear keys and post-tensioning improve the results for the bridges with those features. The presence of a composite slab does not have a large effect on the stress levels under this load, because the loads and stress effects are concentrated in the shear key area.

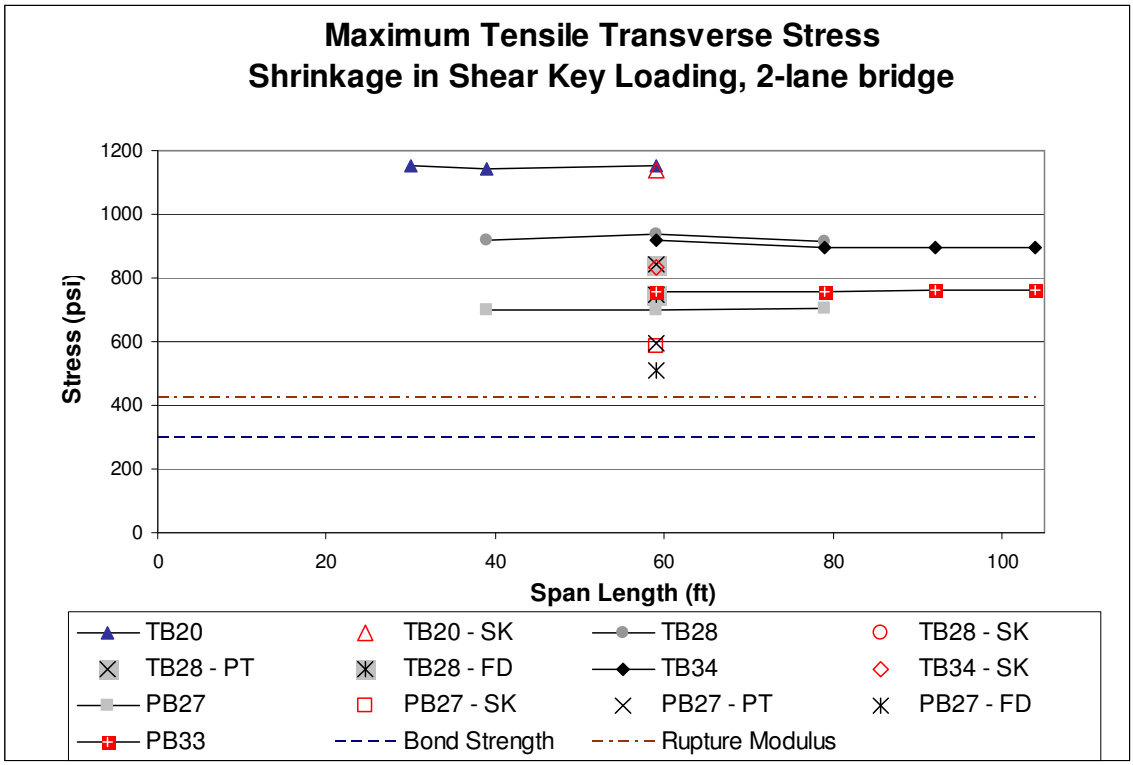

Figure 50: Maximum Transverse Stress due to Shear Key Shrinkage in 2-Lane Bridges

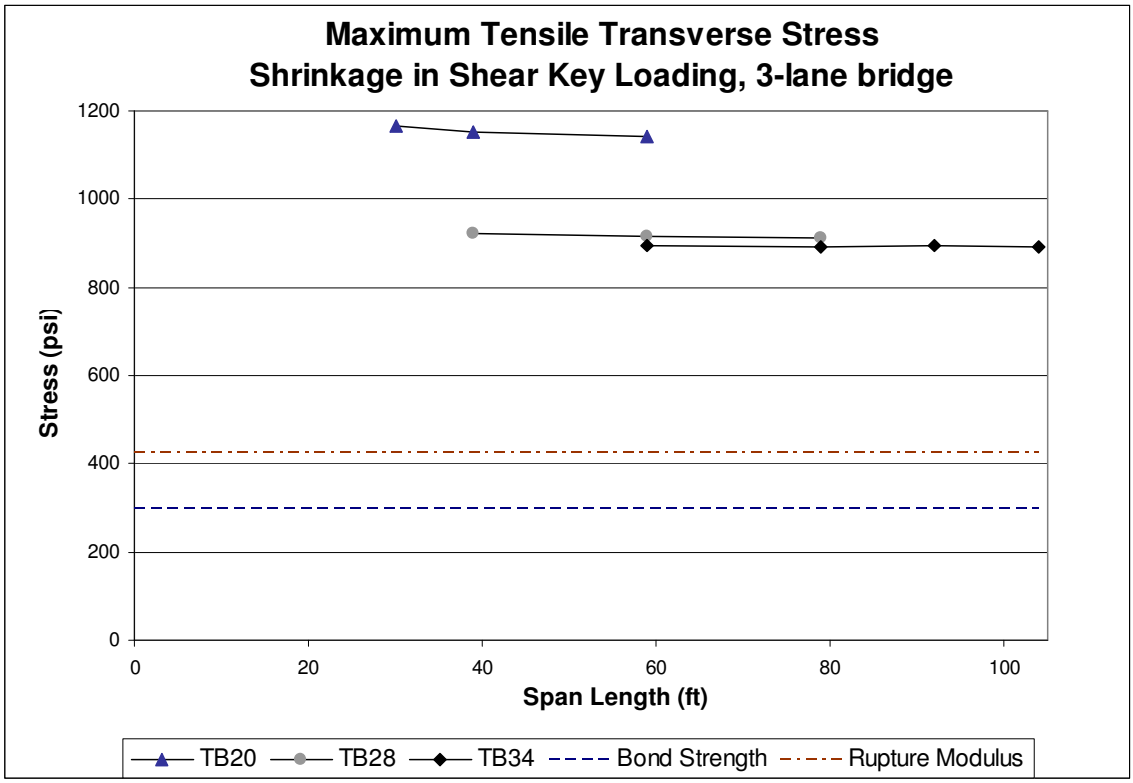

Figure 51: Maximum Transverse Stress due to Shear Key Shrinkage in 3-Lane Bridges

The stress profiles for a typical TxDOT and PCI bridge are shown in Figure 52 and Figure 53. The TxDOT bridges have the highest tensile stress just below mid-depth. The PCI bridges have the highest tensile stresses at the top of the slab and near the bottom of the keyway. When stresses are reduced to match the submodel results, the values are still above the failure criteria.

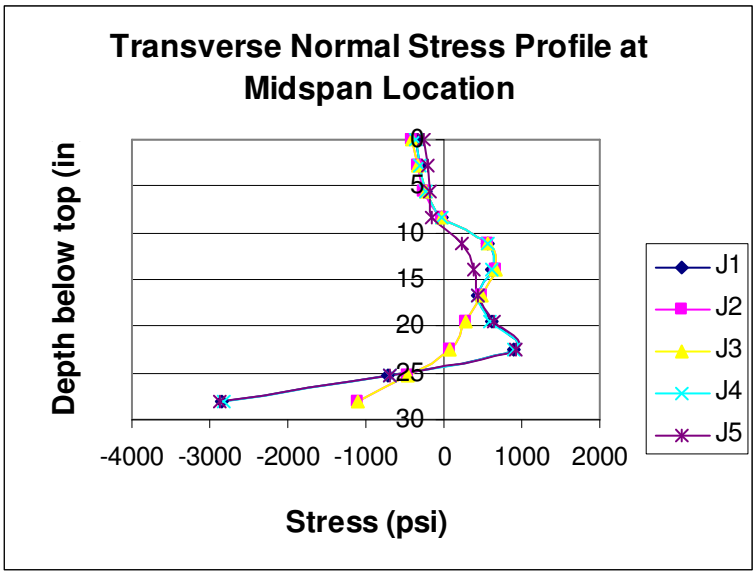

Figure 52: Stresses in Joint for TxDOT Bridge Under Shear Key Shrinkage (2-Lane TB28 - 59)

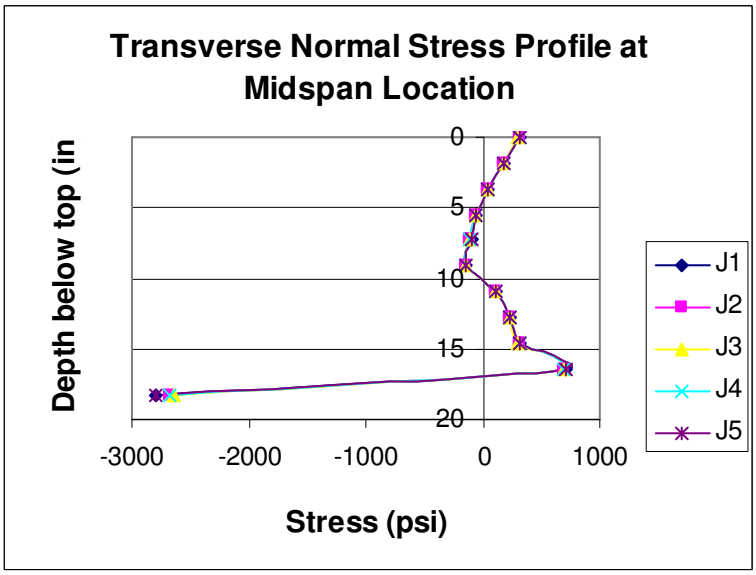

Figure 53: Stresses in Joint for PCI Bridge under Shear Key Shrinkage (2-Lane PB27 - 59)

Results for Temperature Loading

(+) Positive Thermal Gradient

The thermal gradient load considers the effect of solar heating on the top surface of the bridge, while the bottom regions of the bridge remain at lower temperatures. The transverse stresses due to thermal expansion are applied using the recommended temperature profiles from AASHTO. The submodel analysis showed very little difference with respect to the global model maximum tensile stresses, so no adjustment factor is needed for this load case.

The results from Figure 54 and Figure 55 show that the Texas box girders much lower tensile stresses versus the PCI sections with regard to thermal differential loads. None of the standard Texas bridges has stresses above the failure criteria, but similar bridges using a PCI shear key will have much higher stresses. Bridges without a composite slab or without a shear key also have much higher transverse stresses in the joint. Post-tensioning (bridges listed with – PT) reduces the tensile stresse, but a full-depth shear key reduces the tensiles stress even further in PCI bridges.

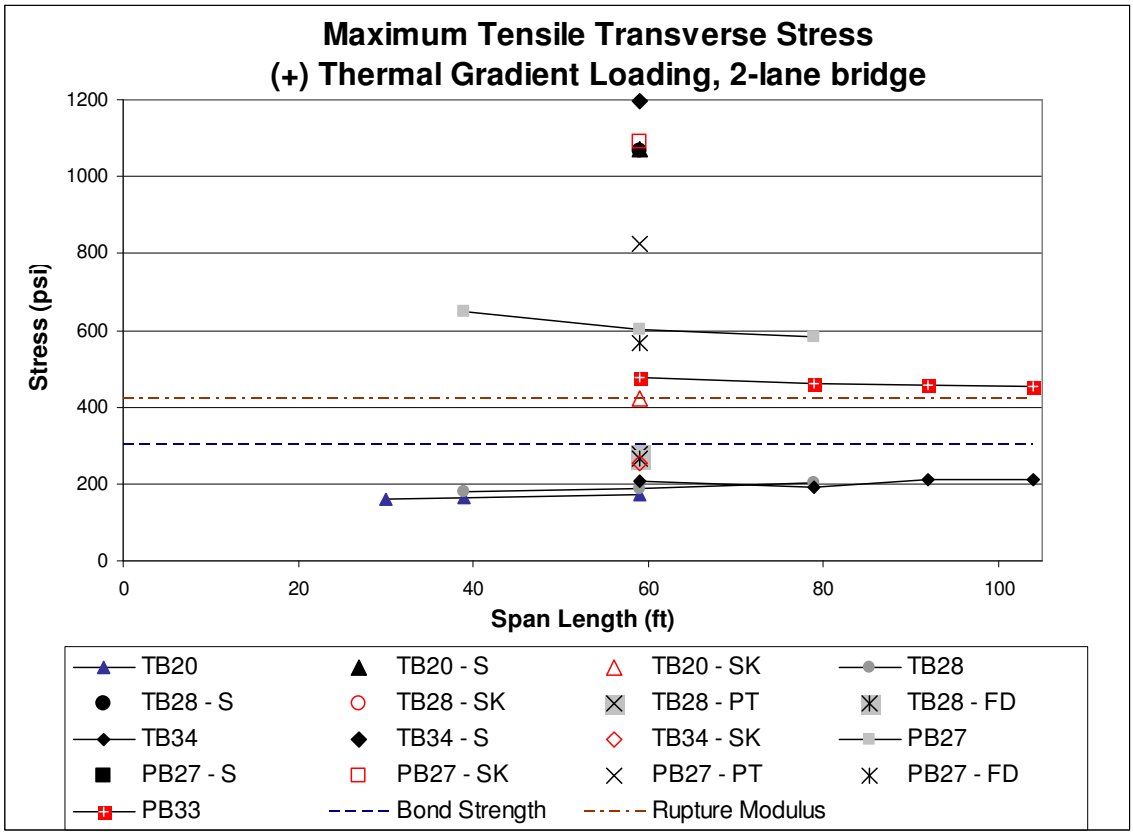

Figure 54: Maximum Transverse Stress due to Positive Thermal Gradient in 2-Lane Bridges

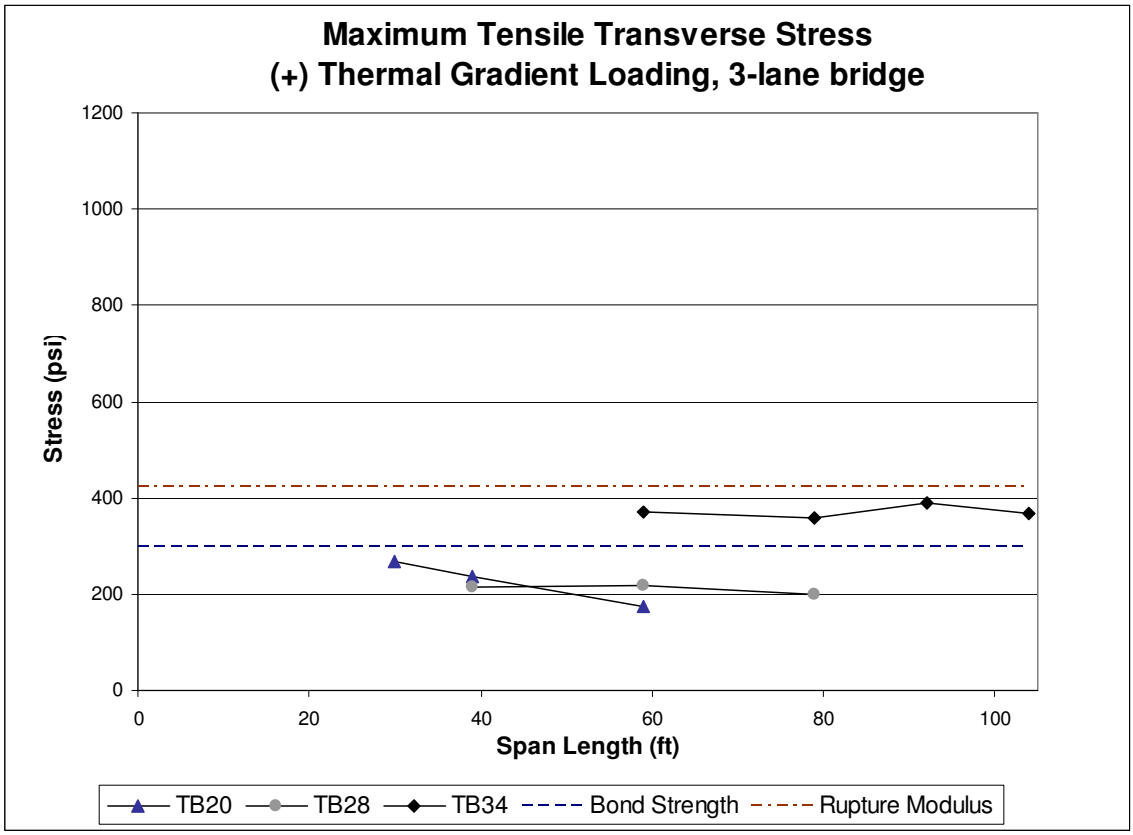

Figure 55: Maximum Transverse Stress due to Positive Thermal Gradient in 3-Lane Bridges

The stress profiles of typical TxDOT and PCI bridge joints are shown in Figure 56 and Figure 57. All joint locations show similar stress levels, and the highest tensile stresses occur about mid-depth of the joint. The results shown in these figures are for stress at mid-span, but the higher stresses shown in Figure 54 are near the end of the span.

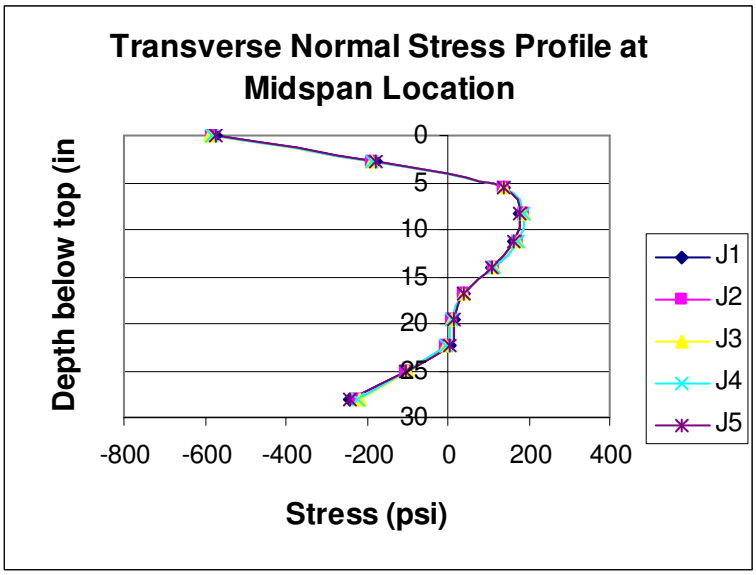

Figure 56: Stresses in Joint for TxDOT Bridge due to Positive Temperature Gradient

(2-Lane TB28 - 59)

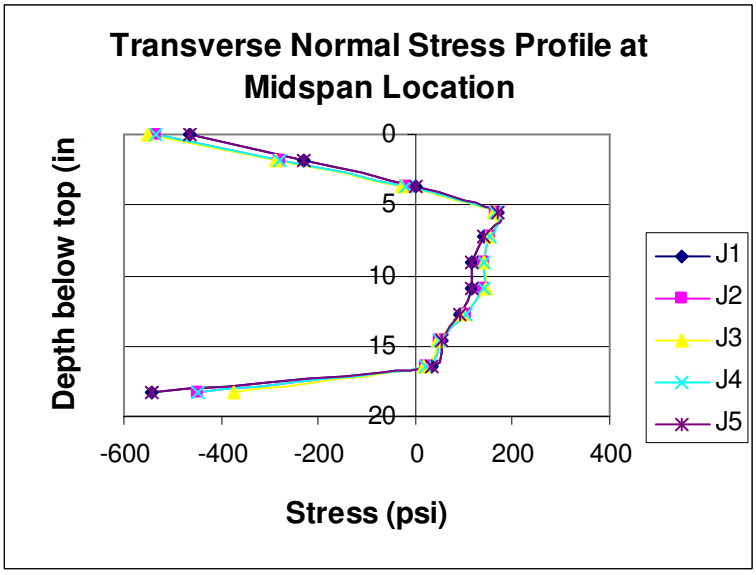

Figure 57: Stresses in Joint for PCI Bridge due to Positive Temperature Gradient

(2-Lane PB27 - 59)

(-) Negative Thermal Gradient

The counterpart to the solar induced thermal effects is the loss of thermal energy to the night sky. The temperature differential is less, but the top surface of the bridge can experience large tensile stresses. The temperature profiles are applied using the AASHTO negative thermal gradient specifications similar to the other thermal gradient load case. The submodel analysis indicated that this load case would underestimate the stresses, so the stresses shown in the results should be scaled up by about 20%.

The results in Figure 58 and Figure 59 show that most bridges have stress values below the failure criteria. Only bridges built without a shear key are close to the cracking stress, but these bridges would not experience problems with debonding because the slab is typically a monolithic pour.

The stress profiles for a typical TxDOT and PCI bridge for this load case are shown in Figure 60 and Figure 61. The results indicate that high tensile stresses exist near the top surface for both TxDOT and PCI bridge, but the stresses are below the failure criteria even after scaling up to match the submodel results.

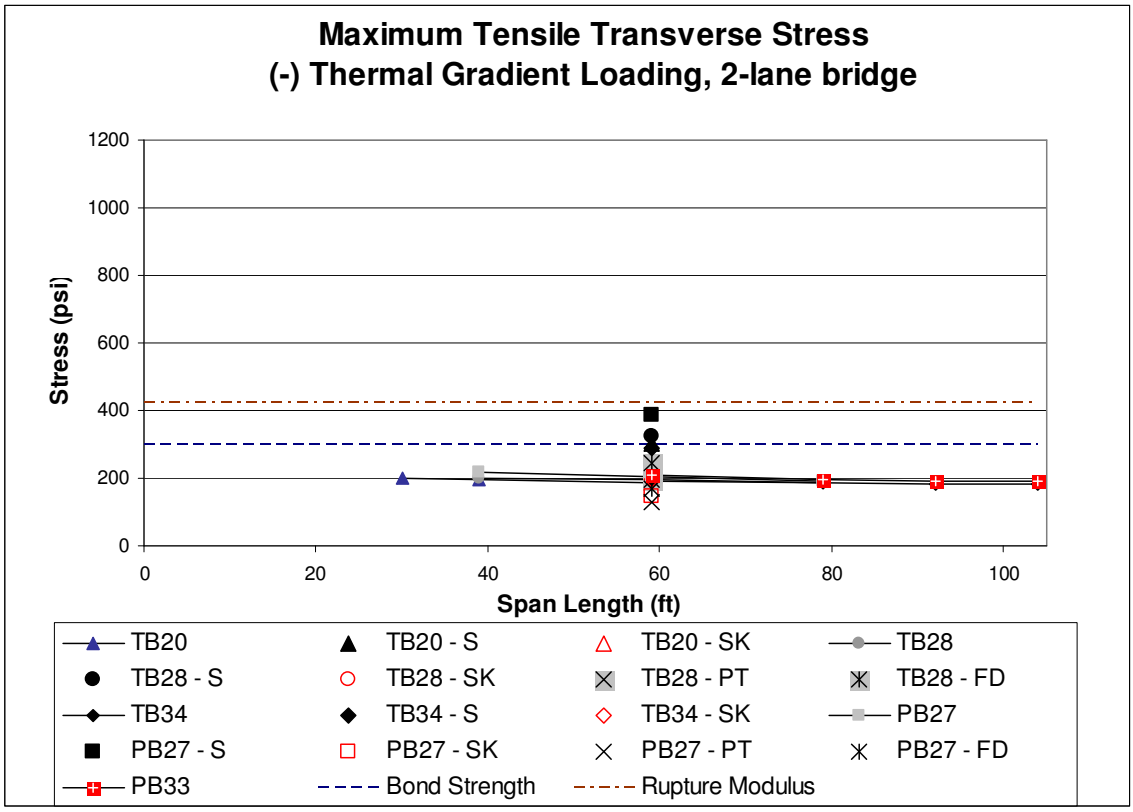

Figure 58: Maximum Transverse Stress due to Negative Thermal Gradient in 2-Lane Bridges

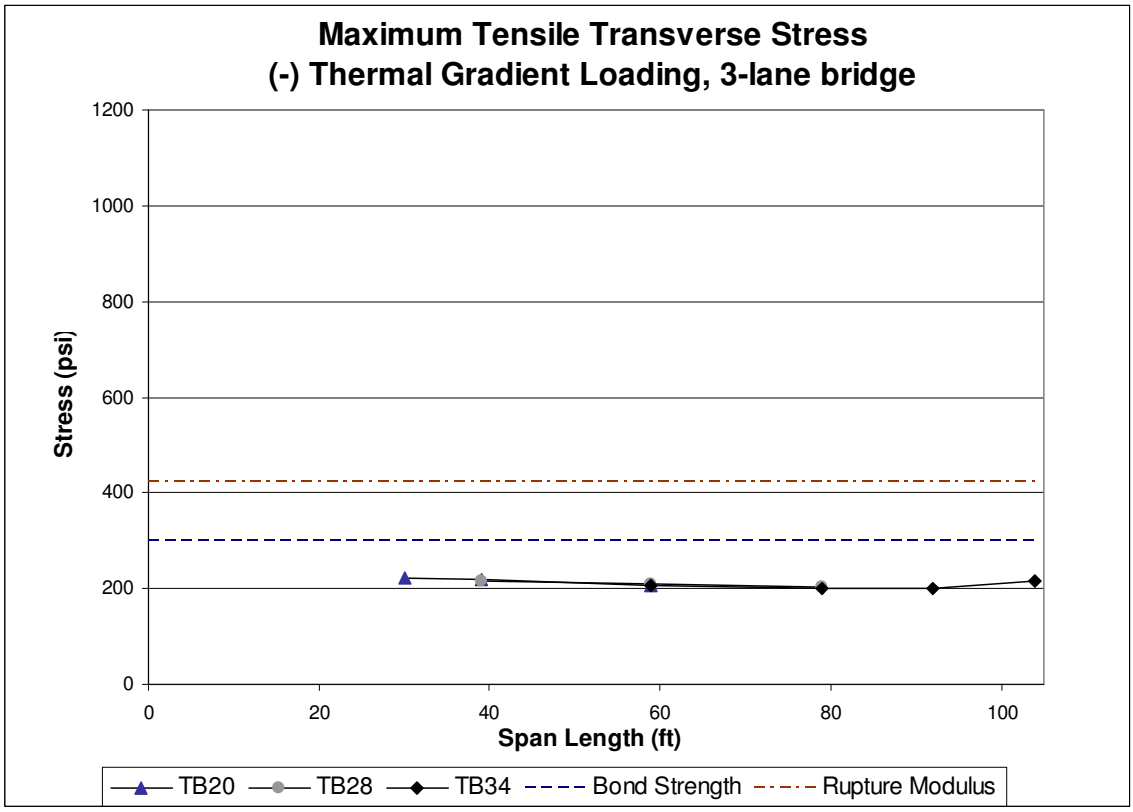

Figure 59: Maximum Transverse Stress due to Negative Thermal Gradient in 3-Lane Bridges

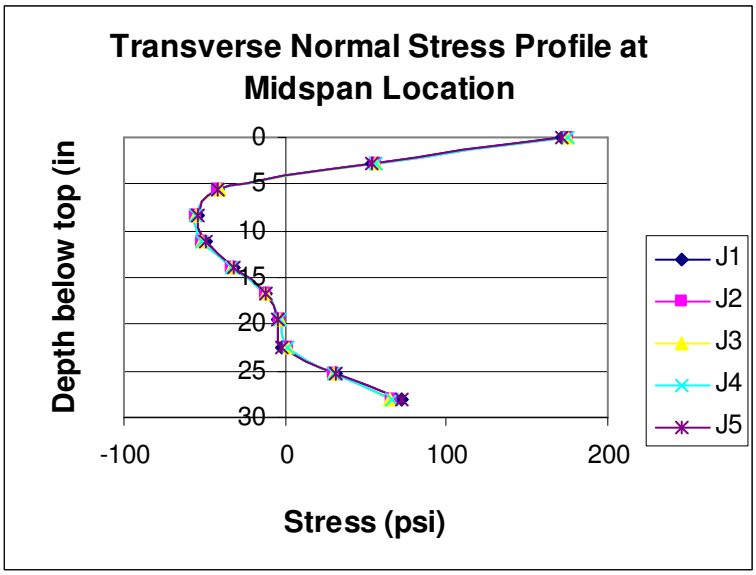

Figure 60: Stresses in Joint for TxDOT Bridge due to Negative Thermal Gradient

(2-Lane TB28 - 59)

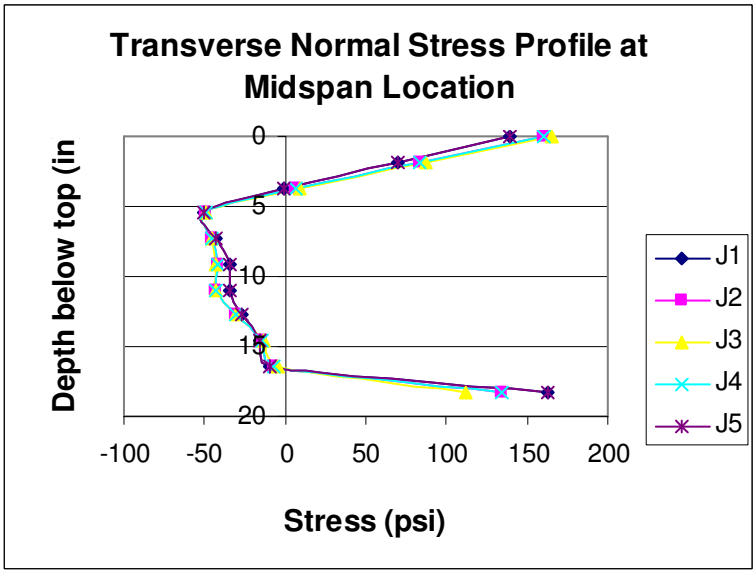

Figure 61: Stresses in Joint for PCI Bridge due to Negative Thermal Gradient

(2-Lane PB27 -59)

Results for Vehicular Loading

HS-25 Design Truck

The HS-25 truck load results produced by a single truck are shown in Figure 62 and Figure 63. The submodel analysis indicated that the results from the global models would underestimate stresses, so the results presented here should be scaled up by 20% to take this into consideration.

One problem with the data shown in the figures is that actual truck loadings are generally more complicated than the simple static loads presented here. There can be several lanes loaded at one time and dynamic interactions between the truck and the bridge, so the effects of truck loads can result in higher stresses than what is shown by a single static truck load.

There is not an increase in transverse stresses when multiple trucks are placed on the bridge, because the additional trucks effectively reduce bending in the transverse direction. Placing a truck in every lane causes all box girders to deflect similarly, so shear across the shear key is reduced. Therefore trucks in multiple lanes were not considered. Likewise, multiple trucks in the same lane were not considered, but the stresses from this situation could be much higher than for a single truck.

The issue of "impact loading" or higher stresses due to dynamic effects of the moving wheel loads is discussed in the AASHTO bridge manual, but no impact factor was incorporated in this study.

As shown in the results, all of the bridges have stresses below the rupture modulus, and only the PCI Bridge without a composite slab is significantly above the

stress level that would cause debonding. The increase of tensile stresses by 20% to match the submodel results means that more bridges would be above the failure criteria for debonding, but still none would be above the failure criteria for cracking. The TxDOT three lane bridges are also below the stress levels for cracking and debonding.

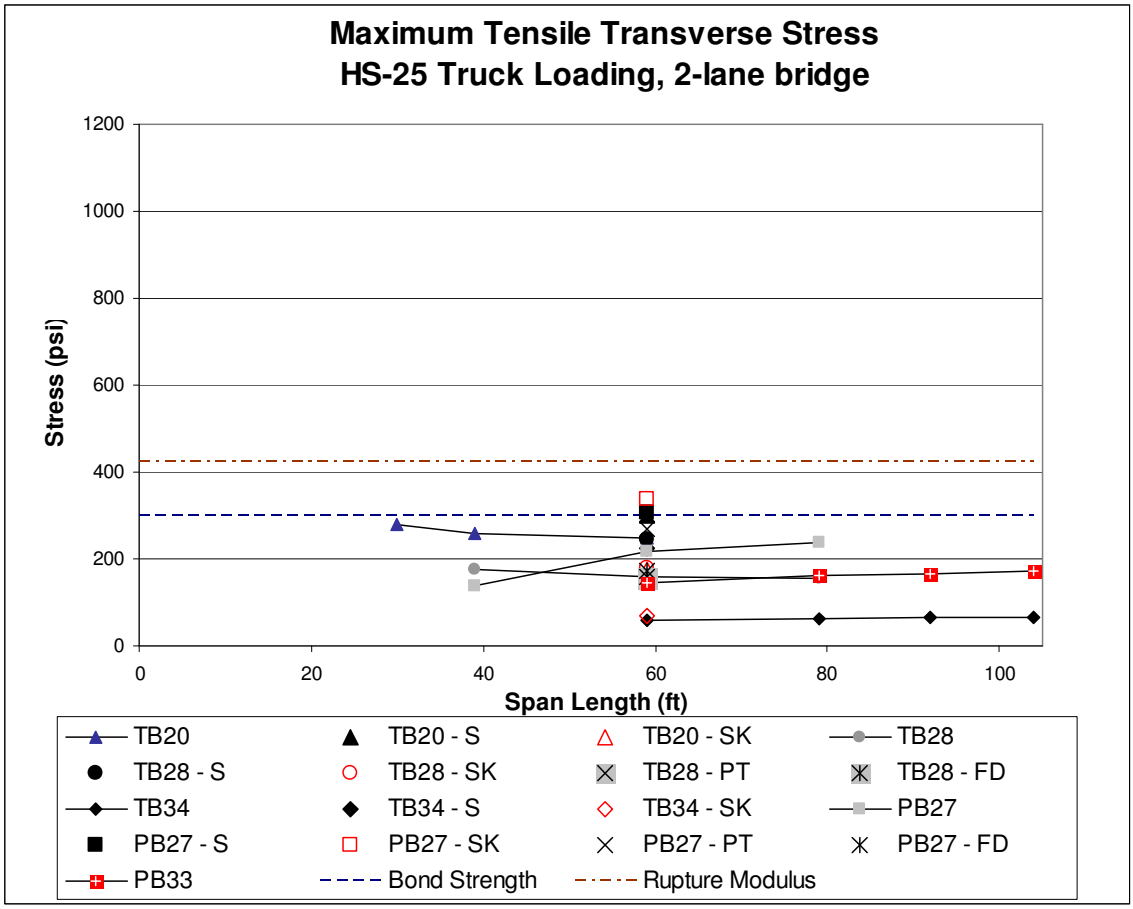

Figure 62: Maximum Transverse Stress due to HS-25 Loading in 2-Lane Bridges

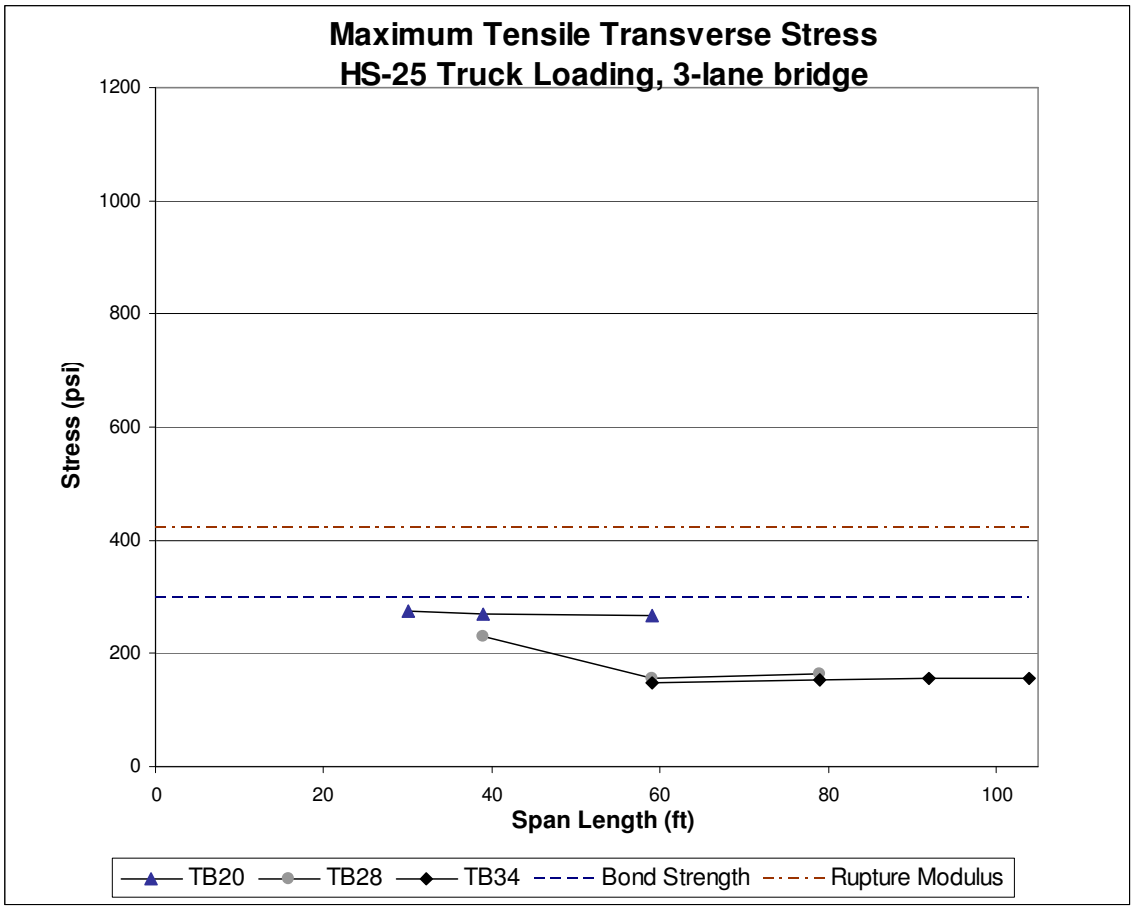

Figure 63: Maximum Transverse Stress due to HS-25 Loading in 3-Lane Bridges

The stress profiles for a typical TxDOT and PCI bridge are shown in Figure 64 and Figure 65. The maximum tensile stress for a joint at midspan exists below the wheel loads, and the stresses decrease as one moves further away from the wheel loads. The TxDOT bridges have small stresses at each joint at midspan, but the tensile stresses near the ends of the bridge are much higher. The PCI bridges have high tensile stresses in their joints at the midspan location as well as near the ends.

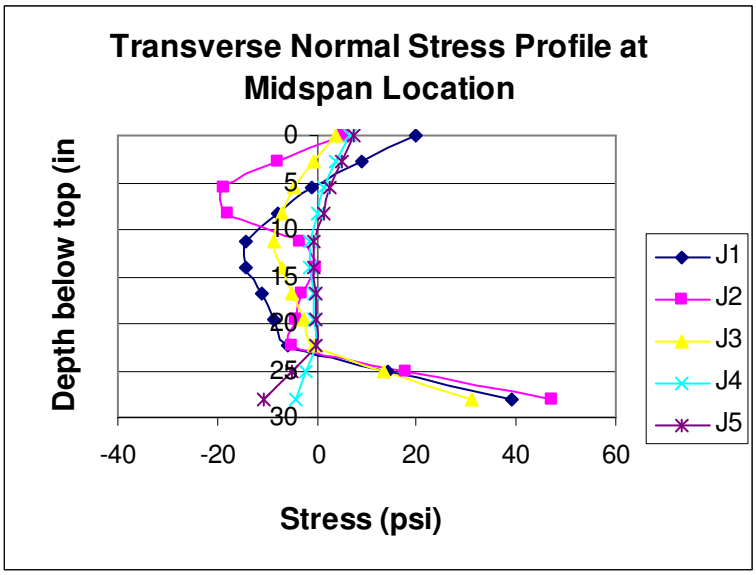

Figure 64: Stresses in Joint for TxDOT Bridge due to Truck Loading (2-Lane TB28 - 59)

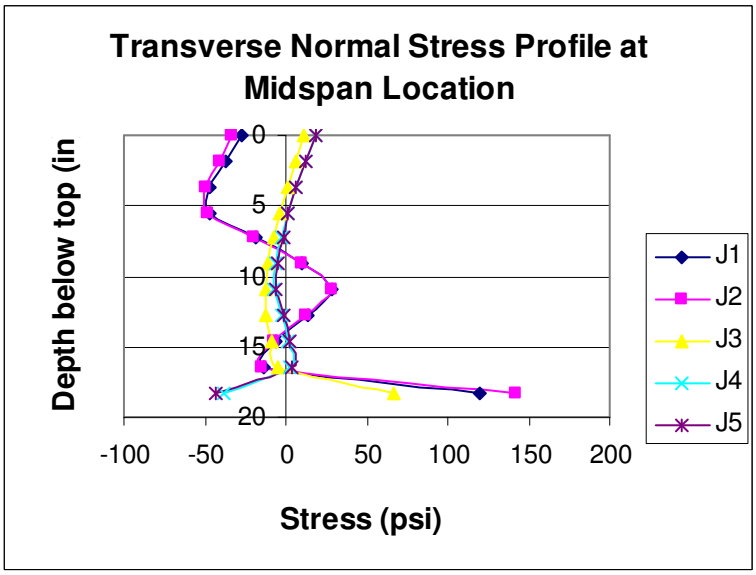

Figure 65: Stresses in Joint for PCI Bridge due to Truck Loading (2-Lane PB27 - 59)

Discussion of Bridge Features

The role of composite slabs, shear keys, transverse post-tensioning, full depth shear keys, and bridge width are discussed here to highlight the differences between the various bridge features.

Effect of Composite Slab

The effect of adding a composite slab serves to increase the load transfer mechanism and protect the shear keys from large tensile stresses. The bridges without composite slabs show higher stresses for most loading conditions. The major benefit of a composite slab is that it contains reinforcing steel and so would not be expected to lose the ability of load transfer once cracking occurs. However, the large shrinkage strains in a composite slab are a concern.

Effect of Shear Keys

The construction of a bridge with a composite slab but without a shear key produces stresses that are above the failure criteria when shrinkage and thermal loads are considered. The stresses due to the HS-25 load case are comparable to other bridge designs, as shown in Figure 66. The stresses due to thermal loads are very high, as shown in Figure 67. The experience of TxDOT with using these box girder bridges confirms these predictions (Jones 1999). The slabs developed large reflective cracks over shear keys and sometimes over the center of a girder. This is most likely related to shrinkage, but even without shrinkage the thermal stresses are high enough to cause

failure. It is unknown whether any PCI box girders have been built without shear keys, but the results would be similar to the TxDOT designs discussed here.

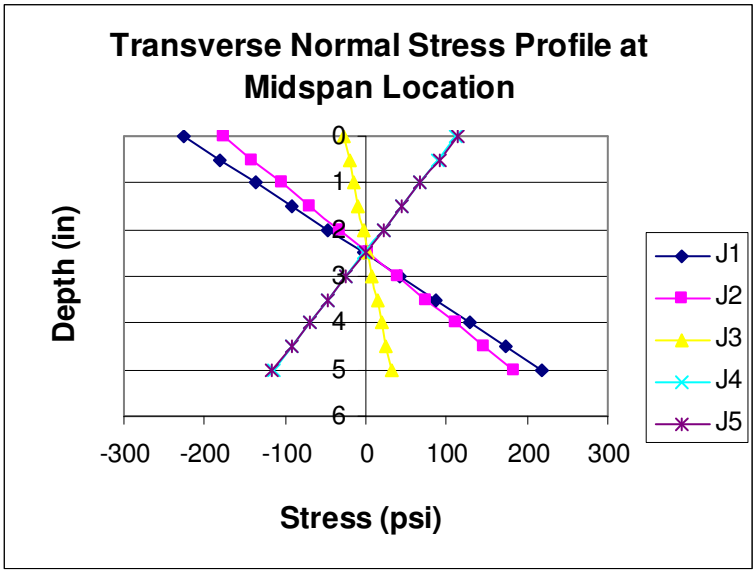

Figure 66: TxDOT Bridge with no shear key under HS-25 loads (2-Lane TB28 – S 59)

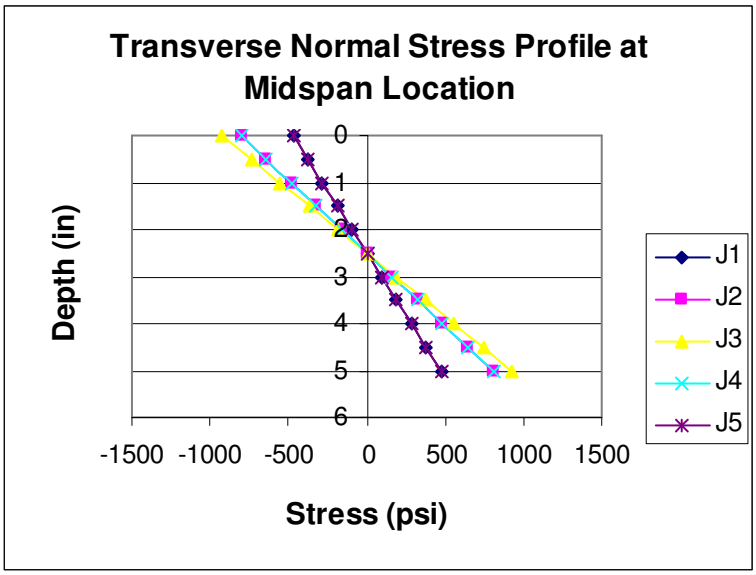

Figure 67: TxDOT Bridge with no shear key and (+) Thermal Gradient Loads (2-Lane TB28 - S 59)

Effect of Full Depth Shear Key

The use of a full depth shear key means that the shear key material extended to the bottom of the section. This is accomplished by including additional small elements below the gap of the typical shear key, but otherwise the models are similar to other bridges. The effect of the full-depth key is somewhat dependent on the original shear key configuration, as the PCI key is typically much smaller than the TxDOT key. This means that there will be a greater difference in the PCI bridges than for the TxDOT bridges. For example, a TxDOT B28 section will have a shear key extending 23" below the top (Figure 68). A PCI B27 (IB) will have a shear key that is only 13" below the top surface, so the key extends only about halfway down the section (Figure 69).

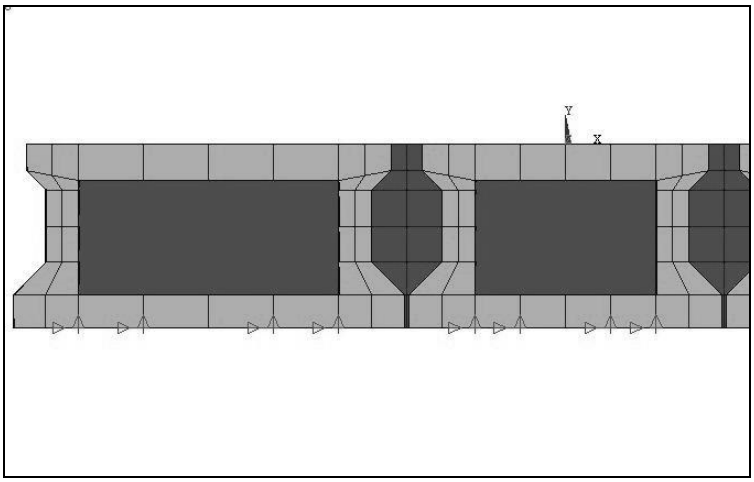

Figure 68: Texas Box Girder (TB28) with Full Depth Shear Key

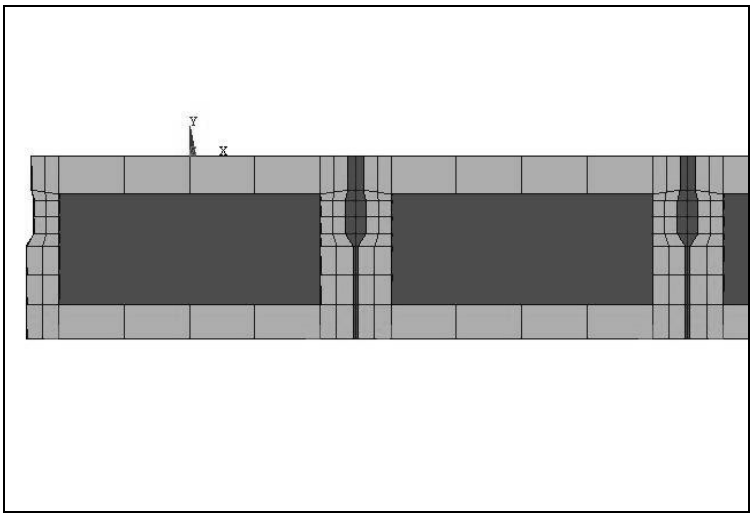

Figure 69: PCI Box Girder (PB27) with Full Depth Shear Key

The full depth shear key allows the bridge to transfer transverse normal stresses more effectively across joints, and there is less of a stress concentration at the bottom of the shear key. This might be difficult to accomplish with current designs, but would

result in lower tensile stresses in the shear key region under the same loads as a partial depth shear key. Another aspect of full depth shear keys is that they are less likely to act like a hinge, and more likely to transfer moment to adjacent girders.

Adding a full depth key to a bridge without a composite slab does lower the maximum tensile stresses as shown in the results. In addition, the use of a full depth key decreases the effect of the stress concentration at the bottom of the current shear key design. This area has an abrupt geometry change and could potentially be a crack initiator. This effect was not explored in this study, but the use of a full depth key decreased tensile stress levels for most bridges and load cases.

The improvements associated with using full depth keys were not evident in the Texas bridges that already have large shear keys. The use of a full depth key in the bridges was effective in lowering the tensile stresses for most load cases, and the results for the HS-25 load case is shown in Figure 70. The full-depth key did not lower the stresses for the negative solar radiation load, as shown in Figure 71.

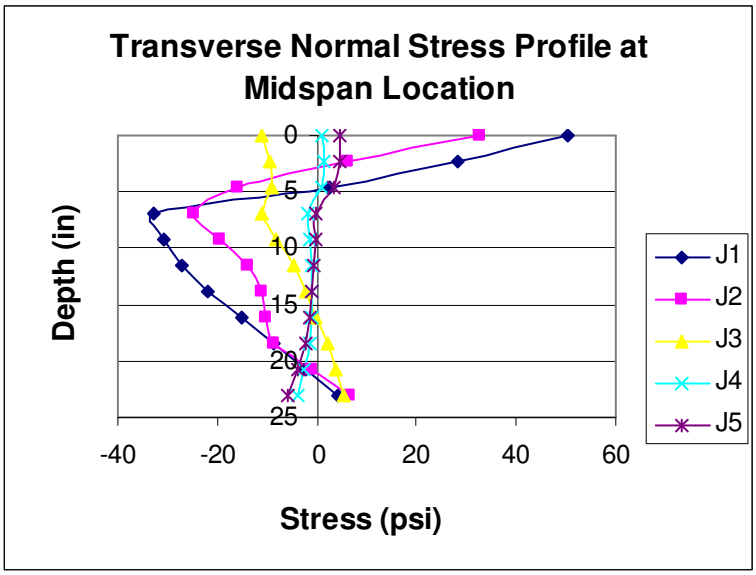

Figure 70: TxDOT Bridge with Full-Depth Key under HS-25 Loads (2-Lane TB28 - FD 59)

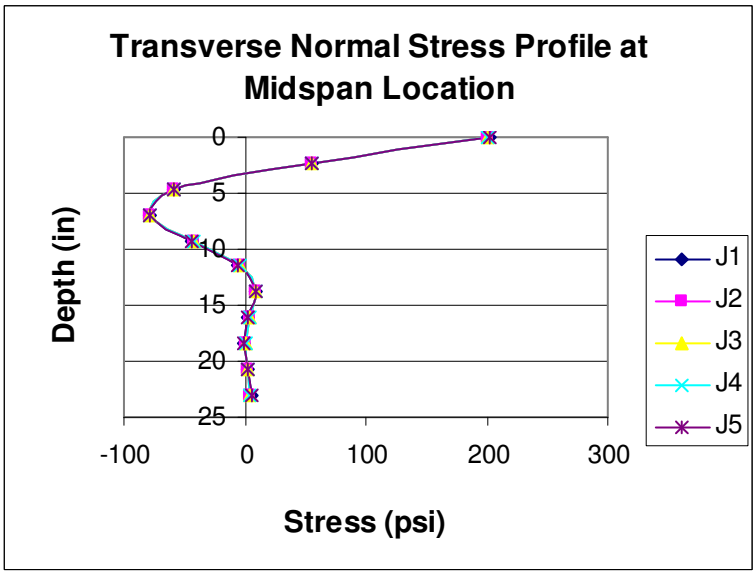

Figure 71: TxDOT Bridge with Full-Depth Key under (-) Thermal Gradient Loads

(2-Lane TB28 - FD 59)

Effect of Transverse Post-Tensioning

The models with post-tensioning are similar to the other models with three main differences. The first is that point loads are applied at the post-tensioning reaction locations simulating the effect of unbonded post-tensioned strands. The second difference is that internal diaphragms are included according to TxDOT or Ohio DOT standards. The last major difference is that no composite slab is used. The Texas bridge standard requires that when post-tensioning is used, diaphragms must be included in the exterior girders spaced every 10 feet with tendons at the same spacing tensioned to 45,000 lbs each. The PCI bridge has diaphragms (at the exterior girders) and tendons only at the ends and midspan locations, and each tendon is tensioned to 30,000 lbs. The effectiveness of post-tensioning had been dismissed by earlier studies, but in the models used for this study it was found to limit the maximum tensile transverse stresses in some cases. The overall improvements were small, and some load cases showed no apparent improvement in reducing transverse tensile stresses. Thus, the use of a small amount of post-tensioning does not appear to justify the additional expense.

One of the problems discussed with post-tensioning is that a close spacing and high tensile forces must be used if a compressive stress is needed for the entire shear key along the entire length of the bridge. The joints at the interior of the bridge have the most consistent compression, whereas the exterior joints have higher compression near the tendon reactions and lower compression halfway between reaction locations.

In the bridges discussed here, the strand is located at the mid-depth of the shear key. However, higher compressive stresses develop at the top and bottom of the shear

key due to the relative flexibility of the box girder walls. The average normal stress in a typical TxDOT bridge is shown in Figure 72.

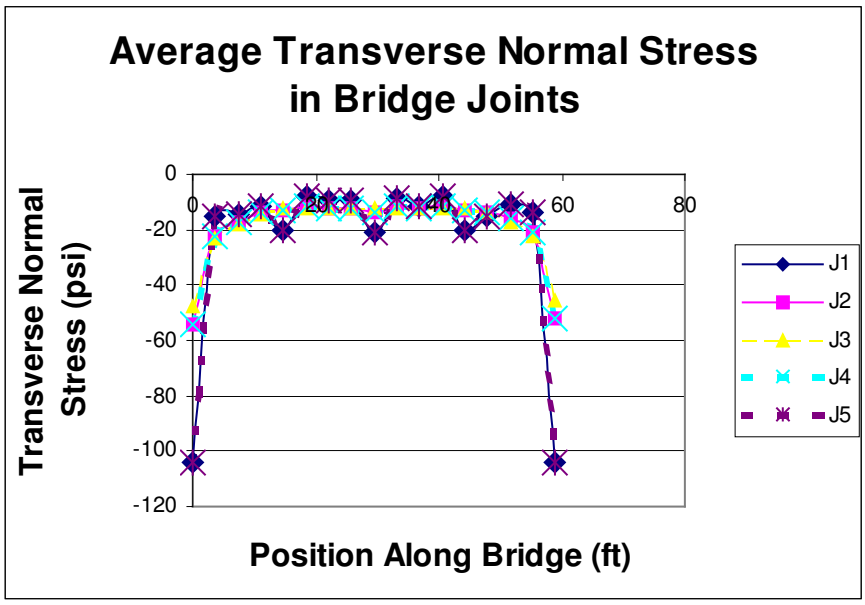

Figure 72: Average Stress in TxDOT bridge from Post-Tensioning Force (2-Lane TB28 – PT 59)

The stress profile through the depth of the shear keys in a typical TxDOT post-tensioned bridge with no composite slab is shown in Figure 73. The profile shown in Figure 74 is similar but taken at the L/4 (the quarter-point of the span) location, which is halfway between tendon locations. The joints in this model show a similar level of stress for all the interior joints, but the exterior joints show a 50% decrease from the level shown in the results from the midspan location. So, the interior joints will have a net compressive force that is consistent along the entire length of the bridge, but the

exterior joints can only be assured of half of that compressive force at locations away from strand reactions.

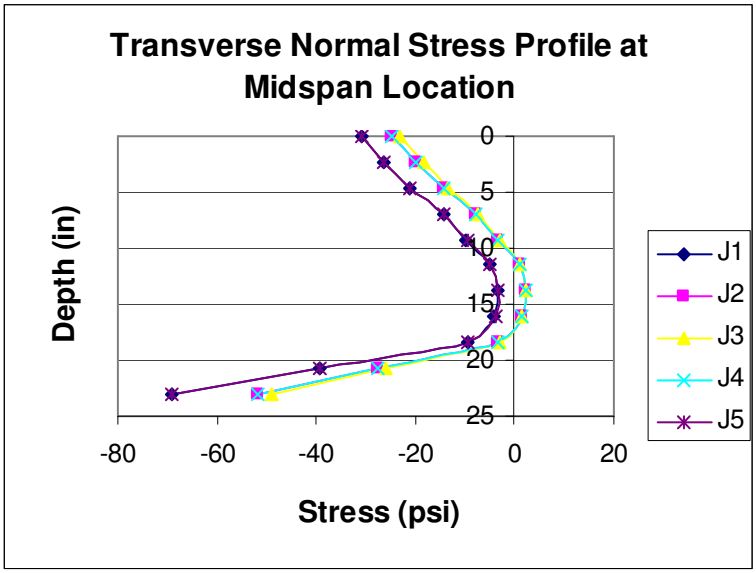

Figure 73: Post-Tensioned TxDOT Bridge without Loads Applied (2-Lane TB28 – PT 59)

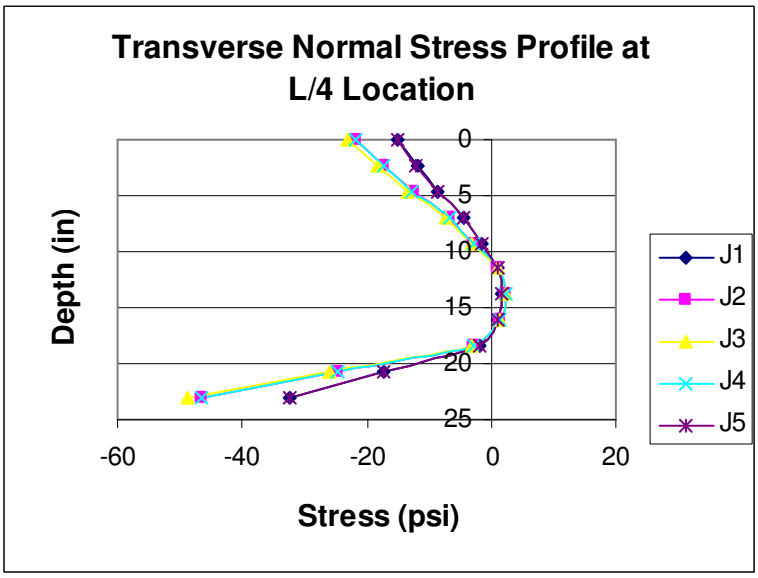

Figure 74: Post-Tensioned TxDOT Bridge without Loads Applied (2-Lane TB28 – PT 59)

The PCI bridge with post-tensioning according to OHIO DOT specifications uses three strand locations and 30,000 lbs of force at each location. The average compressive stress as a function of location along the span length is shown in Figure 75. From these results, it can be seen that the compressive stress decreases quite rapidly when one moves away from the post-tensioning strands.

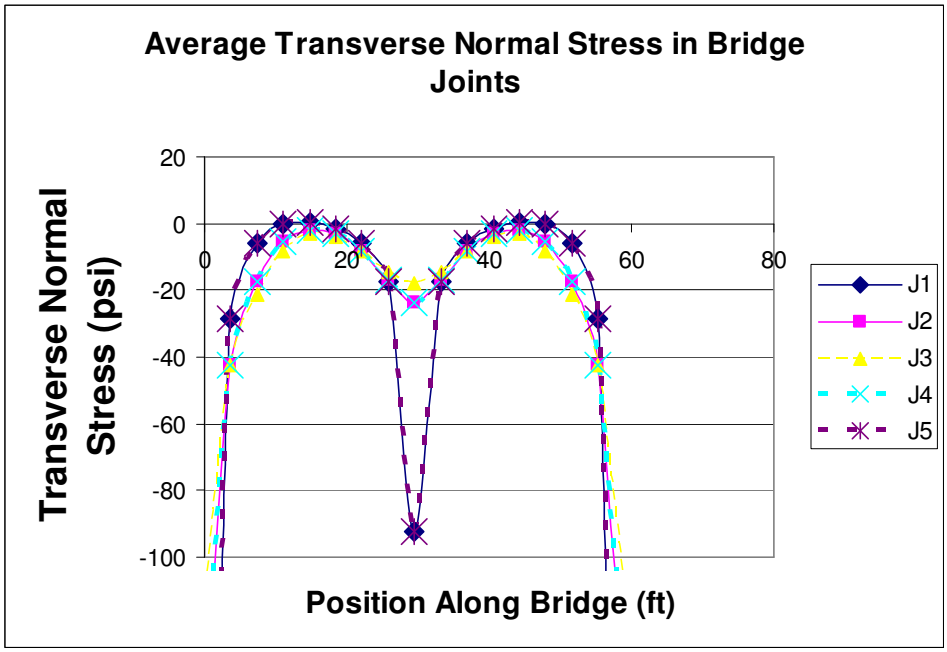

Figure 75: Post-Tensioned PCI Bridge without Loads Applied (2-Lane PB27 – PT 59)

The stresses through the depth of the joint section at midspan are shown in Figure 76. The highest compressive stresses are at the bottom of the joint, but this effect could be a reflection of the post-tensioning strand location. The post-tensioned strands were assumed to be at mid-depth of the shear key since no location was specified.

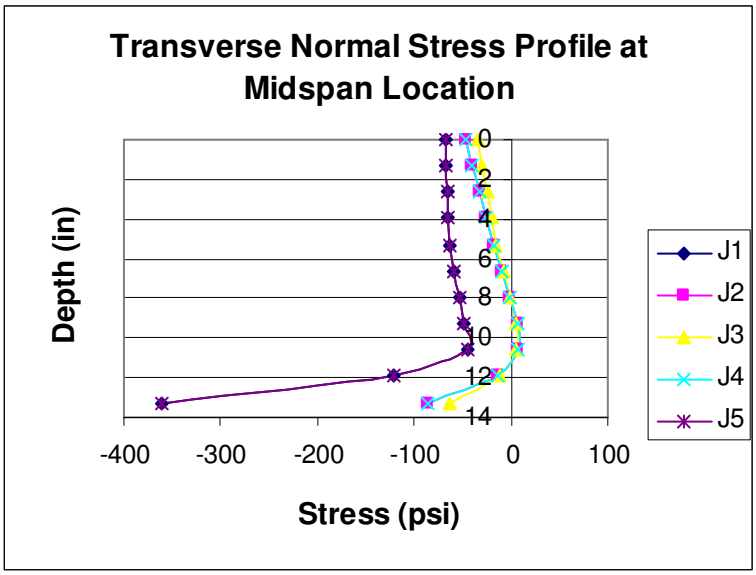

Figure 76: Post-Tensioned PCI Bridge without Loads Applied (2-Lane PB27 – PT 59)

The TxDOT bridges with post-tensioning have a measurable level of compression for each joint along the length of the bridge. However the compressive stress was about 15 psi on average and only half this value away from strand locations. This is not high enough to prevent cracks from forming, but may help control the opening of cracks and limit their width. If crack prevention is desired, much higher post-tensioning force is needed to ensure compressive stresses high enough to counteract the tensile stresses along the entire bridge.

Alternatively, if the maximum tensile stresses occur only in certain areas of the bridge, then the location of the post-tensioning can be optimized as an effective way to reduce cracking. For example, if cracking is a problem only at the end of span and midspan locations, then the current specifications may prevent shear key failure to a

certain extent. However, it should be noted that other techniques were much more reliable and effective at reducing tensile stresses such as using a composite slab or a full depth key.

The post-tensioned PCI bridges have two main problems. The first is that the compressive forces are too small to resist cracking. The second problem is that there is no consistency in compressive stresses at the joints along the length of the bridge. Between the post-tensioning locations, the average compressive stress drops to zero. If post-tensioning is needed to resist the large tensile stresses experienced by the shear keys, then a closer spacing of strands is necessary to ensure a consistent compressive stress along the length of the bridge.

Effects of Bridge Width

The differences between bridges of different widths were not significant when considering the maximum transverse normal stresses. The results for a 2 lane bridge were similar to the results for a 3 lane bridge under each loading case. This is because the highest stresses due to vehicular loads do not extend very far beyond the girders supporting the loads, and the secondary loads (shrinkage and temperature) remain consistent across every joint.

SUMMARY AND CONCLUSIONS

Summary of Project

The purpose of this study is to determine why shear keys are failing in multi-beam box girder bridges. Texas box girder bridges as well as PCI/AASHTO box girder bridges are investigated, because both of these have developed reflective cracks in the past. Other research has been carried out on this topic and several important discoveries have been made, including what loads are likely to cause reflective cracking and the strength of different materials currently used as shear keys. This study aims to build on previous work to create realistic computer models that will provide more information on the topic of reflective cracking.

Previous laboratory and computer analyses, as discussed in the literature review, indicate that shear keys should withstand normal vehicular loads. The shear key designs of most box girder bridges are theoretically strong enough to perform their intended function. In service, however, many box girder bridges utilizing shear keys have experienced problems, and reflective cracking is present on many bridge decks.

This study suggests that secondary loading effects are the principal cause of reflective cracking, or that they act in conjunction with vehicular loads to cause reflective cracking. Secondary loads reflect local conditions, such as the final shrinkage of the concrete used in a specific bridge or the temperature differential of a particular bridge shortly after construction. It is possible that secondary loads can be high in some bridges (those with reflective cracking), while remaining small in most bridges (those with no evidence of reflective cracking).

In addition, secondary loads are proposed as a contributor of reflective cracking because when bridges are closely evaluated under normal environmental conditions they show some kind of reflective cracking above the shear keys, whereas in a controlled laboratory setting most test specimens achieve adequate failure loads. In both Texas and PCI box girder designs, some bridges appeared to develop cracking before the bridge was open for traffic (Jones 1999, Hucklebridge 1995). This clearly indicates the importance of secondary loading effects such as thermal expansion or shrinkage.

Finite element models are a central part of this study, and much work has been carried out to understand how a box girder bridge can be modeled using finite elements as well as how different loads can be applied correctly to these models. Many individual experiments involving convergence tests, comparisons of finite element models, previous published results, and experience from other finite element projects have been used in this particular study.

The finite element models in this study are similar to those used in previous research efforts, but some refinements have been made. First, the specific geometry of the shear key and box girders have been modeled, along with interior diaphragms and composite slabs. A second improvement is the addition of elastic support conditions, reflecting the common use of elastomeric bearing pads. The stiffness, size, and location of these bearing pads have an effect on the transverse loads near the supports, and so these are included within the finite element models.

Solid elastic elements were chosen to represent all of the bridges because many of the bridge components did not meet the requirements for beam or shell element

assumptions. The use of solid elastic elements allows the true geometry of the bridge to be used in the model, avoiding the assumptions required to transform the problem into one involving beam or shell elements.

Another benefit of using solid elastic elements is that loads can be applied directly to nodes in a simple manner. This is important when secondary loads are considered. Thermal differentials and shrinkage effects can be input as loads directly at the locations that they act upon, so complicated strain profiles such as temperatures can be applied as intended. Another benefit of having many nodes available is that stress profiles reflect what is truly happening in a given section, rather than back-calculating stresses based on an assumed strain profile as when classical beam theory is used.

Summary of Results

The results show that most multi-beam box girder bridges considered in this study have shear keys that can safely and effectively transfer vehicular loads. An HS-25 design truck loading will not cause stresses high enough to create cracking problems in the center of the bridge. This is in agreement with most previous studies, and the data shows that the static loading of a truck is not sufficient to cause reflective cracking of multi-beam bridges. However, truck loading does create high stresses near the ends of the bridge, and as a truck passes over the end of the bridge the stresses can be quite large.

Also, secondary loading effects including shrinkage and temperatures result in much higher stresses than vehicular loading. This was true for all of the bridges studied.

The effect of a design temperature gradient as specified by AASHTO causes tensile stresses high enough to cause cracking in some shear keys. The Texas shear keys, by virtue of their larger section, developed lower stresses than the PCI shear keys and would not be expected to have problems with temperature gradients. The other secondary loading situation considered was shrinkage of the shear key and composite slab. If shrinkage values approached the levels used in this study, then all bridges would develop problems with cracking in the shear key and the composite slab.

The results show that section depth and shear key size are the most important factors. Also important are the number and locations of the bearing pad supports, and the presence of a composite slab. Span length does not appear to be an important factor for maximum transverse stress. The presence of post-tensioning does appear to limit the tensile stresses in the shear key, but the improvement is not evident for every load case considered. Another proposed solution, the use of a full depth shear key, resulted in lower tensile stresses, but once again the improvement was not seen for every load case.

Conclusions

Based on the results, several conclusions can be drawn from this study. First, the stresses caused by secondary loadings cannot be ignored when designing and analyzing a multi-beam bridge that will use shear keys. The ACI 318 specifications require that unreinforced concrete elements be analyzed for these effects, but this does not seem to have been addressed in current designs.

Another finding from the computer models is that the largest stresses often occur at the ends of the bridge. The regions near the supports have been found to crack often in previous research, and so the boundary conditions and elastomeric bearing pads must be carefully designed to protect the bridge joints from high stresses.

Another conclusion that can be drawn from the data is that HS-25 truck loads are not large enough to cause shear key failure independently of other loads. If problems with reflective cracking exist along the entire length of the bridge, then shrinkage of the slab and shear key is the most probable candidate. Temperature loads can be large enough to cause cracking and daily temperature fluctuations can cause large stress reversals.

The solutions proposed for shear key failures in past research include transverse post-tensioning and design changes such as the use of a full depth key. These solutions did show improvements compared to a bridge without these features, but the use of a composite slab was the most effective way to decrease tensile stresses. The full depth key was more effective than transverse post-tensioning, but neither reduced tensile stresses for every load considered.

Recommendations for Further Research

The finite element models used in this study were not able to model what would happen after initial cracking. This behavior would be an important step to understanding the consequences of shear key failure. Specifically, the difference in behavior between a fractured shear key and a debonded shear key is essential to determining whether this

has an effect on the composite deck slab. If a debonded shear key is able to transfer load between girders and does not cause cracking in the slab above, then this system would be a good candidate for creating a waterproof joint. However, if a slab is affected by a debonded shear key then the problem with the shear key itself must be corrected.

Another recommendation is to study the impact that the elastic bearing conditions have on transverse stresses near the supports. These locations consistently experienced the highest stresses in the bridge models, and so altering the location or size of the bearing pads could have benefits for the shear keys.

A final recommendation for further work is to measure transverse shrinkage in a composite deck slab as it is installed on a bridge. The shrinkage loadings produced the highest tensile stresses in the bridge models, but the values used for ultimate shrinkage strain were based on limited information. Better knowledge about this effect could lead to slab designs that are able to withstand reflective cracking better than previous bridges.

REFERENCES

American Association of State Highway and Transportation Officials (AASHTO). (1992). *Standard Specifications for Highway Bridges*, Fifteenth Edition. Washington, DC.

American Association of State Highway and Transportation Officials (AASHTO). (2004). *Load and Resistance Factor Design (LRFD) Bridge Design Specifications*, Third Edition. Washington, DC.

American Concrete Institute (ACI). (2002). *ACI-318-02, Building Code Requirements for Reinforced Concrete*. Detroit, MI.

American Society for Testing and Materials. (1993). *ASTM Standards Volume 04.02.* Philadelphia, PA.

Annamalai, G., and Brown, R. C. (1990). "Shear Strength of Post-Tensioned Grouted Keyed Connections in Precast Concrete-Framed Structures," A*CI Structural Journal*, 87(1), 53-59.

ANSYS, Inc. (2005). *ANSYS Theory and Reference Manual*, Version 8.0. http://sc.tamu.edu/softwareDocs/ansys80/

Cusens, A. R., and Pama, R. P. (1965). "Design of Concrete Multibeam Bridge Decks," *Journal of the Structural Division*. October, 254-278.

El-Remaily, A., Tadros, M. K., Yamane, T., and Krause, G. (1996). "Transverse Design of Adjacent Precast Prestressed Concrete Box Girder Bridges." *PCI Journal*. 41(4), 96-113.

Federal Highway Administration (FHWA). (2005). "National Bridge Inventory." <http://www.fhwa.dot.gov/bridge/nbi.htm>

Grata, J. and M. Saxton. (2005). "Road salt, hits from trucks likely led to bridge collapse." Pittsburgh Post-Gazette. December 24.

Gulyas, R. J., Wirthlin, G. J., and Champa, J. T. (1995). "Evaluation of Keyway Grout Test Methods for Precast Concrete Bridges," *PCI Journal*. 40(1), 44-57.

Huckelbridge, A. A., and El-Esnawi, H. H. (1997). "Evaluation of Improved Shear Key Designs for Multi-Beam Box Girder Bridges," Final Report, Ohio Department of Transportation, FHWA/OH-97/009. Columbus, OH.

Huckelbridge, A. A. Jr., El-Esnawi, H., and Moses, F. (1995). "Shear Key Performance in Multibeam Box Girder Bridges." *Journal of Performance of Constructed Facilities*. 9(4), 271-285.

Issa, Mohsen A., Ribeiro de Valle, C. L., Abdalla, H. A., Islam, S. H., and Issa, Mahmoud A. (2003). "Performance of Transverse Joint Grout Materials in Full-Depth Precast Concrete Bridge Deck Systems." *PCI Journal*. 48(4), 92-103.

Jones, H. L. Multi-Box Beam Bridges with Composite Deck. (1999). FHWA-TX-00-1709-1. Texas Transportation Institute. Texas A&M University, College Station, TX.

Kaneko, Y., Connor, J. J., Traiantfillou, T. C., and Leung, C. K. (1993a). "Fracture Mechanics Approach for Failure of Concrete Shear Key I: Theory." *Journal of Engineering Mechanics, ASCE*. 119(4), 681-699.

Kaneko, Y., Connor, J. J., Traiantfillou, T. C., and Leung, C. K. (1993b). "Fracture Mechanics Approach for Failure of Concrete Shear Key II: Verification." *Journal of Engineering Mechanics, ASCE*. 119(4), 701-719.

Lall, J., DiCocco, E. F., and Alampalli, S. (1997). "Full Depth Shear-Key Performance in Adjacent Prestressed-Beam Bridges." Special Report 124, Transportation Research and Development Bureau, New York State Dept. of Transportation, Albany, NY.

Miller, R. A., Hlavacs, G. M., and Long, T. W. (1998). "Testing of Full-Scale Prestressed Beams to Evaluate Shear Key Performance," Final Report, Ohio Department of Transportation, FHWA/OH-98/019, Columbus, Ohio.

Moreton, A. J. (1981). "Epoxy Glue Joints in Precast Concrete Segmental Bridge Construction," *Proc. Instn. Civ. Engrs*. 70(1), 163-177.

Nottingham, D., Gulyas, R. J., Wirthlin, G. J., and Champa, J. T. (1995). "Reader Comments - Evaluation of Keyway Grout Test Methods for Precast Concrete Bridges," *PCI Journal.* 40(4).

Ohio Department of Transportation (ODOT). (2005). "ODOT Bridge Design Manual." <http://www.dot.state.oh.us>

Texas Department of Transportation (TxDOT) (2001). "TxDOT Bridge Design Manual." <http://manuals.dot.state.tx.us/dynaweb/colbridg/>

Yazdani, N., S. Eddy, C. S. Cai. (2000). "Effect of Bearing Pads on Precast Prestressed Concrete Bridges." *Journal of Bridge Engineering*, ASCE. 5(3), 224-232.

VITA

Graeme Peter Sharpe graduated with a Master of Science degree in civil engineering from Texas A&M University in August 2007. His thesis advisor was Dr. Harry Jones, and he worked with Dr. Ray James and Dr. Jones as a research assistant for the Texas Transportation Institute before finishing work on his thesis. Graeme received his Bachelor of Science degree in civil engineering from Carnegie Mellon University in May 2002. He has been an engineer at the firm of Silver Creek Engineering, Inc. of Indianapolis, IN since July, 2005.

Contact Information:

Graeme Peter Sharpe

400 S. Ritter Avenue

Indianapolis, IN 46219

United States of America

Email: graeme.sharpe@gmail.com